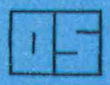

ORKUSTOFNUN
NATIONAL ENERGY AUTHORITY

THE UNITED NATIONS UNIVERSITY

GEOPHYSICAL EXPLORATION FOR GEOTHERMAL RESOURCES
Principles and application

Gylfi Pall Hersir and Axel Bjornsson

UNU Geothermal Training Programme
Reykjavík, Iceland
Report 15, 1991

Report 15, 1991

GEOPHYSICAL EXPLORATION FOR GEOTHERMAL RESOURCES
Principles and application

Gylfi Páll Hersir and Axel Björnsson

National Energy Authority, Geothermal Division
Grensásvegur 9
108 Reykjavík
ICELAND

LIST OF CONTENTS

LIST OF FIGURES

LIST OF TABLES

FOREWORD

These lecture notes are compiled for students attending the UNU Geothermal Training Programme in Iceland. This is not a textbook on geophysical exploration, but rather notes containing the essence of the most important texts in a short form, some major formulas and figures and tables with data. It is compiled to help students follow the introductory lectures during the first weeks of the programme. Hence, the level of these notes is meant for non-geophysicists who want an overview of the basic principles of geophysical exploration in geothermal areas, as well as for geophysicists who are starting work in the field of geothermal exploration.

The main emphasis is put on geophysical exploration of geothermal resources in volcanic areas. The material is based on experience of geothermal exploration in Iceland over the last two decades, but exploration in other countries is discussed as well. In the list of references, several books and articles are listed that are not referred to directly in the text. These are general references which the reader might find useful as an addition to the lecture notes.

These notes are mainly based on material compiled by Gylfi Páll Hersir and Axel Björnsson, as well as by Sveinbjörn Björnsson and Guðmundur Pálmason, which has been used in the UNU Geothermal Training Programme over the last few years. Furthermore, we have used material from several geothermal courses organized by Axel Björnsson for the UNDP in various countries.

The authors want to thank Knútur Árnason for reading the manuscript and suggesting several improvements, Ólafur G. Flóvenz for reading chapter 3 and bringing in new aspects, Auður Ágústsdóttir for making the drawings, Marcia Kjartansson for correcting the English and Lúðvík S. Georgsson for making various recommendations.

1. INTRODUCTION

In geophysical exploration we examine the physical properties of the earth's crust. We measure the various parameters connected to geological structure and the properties of geothermal systems. In geothermal exploration the task is the detection and delineation of geothermal resources, the location of exploitable reservoirs and the siting of drillholes through which hot fluids at depth can be extracted.

Almost all geophysical methods have been applied in geothermal prospecting. In oil exploration the seismic reflection method is most widely used. About 90% of all efforts in geophysical exploration in the world is spent on this method. On the other hand, in geothermal exploration the most important methods are various electrical and thermal methods.

The effectiveness of these geophysical methods was greatly increased when emphasis was shifted from prospecting the geology and the structures that contain the geothermal fluids to prospecting the fluids themselves and concentrating on determining those parameters which are most sensitive to changes in temperature.

Rocks containing geothermal fluids are usually characterized by anomalously low resistivity. Therefore, those methods which measure the electrical resistivity at depth in the ground have been the most useful of all geophysical methods used to prospect for geothermal reservoirs.

Geophysical methods can often provide information as effectively, and certainly at a lower cost, than drilling a borehole.

It should be recognized that no particular technique is universally applicable, and methods should be chosen carefully to suit the situation. Most geophysical methods display a progressive reduction of resolving capacity as they are extended to greater depths.

Further, it should be born in mind that geophysical exploration cannot stand alone, but must be applied along with field geology, geochemistry and drilling in order to resolve the nature of the subsurface geothermal systems in as much detail as possible.

2. GEOPHYSICS AND GEOTHERMAL EXPLORATION - AN OVERVIEW

2.1 Introduction

The fundamental parameters of interest which characterize a geothermal system are:

- Temperature
- Pressure
- Porosity (water/steam content)
- Permeability
- Chemical composition of the fluid

A good geothermal reservoir has high temperature, high pressure, high porosity and permeability, and low content of dissolved solids and gases in the water. Most exploration methods estimate the fundamental parameters indirectly.

The most important methods in geothermal exploration are:

- Geological mapping: Regional and local stratigraphy, geological formations, faults, fissures, dip, thermal springs
- Chemical study of thermal water: Dissolved solids, thermometers, isotopes
- Geophysical measurements: Direct methods (temperature, resistivity), structural methods (seismics, gravity, magnetics)
- Exploratory drilling, logging

It is not possible to tell from geophysical data alone as to whether or not there is an economically exploitable geothermal field in a certain area.

It is essential to combine geophysics with geology, geochemistry and borehole data in order to obtain significant information on the geothermal field under investigation.

The **primary aim** of geophysical exploration of geothermal areas is to:

- Find geothermal prospects
- Outline drilling fields
- Locate aquifers and site wells
- Estimate properties of the system

Geophysical exploration of geothermal areas can be divided into: Surface geophysics (exploration) and borehole geophysics (logging).

The **success of a geophysical survey** is measured by the time, effort and money which the survey has saved in delineating a prospect area and in siting successful wells. The success of a survey is highest if it can be used to lower the total number of drillholes and assist in avoiding the drilling of unsuccessful wells. A single well may cost about 1 million US dollars, but a resistivity survey, which outlines a drilling field and helps siting several wells, costs only some 0.2 million US dollars.

The **basic geophysical methods** measure some physical properties related to the geothermal

system. The physical properties must differ from those of the host rock in order to create an anomaly. If the variation in physical properties is related directly to the geothermal system (e.g. temperature), then we talk about direct exploration methods. If the anomaly is caused by associated geological formations or structures (e.g. dykes, faults), then the method is called an indirect exploration method.

The most important physical properties measured in geothermal exploration are:

- Temperature [°C]
- Electrical resistivity [Ωm]
- Magnetization [A/m]
- Susceptibility [dimensionless]
- Density [g/cm^3]
- Elasticity [N/m^2]
- Seismic velocity [m/s]
- Thermal conductivity [W/m°C]
- Electrochemical or streaming potential, SP [V]
- Radioactivity (in logging)

The best results are obtained through the combined use of two or more methods.

2.2 Performing a geophysical survey

The first step is to collect all available existing data on the geothermal field.

- Topographical information; maps 1:50,000 - 1:100,000, accessibility, roads
- Geological information; maps, geological units, tectonics, fumaroles, alteration
- Existing geophysical data; review all available data
- Drilled wells; geological sections and logs
- Geochemistry; minerals in water and steam, chemical thermometers

The most promising geophysical method is selected by using all available data. A trial survey ought to be carried out, at the least, before a large-scale geophysical campaign is started in a new or unknown area. It is important to stake the area in detail before field measurements start.

The best routine depends on the method used. Organize the field setup to minimize time. Organize your collected data. Record field observations on standardized paper with printed columns and lines. Include date, time, area, observer, number of site, instrument and remarks.

Judge the data in the field. Look for errors, repeat if necessary (this is less expensive than repeating a whole survey later).

Most geophysical instruments are delicate and expensive (a gravimeter costs 30,000 US dollars; a resistivity instrument costs 40,000 US dollars). Be careful!! Failure can result in one year's delay.

Preparation and presentation of the data: The readings of the field data are converted to appropriate units, corrected if necessary, and then plotted on a map. Two methods are common in presenting geophysical data:

- Iso-anomaly curves or contour lines. Iso-anomaly maps give an overview of the data but usually not all the details
- Profiles or pseudo-sections. The observation station is the abscissa along a line and the measured value (anomaly) is the ordinate on ordinary graph paper. Profiles visualize the continuous variation of anomalies better than contour lines

Iso-anomaly maps and profiles are summaries of the observations and are not geological interpretations. Some qualitative conclusions can be drawn from iso-anomaly maps and profiles: Location of an anomalous body, size and form of an anomaly, strike of faults or dykes, etc. A short wavelength anomaly usually reflects shallow depth; a broad anomaly may reflect great depth. With experience and by considering other data, it is possible to extract good qualitative information from maps and profiles.

Quantitative interpretation usually involves a certain amount of computational work depending on the method and, of course, close cooperation with geologists, geochemists and engineers in order to construct a model of the explored field.

Nowadays, geophysics is becoming more and more complicated. Hence, teamwork and cooperation between experts from different disciplines are essential.

2.3 The most important geophysical methods in geothermics

The most important properties of a geothermal system are temperature, permeability and the chemical composition of the fluid. Various parameters are measured in geophysical exploration. An attempt is made to connect them to the properties of the geothermal system. Geophysical methods are divided into direct and indirect or structural methods. The most important geophysical exploration methods in volcanic areas are:

Thermal methods. The most direct method is to study the subsurface temperature in a geothermal system. Temperature is measured in shallow drillholes and in soil. Estimation of the temperature at depth is made from the temperature gradient. Conduction versus convection in geothermal systems is determined, as well as location of aquifers in geothermal wells.

Electrical resistivity of rocks. The electrical resistivity of rocks is an important parameter which can be related to the properties of geothermal systems. In most rocks near the earth's surface the electrical conduction is mainly electrolytic in an aqueous solution of common salts distributed through the pores of the rock and/or along the rock-water interface. The resistivity depends on the pore structure, amount of water (saturation), salinity of the water, steam content in the water, water-rock interaction (alteration minerals), temperature and pressure. The salinity of the water, temperature, porosity and water-rock interation are of greatest influence. Resistivity measurements are used to delineate geothermal systems, locate aquifers and sometimes to estimate porosity and physical conditions within a geothermal system.

DC-resistivity methods. Several variations of the direct current resistivity method have been used for decades in geothermal exploration with great success. The most widely used is the Schlumberger method. DC-methods are used both for depth-soundings and profiling. Nowadays, two-dimensional modeling is a standard procedure. Near-surface vertical structures can be delineated. The limitations of the DC-methods include a relatively slow progress in the field, tedious two-dimensional model calculations and limited depth penetration.

AC-resistivity methods. MT, AMT, EM, TEM. The magnetotelluric method has been used for deep probing, mainly in sedimentary basins. Various types of electromagnetic methods and time-domain electromagnetic methods have been used in geothermal exploration. The depth of penetration is similar to the DC-methods but field measurements and model calculations are, in some cases, much more economical. In the last few years in Iceland, a TEM method with two concentric loops has proven very successful.

SP survey. This is a low-cost surveying technique and has been applied in many geothermal areas. However, the anomalies are usually small and can be contaminated by noise.

Magnetic survey. A structural method. Numerous aeromagnetic surveys have been carried out over geothermal areas. A correlation between magnetic lows and zones of intense hydrothermal alteration has been found. Detailed ground-magnetic surveys are used in Iceland to trace narrow linear features like dykes and faults where the basement is covered with soil.

Gravity survey. A structural method. This is typically used to find features such as faults, dense intrusions or sediments on a dense basement.

Seismicity, micro-earthquakes. Many geothermal systems occur in volcanic tectonically-active areas and are characterized by a high level of micro-seismic activity. There is, in most cases, no clear one-to-one relationship between the location of micro-earthquakes, and the geothermal reservoir. In some areas micro-earthquakes indicate cooling intrusions.

Seismic methods - Reflection and refraction. Seismic reflection and seismic refraction have both been used, to a limited extent, in geothermal exploration.

Logging in geothermal wells. Logs are performed to give information on well performance, and also to obtain information on lithological structure and physical properties of the geothermal system penetrated by a well.

3. THERMAL METHODS AND TEMPERATURE SURVEYS

Thermal methods directly measure temperature and heat. No other method has such a good correspondence with the geothermal system. There are approximately four measurement sub-categories:

- **Temperature alone;** direct interpretation, mapping
- **Geothermal gradient;** vertical variation of temperature measured in soil or shallow drillholes
- **Heat flow;** calculated from the product of gradient and thermal conductivity
- **Heat budgets**; measuring spring flow and steam output and/or integrating areal heat flow

Measuring the temperature alone or the geothermal gradient is of direct significance in local geothermal work, while measuring the heat flow is of a more regional or global interest.

Heat can be exchanged by:

- **Conduction**; transfer of heat through a material by atomic vibration; often in steady-state
- **Convection;** transfer of heat by motion of mass (solid or liquid); natural circulation of hot water
- **Radiation** (does not play any significant role in geothermal exploration)

Conduction plays a significant role in the transfer of heat in the earth's crust, from below to the surface. Thermal convection is usually a much more effective heat transfer mechanism than thermal conduction and is most important in geothermal systems, as shown in Figure 3.1.

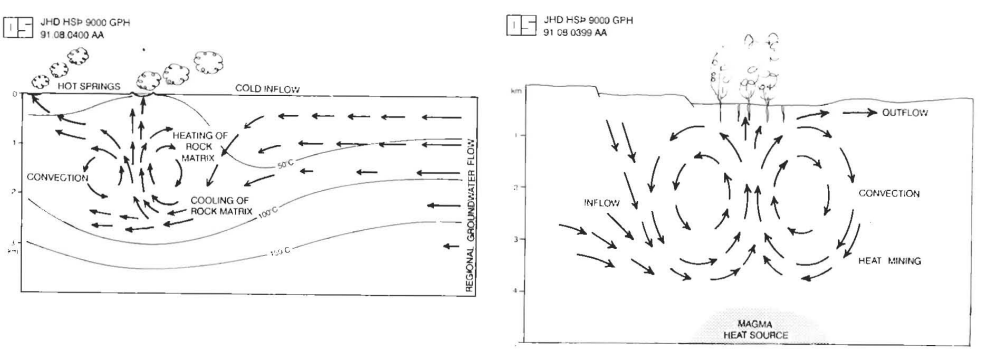

FIGURE 3.1: *Generalized model of convective hydrothermal systems; a low-temperature system to the left and a high-temperature system to the right (modified from Björnsson, 1990; Björnsson et al., 1990)*

3.1 Thermal conduction

If a temperature difference $\Delta T = T_2 - T_1$ [°C] is kept constant along a piece of rod with length L [m] and cross-sectional area A [m^2] (see Figure 3.2), then the amount of heat U [J] flowing through the rod during the time t [s] is given by the equation:

$$U = -A \cdot t \cdot \kappa \cdot \frac{\Delta T}{L} \tag{3.1}$$

(The heat flows from higher to lower temperature, i.e. in opposite direction of the temperature gradient ($T_1 > T_2$). Hence, the negative sign in Equation 3.1). κ is a constant which depends on the material. It is called thermal conductivity and is measured in [W/m·°C] or [μcal/cm·s·°C]. Its value for various rocks is given in Table 3.1. Heat flow density, denoted by Q, is the amount of heat flowing through a unit area during one second. Heat flow density is measured in J/sm^2 or W/m^2. The older cgs-units are still often used in geophysics. One heat flow unit [HFU] is defined as 10^{-2} cal/m^2s and is equal to 42 mW/m^2.

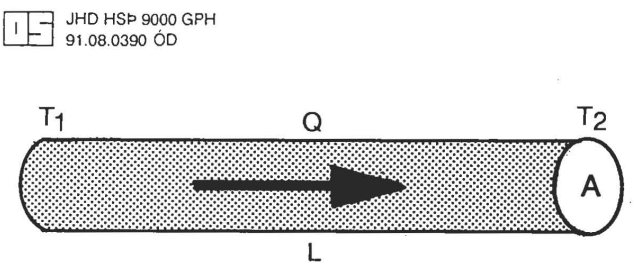

FIGURE 3.2: *Heat flow along a rod is controlled by the temperature difference and the thermal conductivity of the material*

TABLE 3.1: *Thermal conductivity of various rocks at room temperature (taken from Rybach, 1981)*

Rock type	Thermal conductivity [W/m·°C]
Dolomite salt	≈5.0
Peridotite/pyroxenite	4.2-5.8
Granite	2.5-3.8
Limestone	1.7-3.3
Gabbro/basalt	1.7-2.5
Sandstone	1.2-4.2
Volcanic tuffs (depending on porosity)	1.2-2.1
Shale (depending on water content)	0.8-2.1
Deep-sea sediments (depending on water content)	0.6-0.8
Water	0.6

The thermal conductivity varies with different types of rocks (see Table 3.1). It is lower in sedimentary rocks (sandstone, shale) than in crystalline rocks (granite, peridotite). This explains the existence of geothermal systems in the deep sedimentary basins (non-convective geothermal systems), for example around Paris in France, Bejing in China and in Hungary (see Figure 3.3). The sediments act like insulating blankets and the heat from the interior of the earth is accumulated at the basement below the sediments.

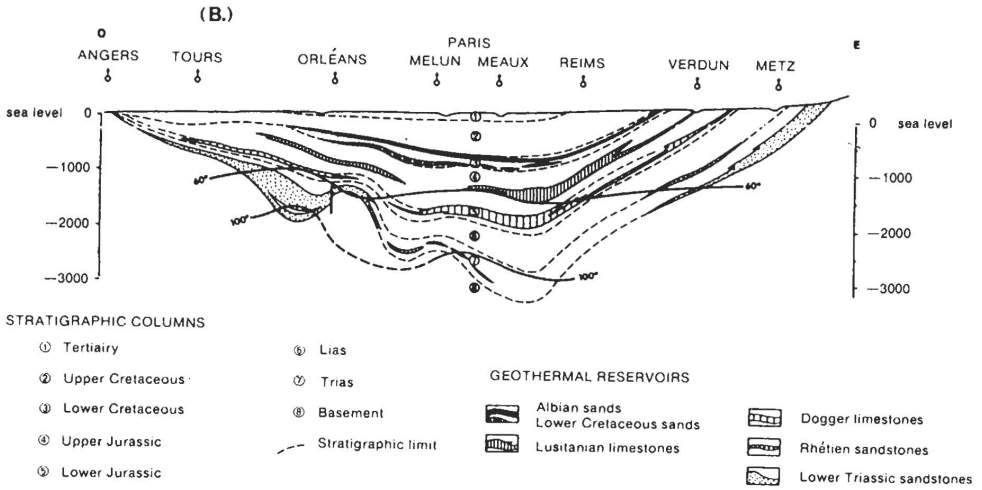

FIGURE 3.3: *Exploitation of heat in normal-gradient conditions in sedimentary basins; a southwest-northeast cross-section through France and the Paris basin (taken from Coudert et al., 1985)*

For porous, water-saturated rocks there exists an approximate relationship between in situ (κ_{is}), intrinsic or bulk (κ_b) and water (κ_w) thermal conductivity and porosity ϕ (Sass et al., 1971):

$$\kappa_{is} = (\kappa_b)^{1-\phi} \cdot (\kappa_w)^{\phi} \tag{3.2}$$

It follows that for low porosity, $\phi \approx$ 10-20%, the water content only plays a minor role in the in situ thermal conductivity.

In the absence of mass movements the linear relationship between conductive heat flow density $\vec{Q}_{cond}$ [W/m^2] and thermal gradient ∇T [°C/km] can be written in a general form as:

$$\vec{Q}_{cond} = -\kappa \nabla T \tag{3.3}$$

Worldwide average conductive heat flow density is estimated to be 60-80 mW/m^2; values in excess of about 80-100 mW/m^2 indicate anomalous geothermal conditions in the subsurface. The total heat output from the earth is $3 \cdot 10^{13}$-$4.3 \cdot 10^{13}$ W (Uyeda, 1988).

Since the heat flow in the earth's crust is mainly vertical, it can be approximated with:

$$Q_{cond_z} = -\kappa \frac{\partial T}{\partial z}, \tag{3.4}$$

where z is the coordinate down into the earth. If time variations in T cannot be ignored, this equation is not valid and has to be replaced by the diffusion equation for heat production.

The temperature distribution in the earth can be described by the heat conduction equation (no convection):

$$\kappa\nabla^2 T + A = \rho c\frac{\partial T}{\partial t}, \tag{3.5}$$

where:

A - the radiogenic heat production in the crust [W/m^3]
ρ - density [kg/m^3]
c - heat capacity [J/kg°C]
$\rho c/\kappa$ - thermal diffusivity [m^2/s]

For a one-dimensional stationary state problem ($\partial T/\partial t = 0$ and T only a function of z) with constant thermal conductivity and heat production, the solution to Equation 3.5 becomes:

$$T(z) = T_0 + \frac{Q_0}{\kappa} z - \frac{1}{2}\frac{A}{\kappa} z^2, \tag{3.6}$$

where T_0 and Q_0 are the temperature and heat flow, respectively, at the earth's surface ($z=0$).

In case of no crustal heat production ($A=0$) we have:

$$\nabla^2 T = 0 \quad \text{and} \quad T = T_0 + g \cdot z, \tag{3.7}$$

where T_0 is the annual mean temperature and g the temperature gradient (see Figure 3.4).

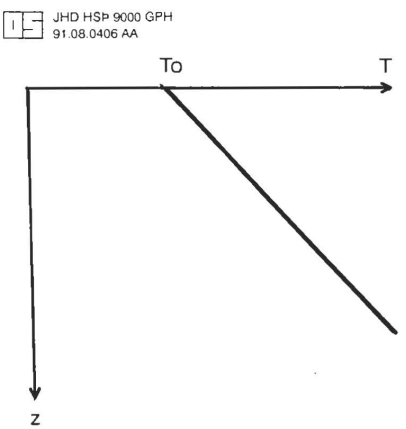

FIGURE 3.4: *Temperature as a function of depth for a one-dimensional stationary state problem with no crustal heat production (T_0 is the mean annual temperature)*

The internal heat of the earth escaping to the atmosphere is called the surface heat flow (Q). Taking into account crustal heat production A(z), it is expressed as:

$$Q = Q_m + \int_0^{z_m} A(z)dz, \tag{3.8}$$

where:

Q_m - mantle heat flow
z_m - the thickness of the crust in which the natural radioelements U, K and Th are concentrated

Heat flow data show that Equation 3.8 can be simplified to a linear equation, showing the relationship between heat flow and radiogenic heat production, thus leading to the recognition of heat flow provinces:

$$Q = Q_m + DA_0, \tag{3.9}$$

where:

Q_m - mantle heat flow or reduced heat flow; heat flow for zero radioactive heat, originating from lower crust and upper mantle
D - characteristic depth of radioactive heat production ($z_m \approx D$), uniform within certain areas termed as "heat flow provinces" (see Table 3.2)

Table 3.3 shows the values of A_0 for several rock types.

TABLE 3.2: *Typical continental heat flow provinces (taken from Jessop and Lewis, 1978)*

Province	Geologic/geothermal characteristics	Mean surface heat flow, Q [mW/m^2]	Reduced (mantle) heat flow, Q_m [mW/m^2]	D [km]
Eastern U.S.A.	Tectonically stable continental area, conductive heat transfer	57	33	7.5
Basin and Range, U.S.A.	Area with active spreading tectonism, strong convective heat flow components	92	59	9.4
Sierra Nevada, U.S.A.	Heat flow transient due to former subduction tectonism	39	17	10.1
Precambrian Shields (average)	Stable continental shield	60	21	14.4

3.2 Corrections of heat flow measurements

Determination of heat flow requires knowledge of two parameters, the temperature gradient and the thermal conductivity as a function of depth.

The thermal conductivity is usually measured in cores or drill cuttings samples from the borehole and is usually a relatively well known physical property. The temperature gradient may, on the other hand, depend on several parameters other than heat production and thermal conduction from the earth's interior. The most important factors are:

- **Topography:** The effect on near-surface heat flow is to decrease the gradient on hills and mountains and increase it in valleys and depressions
- **Paleotemperature:** Changes to air temperature in the past are common in the uppermost tens or even hundreds of meters. Recent upwarming in the near annual temperature can be observed as an inversion on the temperature-depth curve
- **Environmental changes:** Effects of man-made activities such as road building, and deforrestation frequently changes the soil conduction giving use to change in the mean-surface temperature. The effects are similar to paleotemperature changes
- **Sedimentary erosion:** Rapid sedimentation reduces the observed heat flow while the erosion processes have the opposite effect
- **Groundwater flow:** The effect of hydrologically driven water flow can affect the heat flow measurement seriously. This applies particularly to sedimentary basins

In preparing heat flow maps, these factors have to be evaluated and corrected for, where necessary. Several methods for correcting heat flow values are described in: "Handbook of Terrestrial Heat-Flow Density Determination (Haenel et al., 1988).

TABLE 3.3: *Heat production in various types of rocks (taken from Rybach, 1976 and 1986)*

Rock type	Rate of heat production [$\mu W/m^3$]
Black shales	5.5
Granite/rhyolite	2.45
Shales and siltstones	1.8
Granodiorite/dacite	1.48
Diorite, quartz diorite/andesite	1.08
Sandstones - Graywacke	0.99
Sandstones - Arkose	0.84
Sandstones - Quartzite	0.32
Basalt/gabbro	0.31

3.3 Convection

Convection is very important in geothermal systems. Heat is transported by convection in moving fluid (hot water); see Figure 3.1. There are two types of convection:

- **Free convection:** Flow is driven by density gradients, i.e. increase in temperature and the associated decrease in density of the fluid with depth causes instability, which also

depends on permeability. Often a cellular flow; up in the center, down outside

- **Forced convection:** The flow is driven by an external pressure gradient, like hydrostatic head and is more or less independent of the temperature. Often flow along fissures and fault systems

Flow in a geothermal system is often of mixed type. Sometimes free convection dominates in the internal part of the system, but flow towards the system is of forced convection type.

The heat flux to the surface is many times larger in convecting systems than in conductive-type systems. Energy is pumped from the interior of the earth to the surface. Geothermal systems are cooling spots of the earth.

Two non-dimensional numbers are important in understanding convection patterns in cells of circulating water. They are the Rayleigh number, R and the Nusselt number, N:

$$R = \frac{\text{driving force (thermal effect on density)} \cdot \text{permeability}}{\text{viscosity}},$$

$$R = \frac{g \cdot \alpha \cdot \rho \cdot c \cdot \Delta T}{\nu} \cdot \frac{\eta}{\kappa} \cdot D \qquad (3.10)$$

where:

g - gravitational attraction
α - thermal expansion
ρ - density of the fluid
c - heat capacity of the fluid
ν - kinematic viscosity
η - intrinsic permeability
D - vertical extent of the system
κ - thermal conductivity

$$N = \frac{\text{total heat flux with convection}}{\text{heat flux without convection}}; \text{ for same temperature gradient} \qquad (3.11)$$

Convection starts for $R \approx 40$. In most high-temperature geothermal systems $R \approx 100$ - 1000, and $N \approx 5$ - 10. There is a relationship between R and N, as shown in Figure 3.5:

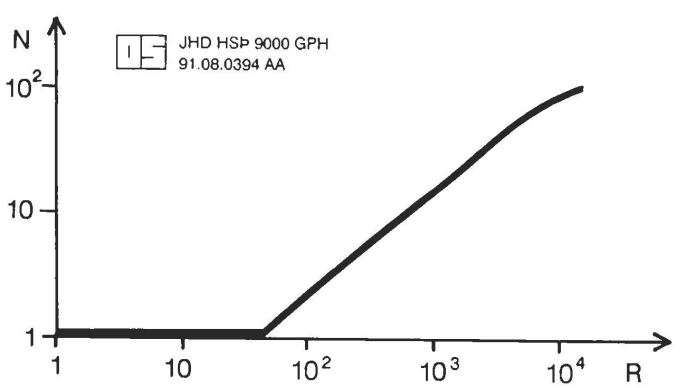

FIGURE 3.5: *Relationship between Rayleigh number R, and Nusselt number N. Convection replaces conduction for R* ≥ 40

3.4 Types of temperature gradients

Where there is no convection (low temperature difference, and low permeability) and no radioactive heat generation, the heat flux is constant everywhere and the temperature distribution is linear for constant κ, i.e. the temperature gradient is constant. If convection takes place ($R \geq 40$) the linear temperature gradient is disturbed (Figure 3.6).

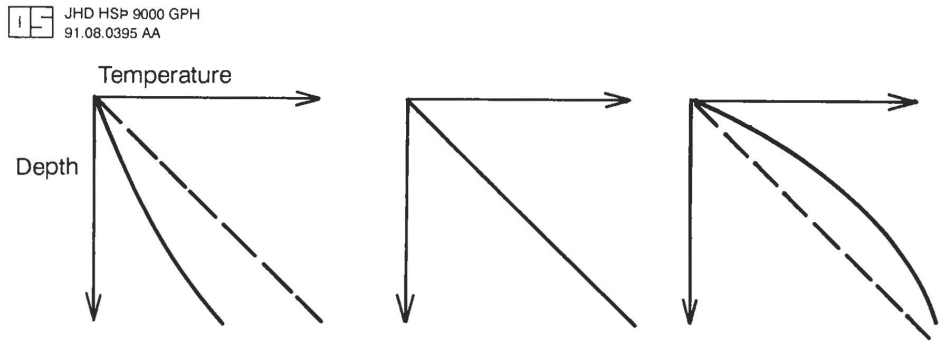

FIGURE 3.6: *Vertical flow: Temperature as a function of depth in a cold downflow zone (figure to the left), undisturbed zone (in the middle) and in a warm upflow zone (to the right)*

The picture is more complicated in cases of lateral flow (Figure 3.7).

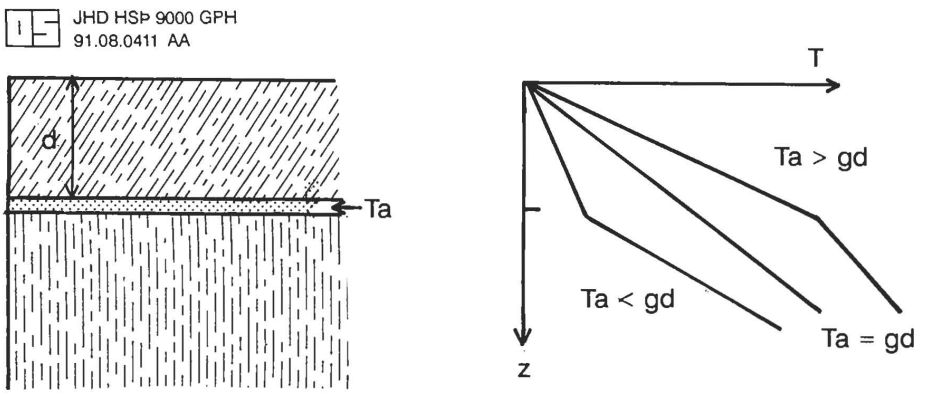

FIGURE 3.7: *Lateral flow: Temperature as a function of depth (T_a is the temperature in the layer, d is the depth to it and g is the temperature gradient)*

If the surface zone is highly permeable and cooled, for example by convection (downflow) of meteoric water, like in many fractured volcanic areas, it is necessary to drill through the surface layer (into the conduction zone) in order to get information about the regional gradient (see Figure 3.8). In the fractured tectono-volcanic zone in Iceland, the depth to the conduction zone is often around 500 m. Some typical temperature profiles from deep drillholes in Iceland are shown in Figure 3.9.

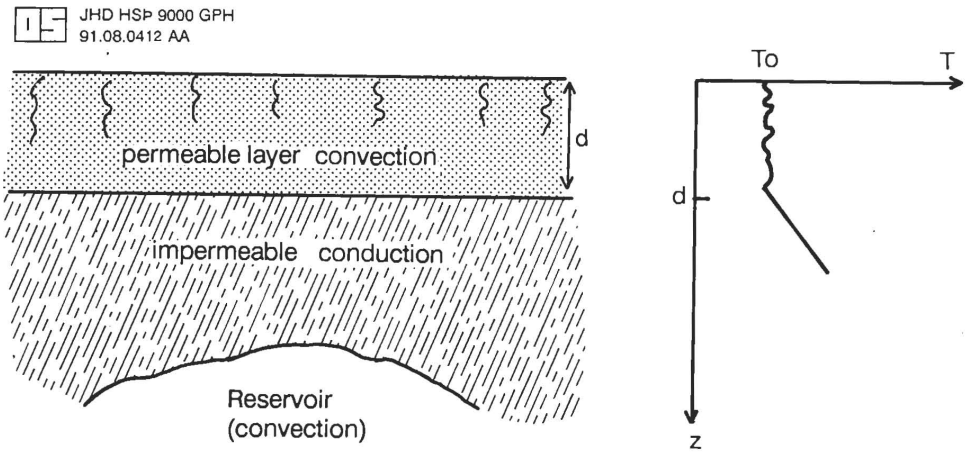

FIGURE 3.8: *Temperature gradient in the presence of a highly permeable surface layer*

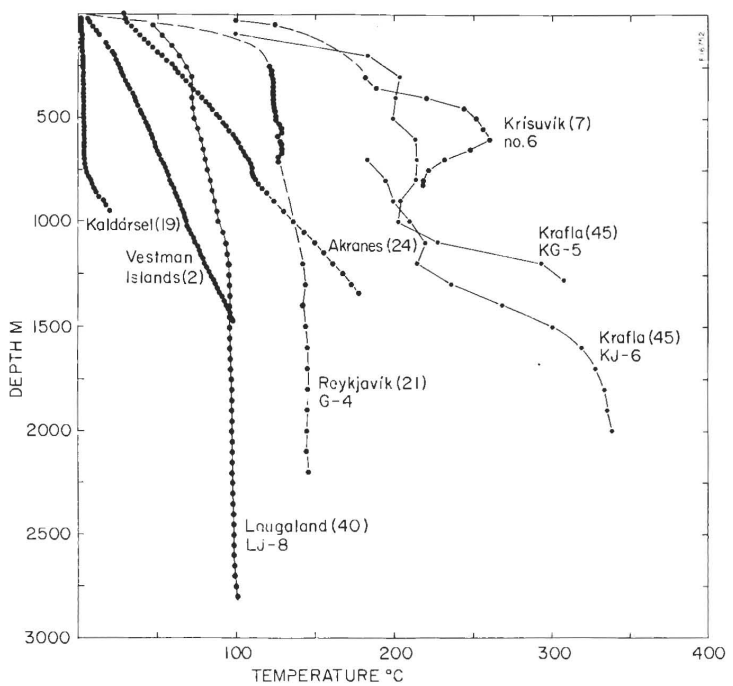

FIGURE 3.9: *Some typical temperature profiles from deep drillholes in Iceland showing disturbances of the crustal temperature by water convection. Drillholes no. 7 and 45 are within high-temperature fields, 21 and 40 are within low-temperature areas, 2 and 24 show relatively undisturbed thermal state of the crust and 19 is a downflow hole (taken from Pálmason et al., 1979)*

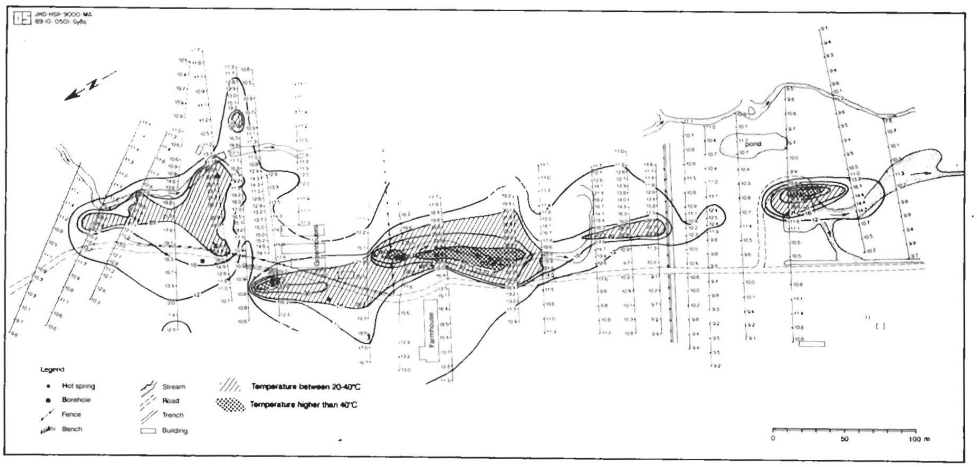

FIGURE 3.10: *A geothermal map from Reykjavellir, S-Iceland based on measurements at 0.5 m depth (modified from Abouriche, 1989)*

3.5 Thermal methods in geothermal exploration

- **Surface measurements of temperature in soil:** Temperature measurements are made at some 0.5 m depth in a grid with an interval of 5-10 m between measurement points. A useful method for strong anomalies, e.g. in the vicinity of springs and fumaroles. It usually gives a similar picture as that indicated by the surface thermal activity. Examples are given in Figures 3.10-3.11.
- **Snowmelt photography** has been used to indicate surface areas of slightly elevated temperatures. Aerial photographs of areas, taken hours to days after light-to-moderate snowfall, made the thermally anomalous areas visible because the snow melted faster over these areas than it did over non-thermal areas. This is a common method in reconnaissance study in Iceland (see Figure 3.12).
- **Airborne thermal infra-red (IR) surveys,** employing infra-red scanners detecting radiated energy, have been used to map the occurrence of warm ground and hot springs in Kenya (Noble and Ojambo, 1976). Previously unknown hot areas in unsurveyed territory were detected. This method has the advantage that large areas can be surveyed rapidly and it provides an instantaneous picture for comparison with pictures at a later date. The disadvantages are low sensitivity, no depth penetration, sensitivity to disturbances by solar radiation and influence of vegetation.
- **Temperature in 20-200 m drillholes:** The main purpose of drilling such medium deep holes is either to measure the temperature gradient or to delineate aquifers. An example is shown in Figure 3.13. These holes are often drilled with air-hammer drilling in 1-2 days, and are, therefore, relatively low in cost. If the hole is not cased, information on aquifers and hydrostatic conditions can be obtained. If only information on the temperature gradient is to be obtained, the hole is usually cased by a plastic or iron tubing. The casing is cemented to prevent flow in the hole between aquifers or between the surface and aquifers. The pipe is capped and filled with water to speed measurements. The main objective of a temperature well is to ascertain the subsurface temperature. This is

difficult to obtain. It can take several weeks for the temperature in the holes to return to equilibrium after drilling. Drilling a hole causes manyfold disturbances of the preexisting temperature distribution:

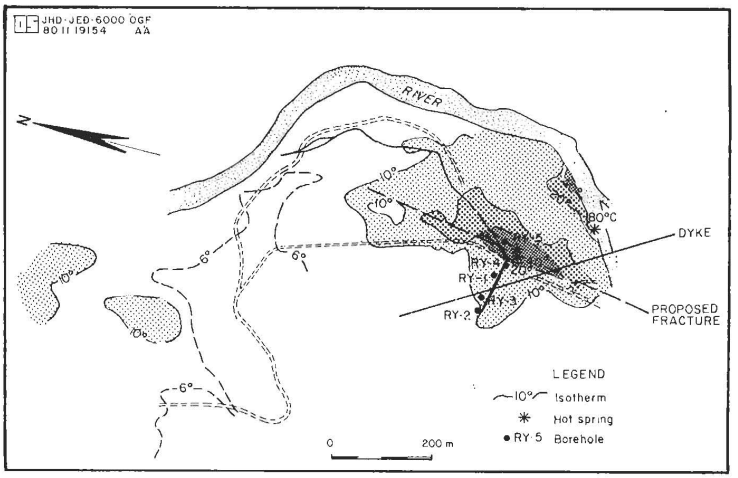

FIGURE 3.11: *Iso-thermal map at 0.5 m depth in the soil at Reykir in Fnjóskadalur, NE-Iceland. The figure also shows the locations of the wells, possible location of a water-bearing NNE-striking fracture in the basement and NW-striking dyke. Two distinctive heat anomalies are observed, one around the two warm springs and another one around the warm spring at the river (taken from Flóvenz, 1984)*

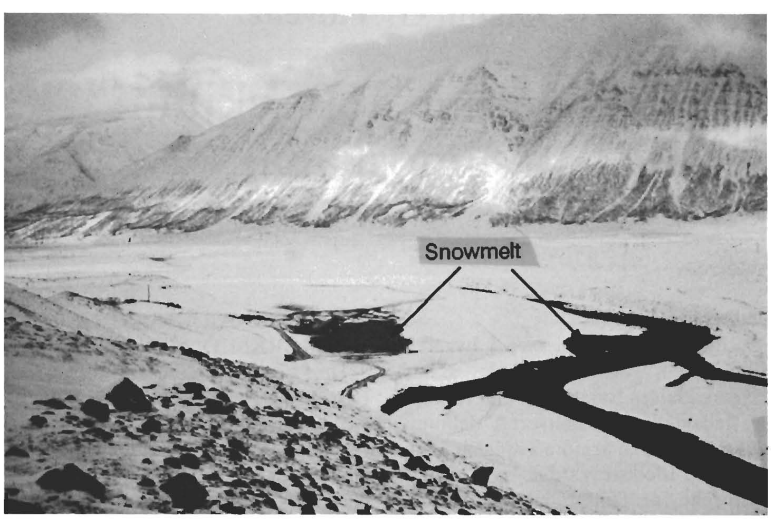

FIGURE 3.12: *Snowmelt in the thermal area at Reykir in Fnjóskadalur, NE-Iceland. The two distinctive heat anomalies in Figure 3.11 coincide with the snowmelt, indicated with the arrows (modified from Flóvenz, 1984)*

- Drilling fluid cools the surrounding rock
- Drilling can connect previously unconnected fluid zones in a well and cause upflow or downflow
- Drilling fluid can flow into permeable zones
- Flow from an aquifer into the well

A hole is usually less disturbed near the bottom than elsewhere. Measurements in temperature gradient wells are made with a resistivity thermometer (thermistor) every 2-5 m along the well with an accuracy of about 0.01°C or only 0.1°C where high anomalies are present like in geothermal areas. Figure 3.14 and Figure 3.15 show the thermal gradient of the Reykjavík low-temperature fields and the temperature at 1000 m depth in Iceland, respectively.

- **Heat flow surveys** can provide information on the areal extent of a geothermal field and the total flow of heat from an area. The conductive heat flow is calculated by multiplying the thermal gradient measured in drillholes and the thermal conductivity measured in rock samples in the laboratory (see Figure 3.16). Topographic corrections may have to be made. Structural complexity and variation in the thermal conductivity make the exact evaluation of the total heat output difficult.

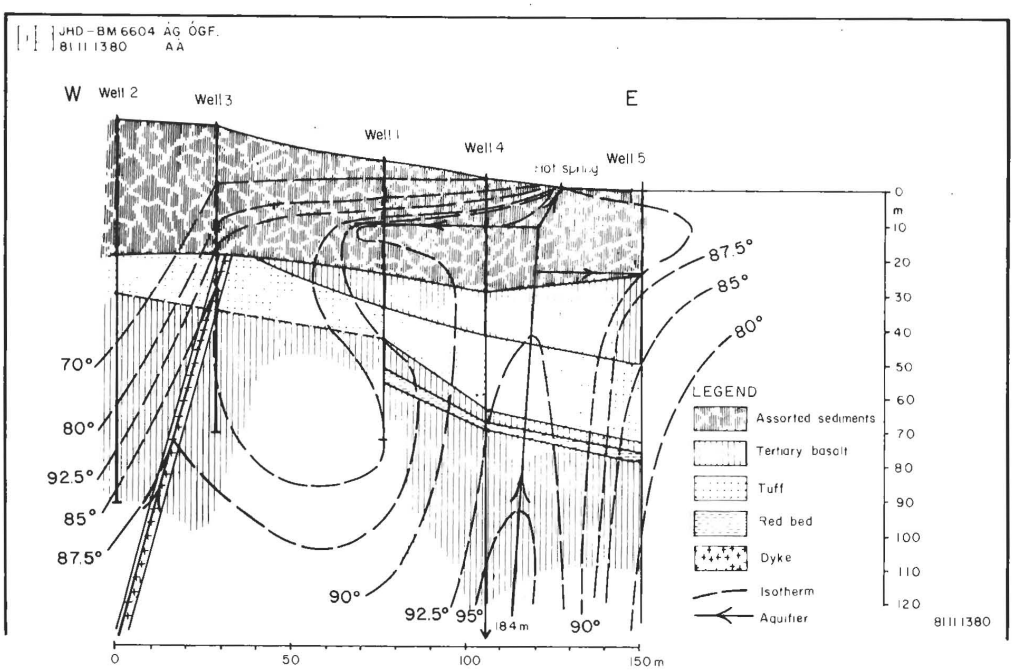

FIGURE 3.13: *A simplified geological cross-section through the wells at Reykir in Fnjóskadalur, NE-Iceland and the location of the main aquifers as calculated from the temperature distribution. The location of the cross-section is shown in Figure 3.11 (taken from Flóvenz, 1984)*

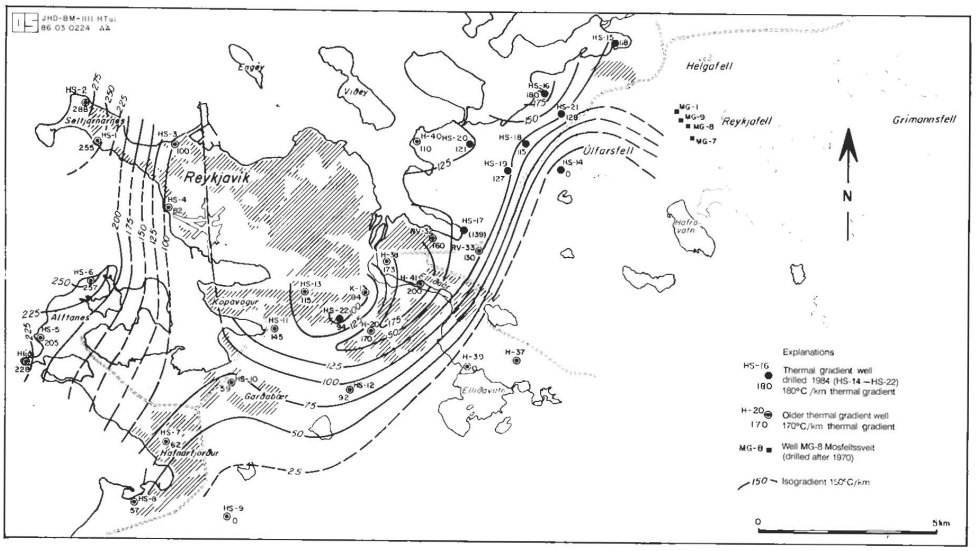

FIGURE 3.14: *Thermal gradient map of the Reykjavík low-temperature fields, SW-Iceland (taken from Tulinius et al., 1986)*

3.6 Model calculations in a conductive environment

If good temperature data is available and a good working model of the reservoir and the upflow zones exists, then much more sophisticated model calculations can be used to study the geothermal system. Interpretation of conduction data can proceed in ways similar to the interpretation of other potential-field data such as gravity, magnetics and groundwater flow.

The time-independent diffusion equation can be solved by using the Galerkin finite element method (Kjaran, 1977). A computer program based on this method is used to find the temperature distribution in the ground around a defined aquifer which cools by conduction. The boundary conditions are the known temperatures at the surface and in the aquifer, and consequently the gradient.

After the temperature has been calculated in sufficient points in a net of triangles, the isolines are drawn. The results of the model calculations are compared with measured data of surface temperature gradients or temperature profiles from drillholes. If better agreement is required, the parameters of the model are changed and a new model calculated (trial and error method).

As an example, we investigate in Figure 3.17 a lateral flow along a dipping aquifer (fissure, fault or dyke). The surface temperature T_0 = 10°C; g = 70°C/km is the normal undisturbed temperature gradient in the area. The aquifer extends from depth and is terminated at 100 m depth beneath overburden, dipping 20° from vertical. The temperature of the aquifer is 60°C at 100 m depth increasing linearly to 80°C at 1000 m depth (the regional temperature).

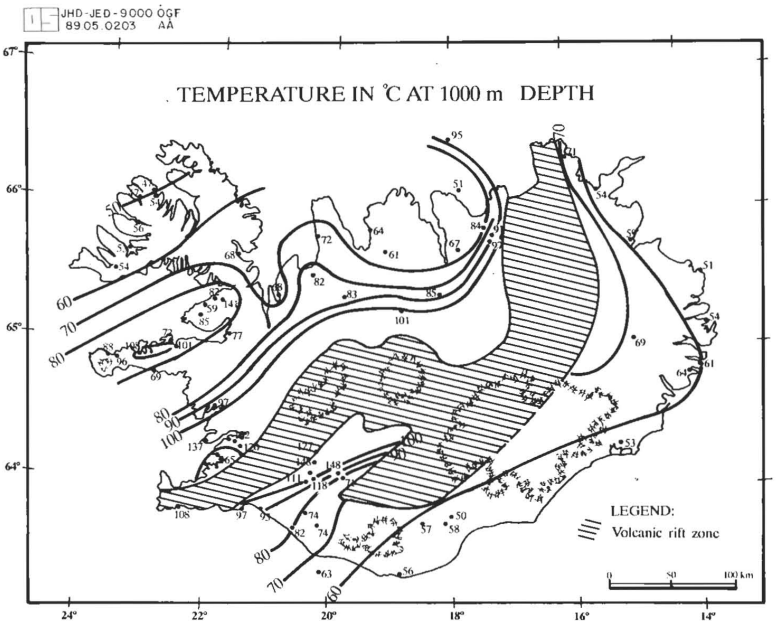

FIGURE 3.15: *Temperature in °C at 1000 m depth in Iceland (taken from Flóvenz and Sæmundsson, 1991)*

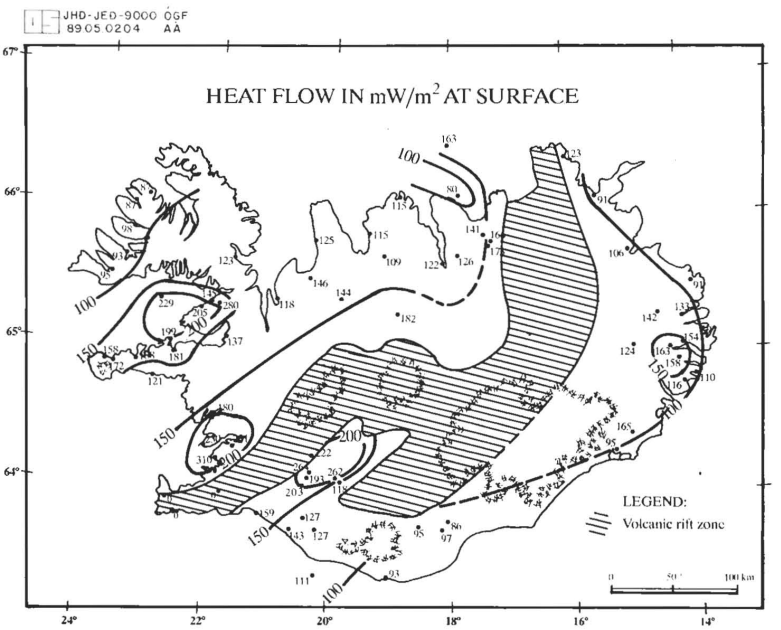

FIGURE 3.16: *Heat flow at surface in Iceland (taken from Flóvenz and Sæmundsson, 1991)*

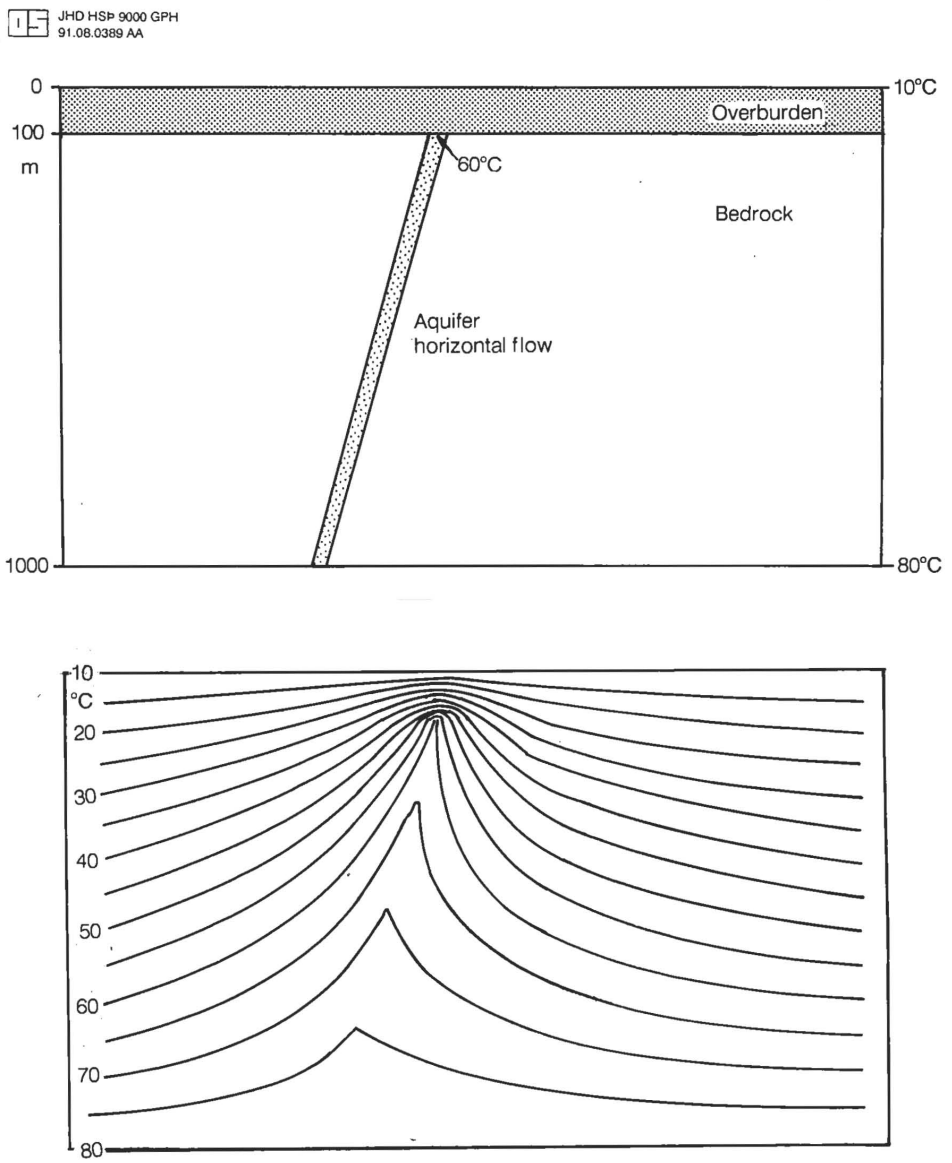

FIGURE 3.17: *Calculated temperature for a dipping-aquifer model*

4. ELECTRICAL RESISTIVITY OF ROCKS - ELECTRICAL METHODS

4.1 Introduction

Measuring the electrical resistivity of the subsurface is the most powerful prospecting method in geothermal exploration. Resistivity is directly related to the properties of interest, like salinity, temperature, alteration and porosity (permeability). To a great extent, these parameters characterize the reservoir.

The specific resistivity, ρ, is defined through **Ohm's law**. The electrical field strength, **E** [V/m] at a point in a material is proportional to the current density, **j** [A/m^2]:

$$\mathbf{E} = \rho \mathbf{j} \tag{4.1}$$

The proportional constant, ρ depends on the material and is called the (specific) resistivity, measured in Ωm. The reciprocal of resistivity is conductivity ($1/\rho = \sigma$).

Resistivity can also be defined as the ratio of the potential difference, ΔV [V/m], to the current, **I** [A], across material which has a cross-sectional area of 1 m^2 and is 1 m long.

$$\rho = \frac{\Delta V}{\mathbf{I}} \tag{4.2}$$

Electrical conductivity in minerals and solutions takes place by the movement of electrons and ions. Most rocks near the earth's surface have low conductivity. Conduction of electricity is mostly through groundwater contained in the pores of the rocks and along surface layers at the contact of rocks and solution.

The common principle of all resistivity sounding methods is to induce an electrical current in the earth and monitor signals, normally at the surface, generated by the current distribution. In conventional direct current soundings such as the Schlumberger soundings, this is done by injecting current into the ground through electrodes at the surface and the signal measured is the electric field (the potential difference over a short distance) generated at the surface. In magnetotellurics (MT) the current in the ground is induced by time variations in the earth's magnetic field, and the signal measured is the electric field at the surface. In transient electromagnetics (TEM) the current is also induced by a time-varying magnetic field, but in this case the current source is not the natural field, the source is of a controlled magnitude generated by a loop or a grounded dipole and the monitored signal is the decaying magnetic field at the surface.

4.2 Conduction in solutions

In aqueous salt-solution the ions of the solid separate and are free to move independently in the solution. In an electric field cations are accelerated to the negative electrode and the anions to the positive one. A viscous drag force limits the velocity of the ions. The **mobility** (terminal velocity/electrical field) of the ions depends on temperature (viscosity) and on concentration.

The conductivity of a solution, σ, may be determined by considering the current flow through

a cross-sectional area of 1 m^2 at a voltage gradient of 1 V/m. It follows that:

$$\sigma = 1/\rho = F \cdot (c_1 q_1 m_1 + c_2 q_2 m_2 + \ldots), \tag{4.3}$$

where:

F - Faraday's number (96,500 coulombs)
c_i - concentration of ions
q_i - valence of ions
m_i - mobility of different ions

Resistivity of water as a function of salinity: Groundwater may have a variety of salts in the solution. Therefore, it is not easy to compute resistivity of water from chemical analysis.

Equivalent salinity is defined as the salinity of a NaCl-solution with the same resistivity as the particular solution. Mobility of the ions does not vary widely. Therefore, equivalent salinity is close to true salinity. Using equivalent salinity, tables or graphs for a single salt only are needed to find how resistivity depends on salinity.

Figure 4.1 shows that salinity of electrolytes, such as NaCl in water, affects resistivity in a nearly inversely linear manner (Keller and Frischknecht, 1966). For T=0°C we have:

$$\rho = 9.545\ C^{-0.937} \approx \frac{10}{C}, \tag{4.4}$$

where C [g/l] is the concentration of NaCl (see Figure 4.1).

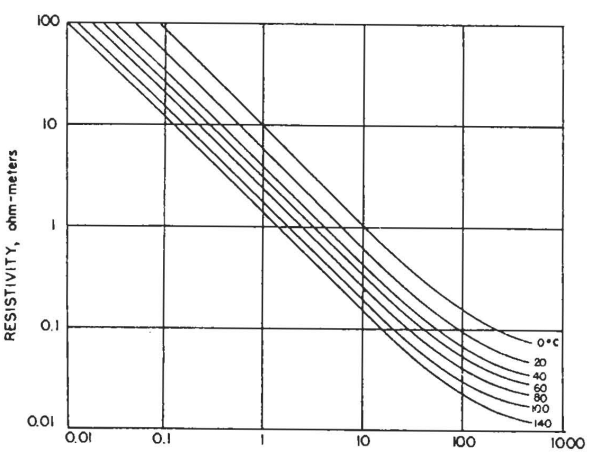

FIGURE 4.1: *Resistivity of solutions of sodium chloride as a function of concentration and temperature (taken from Keller and Frischknecht, 1966)*

Resistivity of water as a function of temperature: At moderate temperatures, 0-200°C, the resistivity of aqueous solutions decreases with increasing temperature (see Figure 4.1). The reason is increasing mobility of the ions caused by a decrease in the viscosity of the water. Dakhnov (1962) has described this relationship:

$$\rho_w = \frac{\rho_{w_0}}{1+\alpha(T-T_0)}, \tag{4.5}$$

where:

ρ_{w_0} - resistivity of the fluid at temperature T_0
α - temperature coefficient of resistivity, $\alpha \approx 0.023\ °C^{-1}$ for $T_0 = 23°C$, and $0.025\ °C^{-1}$ for $T_0 = 0°C$

At high temperatures, a decrease in the dielectric permittivity of the water results in a decrease in the number of dissociated ions in solution. Above 300°C, this starts to increase fluid resistivity (Quist and Marshall, 1968). See Figure 4.2.

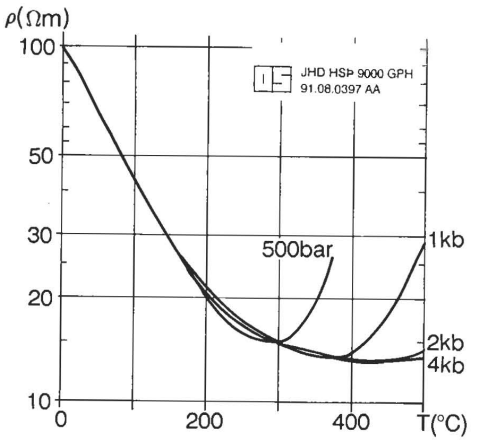

FIGURE 4.2: *Electrical resistivity as a function of temperature at different pressures (modified from Quist and Marshall, 1968)*

4.3 Electrical resistivity of water-bearing rocks

In most rocks near the earth's surface, the conduction is dominated by electrolytic conduction in aqueous solution of common salts distributed through the pores of the rock and/or at the rock-water interface. The rock matrix itself is an insulator. The electrical resistivity of rocks depends on:

- Porosity and the pore structure of the rock
- Amount of water (saturation)
- Salinity of the water
- Temperature
- Pressure
- Water-rock interaction and alteration
- Steam content in the water

The most important factors are the porosity, temperature, salinity and the water-rock interaction. In geothermal areas, the rocks are water-saturated. Ionic conduction in the saturating fluid depends on the number and mobility of ions and the connectivity of flowpaths through the rock matrix. Usually, the saturating fluid is among the dominant conductor in the rock and the degree of saturation is of great importance to the bulk resistivity. The pressure dependence is negligible compared to the temperature dependence, provided that the pressure is sufficiently high so that there is no change in phase.

Porosity is defined as the ratio between the pore volume and the total volume of a material. There are primarily three types of porosity.

Intergranular: The pores are formed as spaces between grains or particles in a compact material (sediments, volcanic ash)

Joints-fissures: A net of fine fractures caused by tension and cooling of the rock (igneous rocks, lava)

Vugular: Big and irregular pores, formed as material is dissolved and washed away, or pores formed by gas (volcanic rocks, limestone)

Pore spaces must be interconnected and filled with water in order that a rock may conduct electricity. In all types of porosity there are larger voids, called storage pores, and finer connecting pores. Most of the resistance to electric current flow (and fluid flow) is met in the connecting pores.

It has been observed for many cases that resistivity of water-saturated rocks varies approximately as the inverse square of the porosity (see Figure 4.3). This empirical relationship is called **Archie's law** (Archie, 1942). It describes how resistivity depends on porosity if ionic conduction in the pore fluid dominates other conduction mechanism in the rocks. It is valid if the resistivity of the pore fluid is of the order of 2 Ωm or less, but doubts are raised if the resistivity is much higher (Flóvenz et al., 1985).

$$\rho = \rho_w \, a \, \phi_t^{-n}, \tag{4.6}$$

where:

ρ - bulk (measured) resistivity
ρ_w - resistivity of the pore fluid
ϕ_t - porosity in proportions of total volume
a - an empirical parameter, varies from less than 1 for intergranular porosity to over 1 for joint porosity, usually around 1
n - cementing factor, an empirical parameter, varies from 1.2 for unconsolidated sediments to 3.5 for crystalline rocks, usually around 2

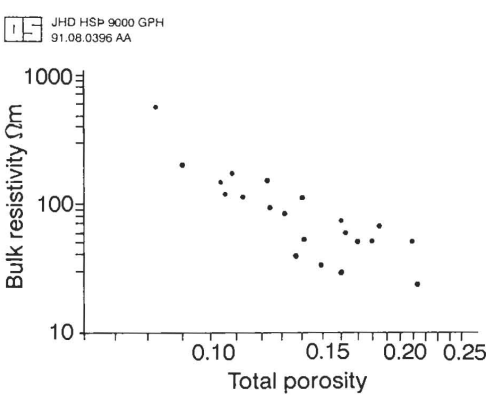

FIGURE 4.3: *Resistivity as a function of porosity at 500 m depth in Iceland. The data have been corrected for variable temperature and refer to the temperature,* T_0 = *23°C. Data from the volcanic rift zone and areas with saline groundwater are excluded (taken from Flóvenz et al., 1985)*

For a first approximation we can usually assume a = 1 and n = 2. According to Archie's law the ratio ρ/ρ_w is constant for a given porosity. This constant is called **formation factor** (F):

$$F = a\,\phi_t^{-n} = \rho/\rho_w \tag{4.7}$$

The relationship between permeability, k [m^2], in crystalline fractured rocks, on the one hand, and the geometric mean fracture width (d) and the mean distance between fractures (F) on the other hand, is presented by the following formula (Lamb, 1932):

$$k = \frac{d^3}{12 \cdot F} \tag{4.8}$$

The bigger the mean fracture width of the pores is, the bigger is the fracture porosity. Therefore, in most cases, high fracture porosity is followed by high permeability.

This close relationship between porosity and, hence, electrical resistivity, on the one hand and permeability on the other hand, has great importance in electrical exploration of potential geothermal areas. That is, for intergranular porosity, high permeability may accompany low resistivity. Typical resistivity values of different rock types are shown in Tables 4.1 and 4.2.

Low resistivity → high permeability → economically exploitable aquifer

Water-rock interaction: Experiments show that Archie's law is only valid for conductive solutions $\rho_w \leq 2\ \Omega m$. The bulk resistivity is decreased by surface conduction along the interface between rock and water. This can be expressed in a formula (Rink and Schopper, 1976):

$$\sigma = (1/F) \cdot \sigma_w + \sigma_s, \tag{4.9}$$

where F is the formation factor. The interface conductivity, σ_s, is caused by fluid-matrix interaction. Experiments show that interface conductivity depends more on the magnitude of the internal surface (porosity) and on its nature (surface conditions) than on the original chemical composition of water and rock. The two main reasons for interface conductivity are the presence of clay minerals (alteration) and surface double-layer conduction.

Since Equation 4.6 only applies for relatively low resistivity values of the pore fluid, several relationships have been developed where interface conduction dominates both matrix and ionic conduction. Flóvenz et al. (1985) established the following equation relating the bulk resistivity ρ, to the fracture porosity ϕ_f, the temperature T and the pore fluid resistivity ρ_{w_0}, at T_0 = 23°C. This equation (an extension of Equation 4.9) has been found applicable for the uppermost 1 kilometer of the Icelandic basaltic crust for temperatures of up to at least 100 °C.

$$\frac{1}{\rho} = \frac{0.22}{\rho_w}\left[1 - (1 - \phi_f)^{2/3} + \frac{(1 - \phi_f)^{2/3}}{1 + (1 - \phi_f)^{1/3} + (1 - \phi_f)^{1/3}\ 4.9 \cdot 10^{-3}}\right] + \frac{\phi_f^{1.06}}{b} \tag{4.10}$$

where:

$$\rho_w = \rho_{w_0}/[1 + 0.023(T - 23)] \quad \text{and} \quad b = 8.7/[1 + 0.023(T - 23)][1 + 0.018(T - 23)]$$

Equation 4.10 is an extension of a double-porosity model put forward by Stefánsson et al. (1982).

TABLE 4.1: *Typical resistivity of Icelandic rocks (taken from Björnsson, 1980)*

Formation	Resistivity [Ωm]
Recent lava flows, above groundwater table	5,000-50,000
Dense intrusives (gabbro, dolerite)	10,000-15,000
Recent lava flows, below groundwater table	100-3,000
Basalts, rather dense	100-300
Palagonite	20-100
Low-temperature areas in basalt formations	30-100
Low-temperature areas in hyaloclastite formations	10-50
Rocks with brine	5-15
High-temperature areas, fresh water	1-5
High-temperature areas, brine areas	1-4

TABLE 4.2: *Typical resistivity of several rock types*

Rock type	Resistivity [Ωm]
Granite, Ultrabasic, Peridotite	1,000-3,000
Marble	400-1,000
Limestone	200-500
Schist	200-300
Limestone, karstified	15-400
Gneiss	30-150
Sediments (depend on sand content)	10-100
Flyss with clay	low
Flyss with sand	high
Surface material with clay	low
Surface material with sand	high

In Icelandic high-temperature geothermal areas, the interface conductivity is caused by alteration of the rock matrix. The type of alteration minerals formed depends upon the temperature and the chemical composition of the fresh rocks and saturating fluid. Results from Nesjavellir, a high-temperature geothermal field in SW-Iceland, show the following correlation between temperature, alteration and resistivity (Árnason et al., 1986 and 1987; Árnason and Hersir, 1991). At temperatures below 200°C clay is the dominant mineral, but chlorite and epidote predominate above 250°C. Between 200°C and 250°C there is a transition, called mixed-layer. Clay minerals are good conductors and can dominate the conductivity of the saturated rock. On the other hand, chlorite and epidote are resistive minerals.

In the center of high-temperature geothermal areas in Iceland, it is common to have high-resistivity below low-resistivity. In the Hengill high-temperature geothermal area, which Nesjavellir is a part of, change in alteration minerals from the more conductive clay minerals to the more resistive, chlorite and epidote, is believed to be the reason for higher resistivity below the low-resistivity layer (Hersir et al., 1990; Árnason and Hersir, 1991). Four additional possible explanations have been given for this phenomena in Icelandic high-temperature geothermal areas. Therefore, we have a total of five:

- Change in rock composition, in particular due to dense and fresh intrusions
- Temperature decreases with depth, mostly because of lateral flow of high temperature water at shallow depth
- High temperature, above 300°C without boiling (remember Figure 4.2)
- Change in alteration minerals, conductive clay minerals - resistive chlorite and epidote
- Boiling, steam-phase is more resistive than water-phase

4.4 Electrical exploration methods - An overview

An electrical method is either *a sounding method* or *a profiling method*, depending on what kind of a resistivity structure is being investigated. The sounding method is used for mapping resistivity as a function of depth. The profiling method maps resistivity at more or less constant depth and is used to map lateral resistivity changes.

Electrical methods can be divided into the following categories and subcategories:

- **DC-methods (direct current methods):** A constant current **I** (independent of time) is introduced into the ground through a pair of electrodes at the surface of the earth. The current creates a potential field in the earth. By measuring the electric field **E** (potential difference over a short interval), the subsurface resistivity can be inferred.
  - Schlumberger soundings
  - Head-on profiling
  - Dipole soundings and profiling
- **EM-methods (electromagnetics, AC-methods):** Alternating current (AC) at various fixed frequencies or a current varying with time in a controlled way is used instead of DC-current. Many different configurations of transmitters and receivers are used. Direct contact with the ground or induction coupling characterize these methods.
  - Magnetotellurics (MT) and audio-magnetotellurics (AMT). The fluctuations in the natural magnetic field of the earth **B** and the induced electric field **E** are measured. Their ratio is used to determine the apparent resistivity
  - Time domain or transient electromagnetics (TEM). A magnetic field is built up by transmitting a constant current into a loop or grounded dipole, the current is turned off and the transient decay of the magnetic field is measured. It is used to determine the apparent resistivity
- **Self-Potential (SP):** Measurement of the natural DC-voltages in the ground. This method does not measure electrical resistivity.

5. DC-RESISTIVITY METHODS

5.1 Introduction

A current **I** is introduced at the surface of a homogeneous half space (earth) with resistivity ρ. The potential V(r), observed at distance r from the current source, is given by the expression:

$$V(r) = \frac{I\rho}{2\pi r} \tag{5.1}$$

If a current is introduced by two electrodes +I at r_1 and -I at r_2, then we have:

$$V(r) = \frac{I\rho}{2\pi}(1/r_1 - 1/r_2); \quad \rho = K \cdot \frac{V}{I}; \quad K = \text{geometrical factor} \tag{5.2}$$

If the earth is not homogeneous, an apparent resistivity, ρ_a is defined as the calculated resistivity from V, I, r_1, and r_2 as if the earth was homogeneous.

Using this formula, it is possible to measure resistivity for homogeneous ground and apparent resistivity for inhomogeneous ground. When current I is introduced by two electrodes at A and B, then the potential difference ΔV measured between two electrodes M and N is given by:

$$\Delta V = V_M - V_N = (I\rho/2\pi)((1/AM - 1/BM) - (1/AN - 1/BN)) \tag{5.3}$$

Consequently:

$$\rho_a = K \cdot \frac{\Delta V}{I}; \quad K = \text{geometrical factor} \tag{5.4}$$

DC-methods can be divided into various subcategories depending on the arrangement of electrodes. The most common ones used in geothermal exploration in Iceland are:

- Schlumberger soundings
- Head-on profiling
- Dipole soundings and profiling

Two types of resistivity measurements can be distinguished:

Geoelectric sounding: Measurements are made at a specified fixed center point for different distances between the electrodes. It is used to sound or measure changes in resistivity with depth at a fixed place.

Geoelectric profiling: The same electrode arrangement with fixed distances is used and measurements are made at various points on the surface, usually along a profile. Geoelectric profiling is mainly used to find lateral changes in resistivity and to locate vertical structures.

Field procedure - Instrumentation: Instruments for DC-resistivity measurements typically consist of a transmitter with an output of about 100-500 W and a maximum voltage of some 1,000 V and a receiver which is basically a voltmeter. The voltmeter must have an input impedance of the order of 10^6 Ω and sensitivity to the order of 1 μV, and SP voltages are

balanced out. A regulated square wave with pulse length of 4, 8 or 16 seconds is transmitted to the earth. The current electrodes are usually iron or aluminum rods. The most common potential electrodes are of the $CuSO_4$ nonpolarizing type. An inductive potential adds to the square wave potential (galvanic potential) when the current changes sign and fades out with time (see Figure 5.1). Therefore, the potential is measured some time after the current changes sign. Usually, several readings are made and stacked in a processor in order to calculate averages and the standard variation of the measurements.

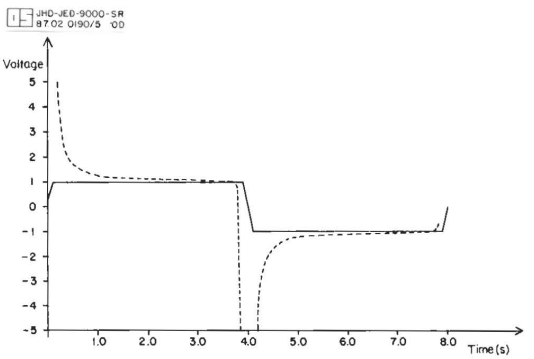

FIGURE 5.1: *Inductive electromagnetic coupling in DC-soundings. The continuous curve shows the galvanic potential and the dashed curve shows the inductive plus the galvanic potential. The signal's pulse length is 8 seconds. This example is calculated for a homogeneous earth of resistivity 1 Ωm and there are 2,000 m between the current electrodes (taken from Árnason, unpublished manuscript)*

5.2 The Schlumberger sounding method

In the Schlumberger array two potential and two current electrodes are placed along a straight line. The array is symmetrical around midpoint O. The setup is shown in Figure 5.2, where the current electrodes are placed at A and B and the potential electrodes are placed at M and N. The distances are given as, AO = OB = S and MO = ON = P.

A current I is injected into the earth through A, and the circuit is closed at B. The resulting potential difference between M and N, ΔV, is measured. The measured values I and ΔV together with S and P are used to calculate the apparent resistivity, ρ_a according to the formula (compare it with Equations 5.3 and 5.4):

$$\rho_a = \frac{\pi}{2} \frac{S^2 - P^2}{P} \frac{\Delta V}{I} \tag{5.5}$$

The depth of penetration of the current increases with increasing electrode separation (AB). Information on resistivity at greater depths is obtained by increasing the distance between the current electrodes stepwise while keeping the distance between the potential electrodes fixed.

The apparent resistivity is plotted on double-logarithmic paper as a function of increasing AB/2 = S (see Figure 5.3). As S increases, the potential difference ΔV becomes lower. At a certain stage ΔV gets close to the detection limit and it is necessary to enlarge P in order to increase ΔV. Because of this, the resulting curve is composed of segments, one for each different P value (see Figure 5.7). It frequently happens that the segments are shifted relative to each other. Measurements are usually made for S from a few meters and up to 1,500 - 3,000 m. The values of S are usually evenly distributed on a logarithmic scale, most frequently with 10 points per decade. There should be at least three overlapping points for successive P

segments. The apparent resistivity curve is interpreted into the resistivity distribution of the earth. This is either done one-dimensionally, where the resistivity is a function of depth only (layered earth), or two-dimensionally where the resistivity also varies along one horizontal direction.

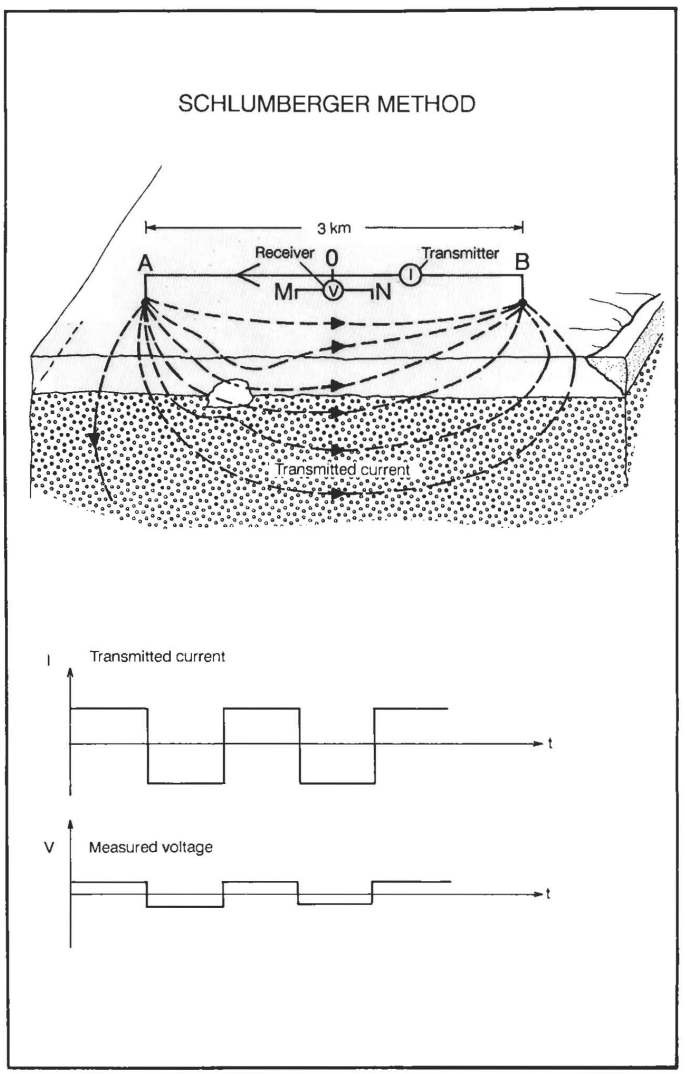

One-dimensional interpretation of Schlumberger soundings (resistivity varies only with depth) was made in the early days with the help of master curves of the apparent resistivity (Orellana and Mooney, 1966). Nowadays, use is made of non-linear least-squares programs for the inversion of Schlumberger soundings. At the UNU Geothermal Training Programme in Iceland, such a program (called SLINV, SchLumberger INVersion) has been implemented on a PC-computer (Árnason and Hersir, 1988a). The program automatically adjusts the layer parameters in order to fit a calculated curve to the measured apparent resistivity curve (see Figure 5.3). SLINV assumes that the distance between the potential electrodes is infinitesimal compared to the distance between the current electrodes (gradient approach), and that the potential changes linearly between the potential electrodes.

FIGURE 5.2: *Schlumberger sounding configuration*

The depth of penetration of Schlumberger soundings is not only a function of the distance

between the current electrodes, 2S. It is actually a function of the shortest distance between the current electrode and the potential electrode, S-P (see Figure 5.4) (Árnason, 1984). For the same S and different P, different values of ρ_a reflect different resistivity at different depths (see Figure 5.5). For instance, if the difference (S-P) in a two-layer case is of the same order of magnitude or less than the depth to the layer boundary, the measured ρ_a value will be dominated by the resistivity of the first layer, ρ_1, independent of the distance between the current electrodes (see Figure 5.4).

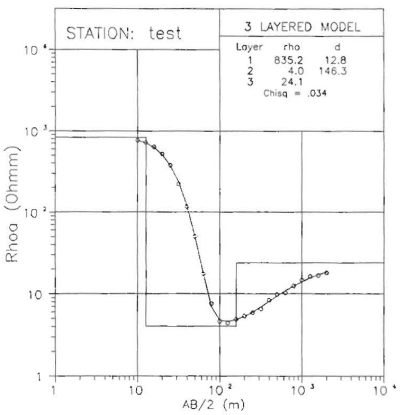

FIGURE 5.3: *One-dimensional interpretation of a Schlumberger sounding using the SLINV program (taken from Árnason and Hersir, 1988a)*

The usual procedure in carrying out a Schlumberger sounding is to keep P as small as possible. As S increases, ΔV decreases, and it becomes necessary to enlarge P. The changes of S and P are reflected in the ρ_a-curve which is composed of shifted segments (see Figure 5.5). These shifts are convergent, because the larger (S-P) becomes, the more the apparent resistivity values, measured with the same S, approach that of the gradient approximation (Árnason, 1984).

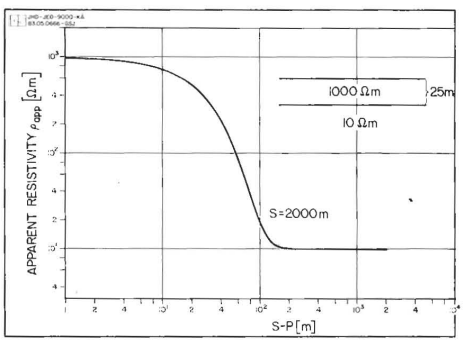

FIGURE 5.4: *Apparent resistivity as a function of S-P for a two-layered model. S-P is the shortest distance between a current and a potential electrode (taken from Árnason, 1984)*

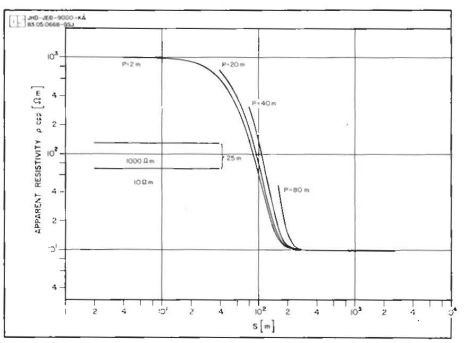

FIGURE 5.5: *Converging shifts in the apparent resistivity curve for a two-layered model (same model as in Figure 5.4) (taken from Árnason, unpublished data)*

In Schlumberger soundings, it is necessary to know the exact amount of both the current injected into the earth and the associated induced potential. Besides the associated potential field, there are always present spurious potential sources such as induced polarization, spontaneous polarization, telluric currents, induction and all kinds of conductors acting as shortcuts (e.g. the sea, if the sounding is close enough to the coast). It is possible to correct for the influence of the sea on the measured ρ_a-curve (Hersir, 1988). Some of these spurious potentials or "noise" can be handled through statistical means by taking many measurement values of ΔV and I, and calculating their mean-values and statistical deviations. Under more difficult conditions, it is possible to obtain a weighted mean-value from all the mean-values where the weighting is determined by the standard deviation in each case. Doing this the random error will be, to at least some extent, averaged out.

There is another kind of effect that affects the shape of the apparent resistivity curve and keeps it different from a "well behaved one", which can easily be treated by one-dimensional interpretation. Two-dimensional resistivity distribution at the site or close to the potential electrodes can provoke a constant shift in the apparent resistivity curve. It can easily lead the interpretation astray (Árnason, 1984). An example is given in Figure 5.6. The way to handle these shifts, is to fix the segment of the curve measured with the largest P used in the sounding, and correct the others by a factor (multiplication coefficient) that forces the segments to tie in. This is done by assuming that the segment of the apparent resistivity curve measured with the largest P has the least local influence. This effect caused by resistivity inhomogeneities can also be compensated for in two-dimensional interpretation.

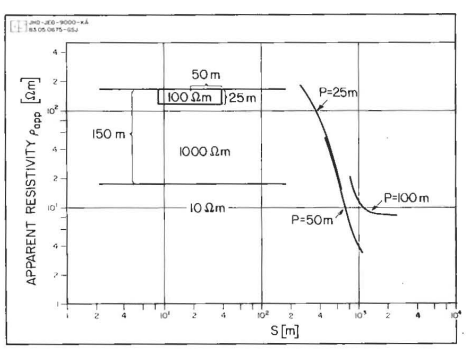

FIGURE 5.6: *Shifts in the apparent resistivity curve due to inhomogeneity at the center of the array (taken from Árnason, 1984)*

Prior to the automatic process in the SLINV program, the shifts (constant and convergent) are handled by a manual procedure. At the National Energy Authority of Iceland, Geothermal Division, a least-squares one-dimensional inversion program (ELLIPSE) for DC-soundings, which automatically corrects for constant shifts, has been developed (Árnason, 1984). It simulates the actual electrode configuration used (instead of using the gradient approach) and computes the apparent resistivity from the potential difference. It optimizes the parameters defining the one-dimensional resistivity model, and multiplication coefficients, for all segments except the one measured with the largest potential electrode spacing. By this method, each shift is resolved into converging and nonconverging parts. Each segment is corrected for the constant part of the shift so that they, except for converging shifts, tie in with the segment measured with the largest potential electrode spacing. By simulating the actual position of the electrodes, ELLIPSE is able to extract the information contained in convergent type shifts, which are due to a finite potential electrode separation and strong resistivity contrasts between layers (see Figure 5.7).

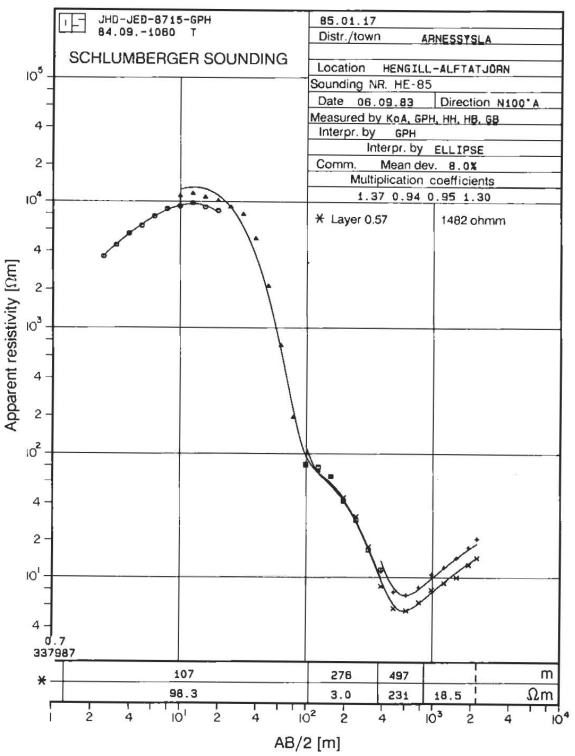

FIGURE 5.7: *One-dimensional interpretation of a Schlumberger sounding from the Hengill high-temperature geothermal area, SW-Iceland, using the ELLIPSE program. The curve shows both converging and constant shifts (notice the multiplication coefficients). The resistive layer (second layer) is an equivalent layer (bell type curve) and the conductive layer (fourth layer) is also an equivalent layer (bowl type curve). Due to additional geological and geophysical information, the resistivity of the conductive layer was fixed at 3 Ωm (taken from Hersir et al., 1990a)*

Errors arise, when topographic and/or two-dimensional effects, are erroneously treated as being caused by a one-dimensional resistivity distribution.

Besides this, there still remains an uncertainty inherent in the method, called equivalence. There are two types of equivalences. In both cases, there is a layer whose thickness and resistivity is undetermined. For both cases, the depth to this layer's interface must be the same or less than the thickness of this undetermined layer, (see e.g. Koefoed, 1979). An example is given in Figure 5.7. The first one is a bell type curve, i.e. a resistive layer which is embedded between two conductive layers. In this case, the only known parameter for the intermediate layer is the transversal resistance, given by the product, $\rho_i\, d_i = T$. The second one is a bowl type curve, i.e. a conductive layer which is embedded between two resistive layers. In this case, the only known parameter for the intermediate layer is the longitudinal conductance, given by the quotient $d_i/\rho_i = S_L$. In the presence of equivalence layers in one-dimensional interpretation, it is advisable to add some independent information from other investigations. If they are not available, correlations can be made utilizing other soundings in the neighborhood.

Examples of the application of Schlumberger soundings, based on one-dimensional interpretation, are shown in Figures 5.8-5.10.

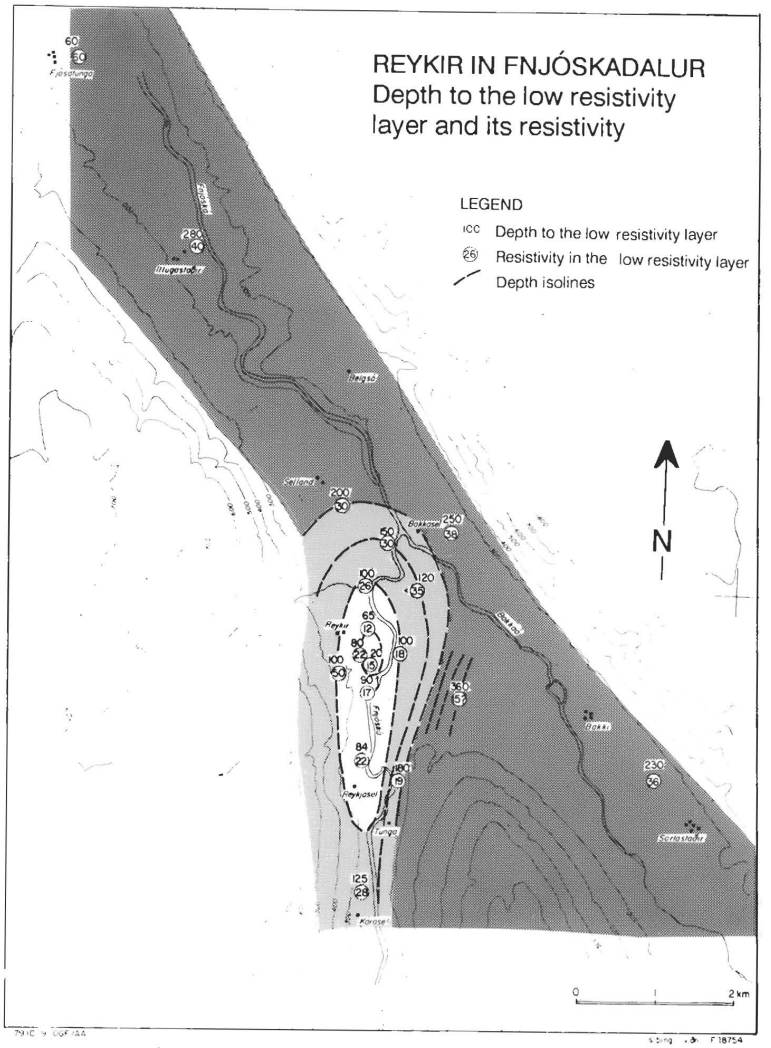

FIGURE 5.8: *A resistivity map of Reykir in Fnjóskadalur, NE-Iceland and the surrounding area based on Schlumberger soundings. The map shows the depth iso-lines down to the top of the low resistivity layer and the numbers within the circles show the values of resistivity. The resistivity surveys indicate very low resistivity in the bedrock below the hot spring area, indicating high porosity (compare the figure with Figure 3.11 and remember to let the N-arrow point in the same direction on both figures). The low-resistivity forms an elongated body along the NNE-striking fault and dyke zone as shown in Figure 3.11 (taken from Flóvenz, 1984)*

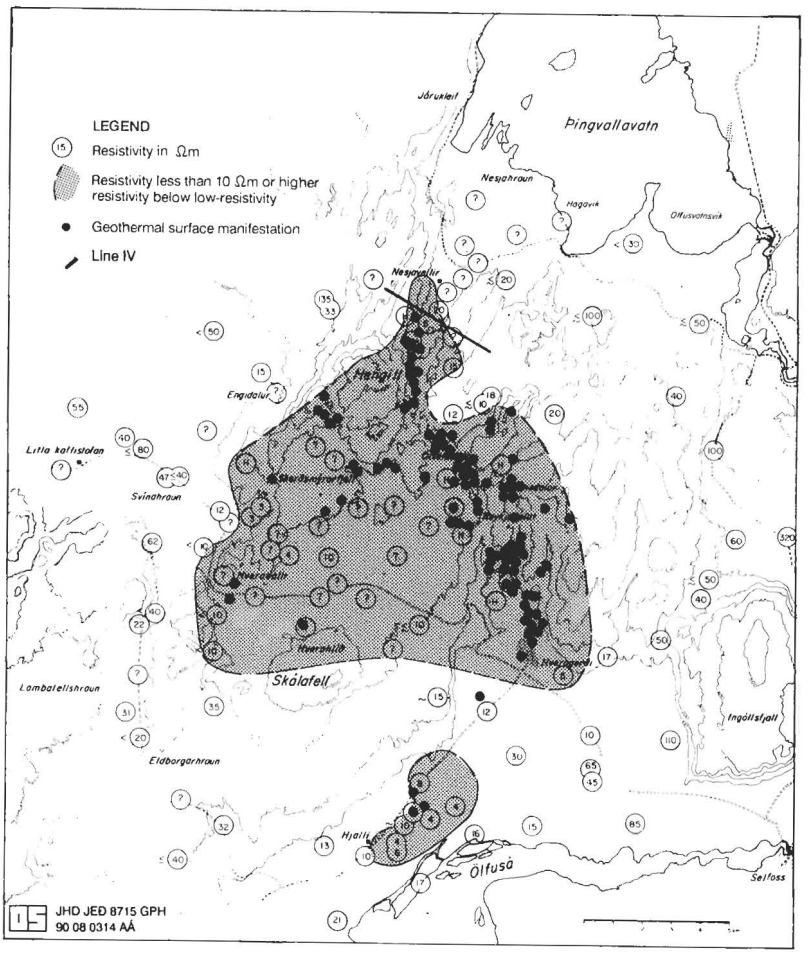

FIGURE 5.9: *Resistivity of the high-temperature geothermal area Hengill, SW-Iceland at 400 m below sea-level. The map is based on one-dimensional interpretation of Schlumberger soundings and shows the geothermal surface manifestations as well. A resistivity low, covering 110* km^2*, roughly indicates the extent of the high-temperature fields at this depth. All surface fumarole activity and altered grounds are within this area. The low-resistivity is associated with water-saturated rock formations with smectite-zeolite alteration (temperature is or has been 50-200°C). Within the hydrothermal systems, higher resistivity is observed below the low-resistivity body. The higher resistivity could be associated with a higher degree of alteration, the chlorite-epidote alteration zone (temperature is or has exceeded 200°C) (taken from Hersir et al., 1990; Björnsson et al., 1986)*

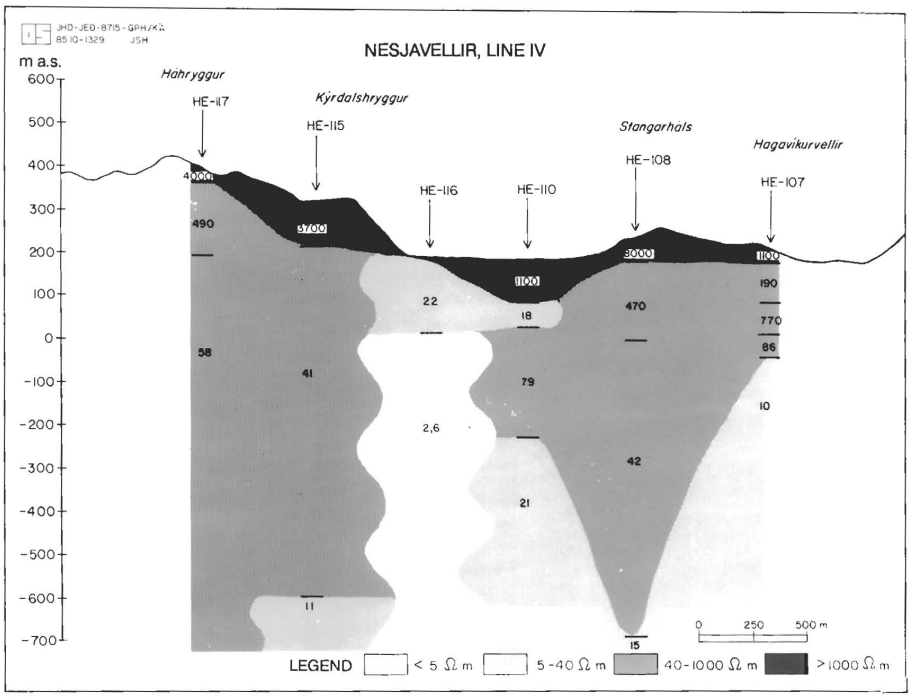

FIGURE 5.10: *One-dimensional interpretation of Schlumberger soundings from Nesjavellir, using the ELLIPSE program. The location of the cross-section is shown in Figure 5.9 and Figure 9.2. The section is based on six soundings; each one is marked with HE. A low-resistivity anomaly is observed (taken from Árnason et al., 1985)*

At the National Energy Authority of Iceland, Geothermal Division, there exists a program for two-dimensional interpretation of DC-soundings (FELIX). The program makes use of the finite element method to evaluate the potential distribution in a two-dimensional resistivity distribution composed of triangular and rectangular resistivity blocks with infinite extension in the third dimension. The surface can be made irregular in order to model the topography. Sometimes Schlumberger soundings are interpreted jointly with head-on profiling data (this method is discussed in the next chapter). This gives a far better resolution in places where strong lateral resistivity contrasts are found. An example of application is given in Figures 5.11-5.12.

Schlumberger soundings: Measurement and interpretation can be divided into:

- Measurement of the transmitted current **I**, and the observed potential difference ΔV for increasing S and P
- Calculation of ρ_a as a function of S and P, plotting
- One-dimensional interpretation, comparison with other soundings and other results, both geophysical and geological
- Two-dimensional interpretation taking the topography into account, comparison with other results
- Geological interpretation, geothermal model of the area

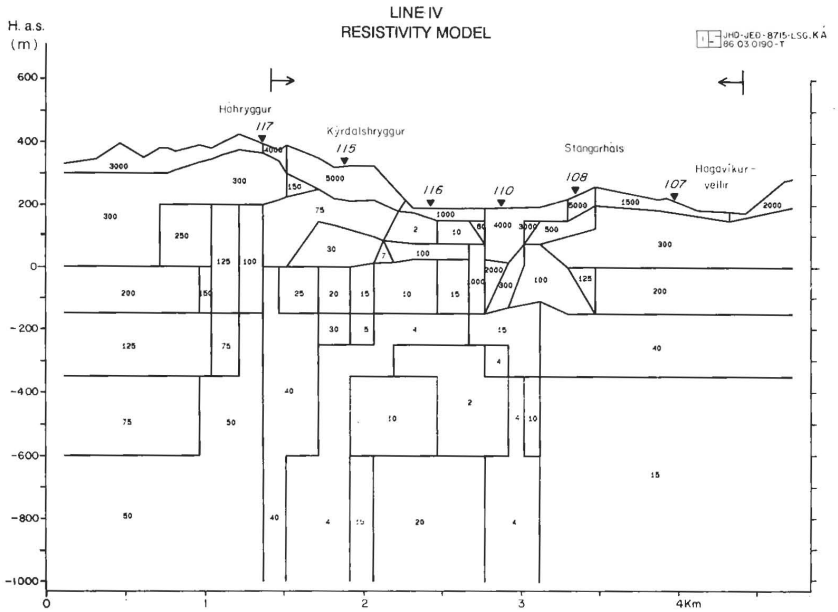

FIGURE 5.11: *Two-dimensional interpretation of resistivity data from Nesjavellir using the FELIX program (same profile as in Figure 5.10). The final model is based on six Schlumberger soundings (shown as triangles) and head-on profiles (lying between the two vertical lines and horizontal arrows). Figures in the blocks denote resistivity in* Ωm *(Árnason et al., 1986)*

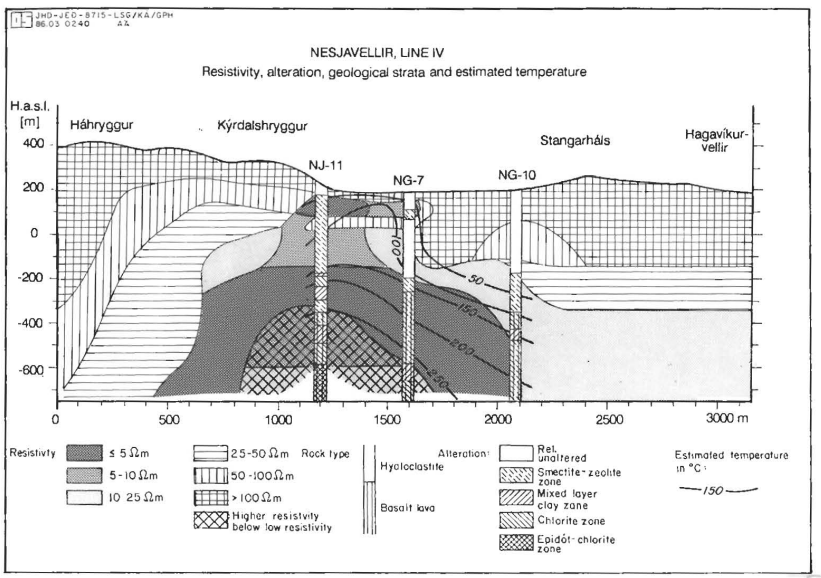

FIGURE 5.12: *Two-dimensional interpretation of resistivity data from Nesjavellir, simplified from Figure 5.11; resistivity, temperature and alteration. A close correlation is found between resistivity, temperature and alteration. Very low resistivity (≤ 5* Ωm*) corresponds to temperature above 100°C and rock formations with smectite-zeolite alteration. Higher resistivity below the low resistivity corresponds to temperature above 250°C and the chlorite-epidote alteration zone (Árnason et al., 1986; Árnason and Hersir, 1991)*

5.3 Head-on profiling

The Schlumberger sounding method cannot detect narrow vertical or near-vertical resistivity structures such as faults, dykes or fractures. Geothermal fluid is often associated with these kinds of structures. Instead, the head-on profiling method has been used successfully for locating these structures. The head-on arrangement is similar to the Schlumberger array (see Figure 5.2) but has an extra current electrode, C, located at a great distance from A and B.

A current I is injected into the earth in three different cases, closing the circuits AC, BC and AB, and the resulting potential difference ΔV between M and N is measured each time. Three resistivity values are calculated:

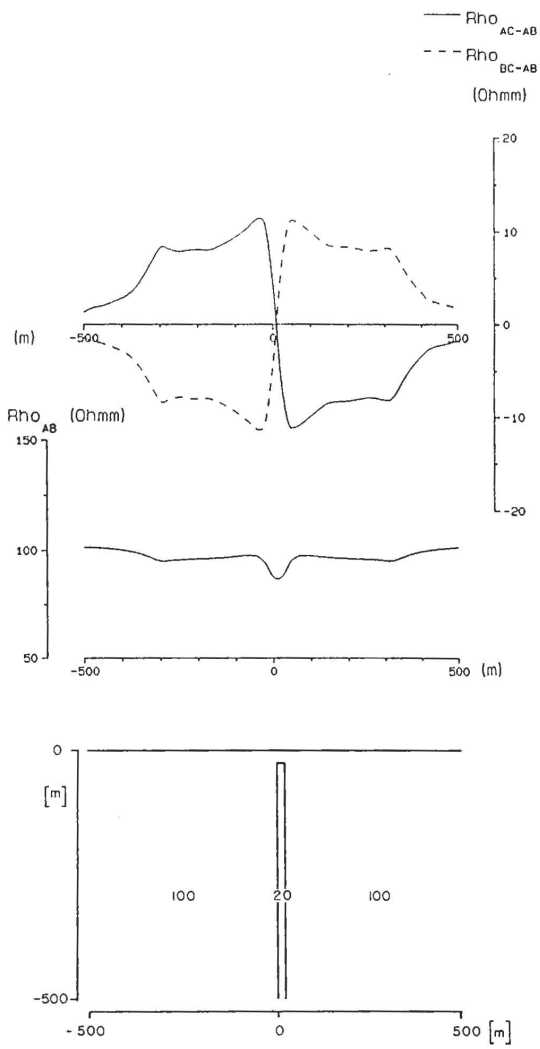

FIGURE 5.13: *Head-on profile over conductive vertical structure. The electrode configuration is from the left to the right, AMNB, and the array is moving to the right. The lower-most figure shows the model and the uppermost figure shows the associated resistivity curves*

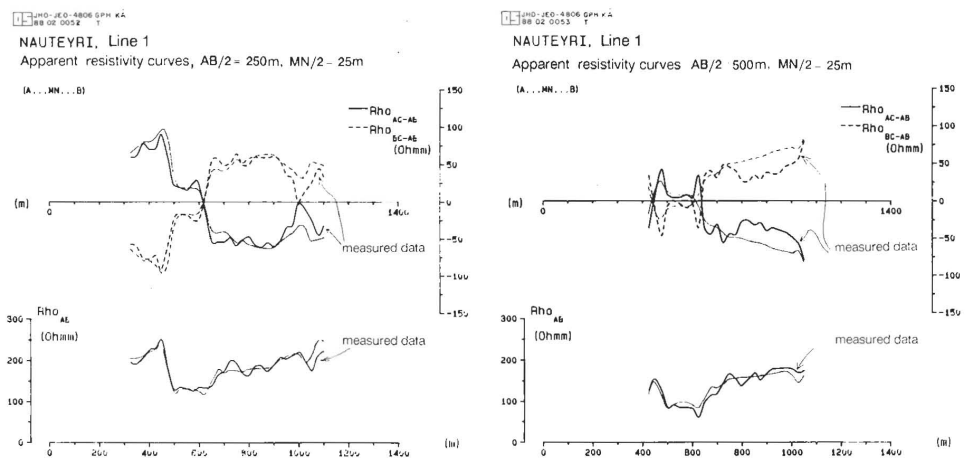

FIGURE 5.14: *Resistivity data of a head-on profile from Nauteyri low-temperature area, NW-Iceland. For location, see Figure 5.16. Both measured data and model response data, as calculated from the model of line 1 in Figure 5.15, are shown (taken from Hjartarson et al., 1988)*

$$\rho_{AC} = \frac{\Delta V_{AC}}{I} \pi \frac{S^2 - P^2}{P} \quad \text{and} \quad \rho_{BC} = \frac{\Delta V_{BC}}{I} \pi \frac{S^2 - P^2}{P} \tag{5.6}$$

for the circuits AC and BC, and the already known (see Equation 5.5)

$$\rho_{AB} = \frac{\Delta V_{AB}}{I} \frac{\pi}{2} \frac{S^2 - P^2}{P} \tag{5.7}$$

for circuit AB. All 4 electrodes AMNB are moved stepwise a certain distance along a profile perpendicular to the vertical structure and a new measurement is made. The three different resistivities ρ_{AC}, ρ_{BC} and ρ_{AB}, are calculated. The common procedure, before plotting the field graphs, is to subtract the apparent resistivities measured at AB, from those measured at AC and BC. The values $\rho_{AC} - \rho_{AB} = \rho_{AC\text{-}AB}$ and $\rho_{BC} - \rho_{AB} = \rho_{BC\text{-}AB}$ are calculated and plotted together with the ρ_{AB} curve as a function of the central position of the array (see Figure 5.13).

If the potential electrodes and the current electrode A are on the same side of the conductive structure, the resistivity $\rho_{AC\text{-}AB}$ will always be positive, and if the potential electrodes and the current electrode A are on opposite sides of the conductive structure, the resistivity $\rho_{AC\text{-}AB}$ will always be negative (see Figure 5.13). As the complete array is moved along a straight line across the conductive structure, the situation reverses, and the curves $\rho_{AC\text{-}AB}$ and $\rho_{BC\text{-}AB}$ will cross each other. This cross is above the vertical conductive structure. An example of application from a low-temperature geothermal area, Nauteyri, NW-Iceland, is given in Figures 5.14-5.16.

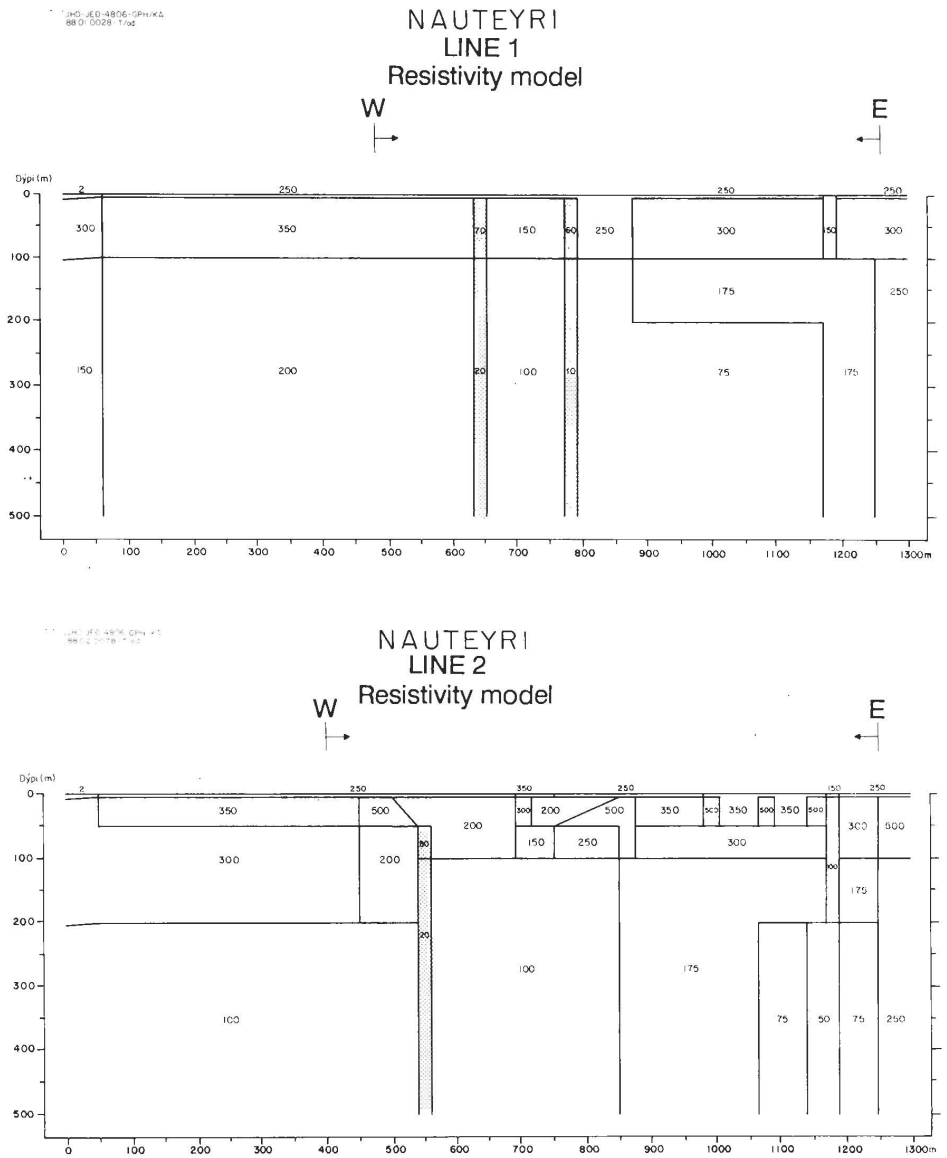

FIGURE 5.15: *Interpretation of head-on profiles (line 1 and line 2) from Nauteyri. For location, see Figure 5.16. In line 1, two low-resistivity fractures are found. In line 2, one low-resistivity fracture is found (Hjartarson et al., 1988)*

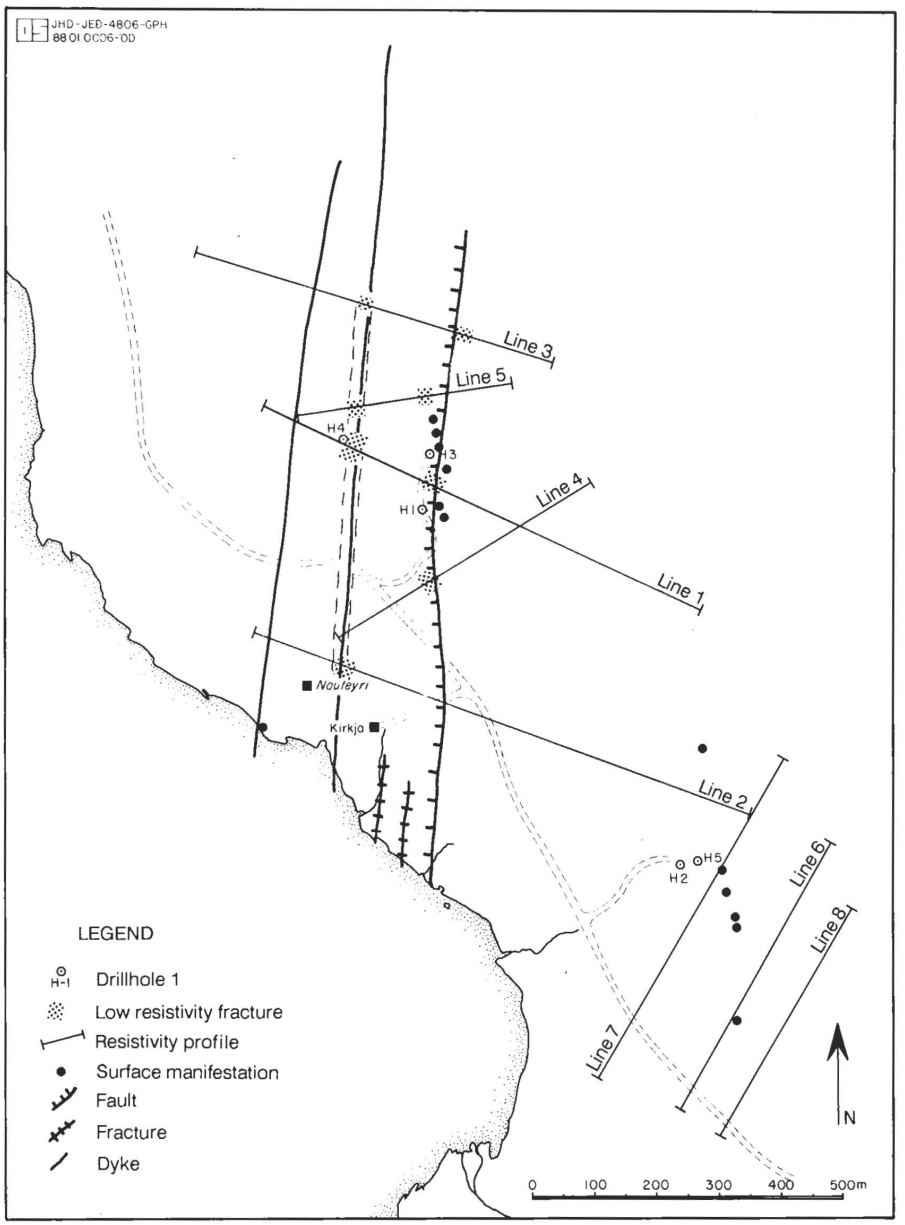

FIGURE 5.16: *Geothermal interpretation of head-on profiles from Nauteyri connecting the low-resistivity fractures as revealed from the head-on profiles. The geothermal surface manifestations in the northern part of the area are associated with a fault (revealed from geological mapping) and a possible low-resistivity fracture (revealed from head-on profiles). Another possible low-resistivity fracture coincides with a dyke. Drilling of drillhole H-4, assumed to cut the low-resistivity fracture at depth, gave very good results although it is at 150 m distance from the surface manifestations (taken from Hjartarson et al., 1988)*

6. ELECTROMAGNETIC RESISTIVITY METHODS

Electromagnetic resistivity methods make use of an alternating current (AC-current) induced in the earth. The alternating current may be artificially induced, as in TEM, or be natural signals, as in MT. Until recently, this method had not been widely used in geothermal exploration. The two categories of electromagnetic methods discussed here, depend on the different sources of the alternating current. They are:

- **Natural-source electromagnetics**
  - MT
  - AMT
- **Controlled-source electromagnetics**
  - TEM (central-loop, grounded dipole)

6.1 The magnetotelluric method (MT and AMT)

In the magnetotelluric resistivity method, the natural electromagnetic field is used as an energy source to probe the earth and to measure electrical resistivity.

The natural EM-field has a very wide spectrum (see Figure 6.1). Low frequencies, 0.0001-10 Hz are used in probing to depths of several tens to hundreds of kilometers (the actual MT-method). Higher frequencies, 10-1,000 Hz are used for shallower investigations in the audio-magnetotelluric method (AMT).

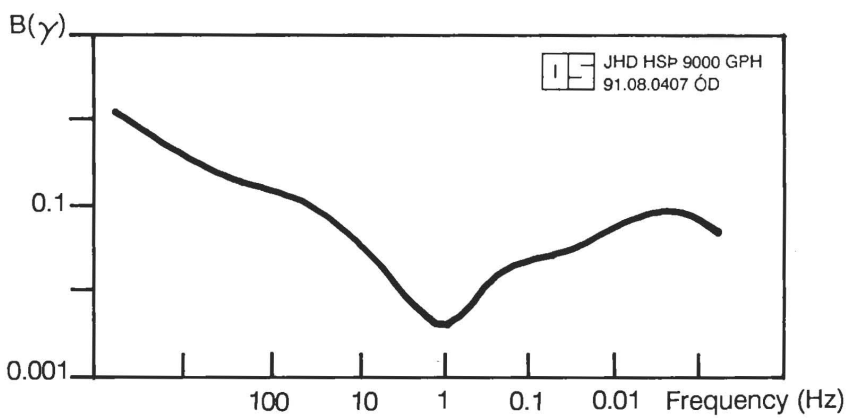

FIGURE 6.1: *The mean amplitude of the natural electromagnetic field (modified from Keller and Frischknecht, 1966)*

The lower frequencies are generated by ionospheric and magnetospheric currents caused by plasma (solar winds) emitted from the sun and interfering with the earth's magnetic field. Some of the higher frequencies (≥1 Hz) are caused by thunderstorm activity near the equator and are distributed as guided waves between the ionosphere and the earth to higher latitudes.

The natural time-varying EM-field can be observed as variations in the earth's magnetic field.

They are called magnetic micropulsations.

Micropulsations induce eddy currents in the ground, called telluric currents (tellus means earth in Greece). The density and distribution of the telluric currents depend on the local conductive structure of the ground.

The subsurface resistivity structure can be studied by simultaneously measuring the magnetic field variations, **B** [γ], at the surface of the earth and the variations in the electric field, **E** [V/m], in the ground for a certain frequency range, ω [Hz]. Because of the skin effect, low frequencies penetrate deeper into the earth than higher frequencies.

$$\mathbf{B},\ \mathbf{E},\ \omega, \quad \rightarrow \quad \rho_\omega(x,y,z) \tag{6.1}$$

If this is compared to the DC-method (see Equation 5.4), then **B** corresponds to the current **I**, **E** corresponds to the measured potential difference ΔV, and ω corresponds to the geometrical factor K.

The primary field $\mathbf{B_p}$, which comes from the ionosphere, creates an electric field **E** and a current **I** in the ground (see Figure 6.2). This current depends on the primary field and the electrical resistivity of the ground. The current, **I**, induces a secondary magnetic field, $\mathbf{B_s}$. $\mathbf{B} = \mathbf{B_p} + \mathbf{B_s}$ and **E** is measured at the surface and delivers the apparent resistivity as a function of ω.

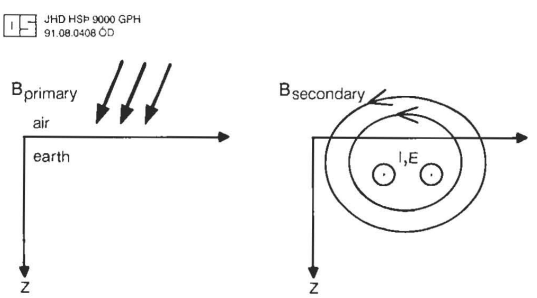

FIGURE 6.2: *The basic principle of the MT-method*

The magnetic field **B** is measured on the ground with magnetometers, such as coils, SQUID or fluxgates (see Figure 6.3). The associated electric field, **E**, is measured with a voltmeter as a potential difference, ΔV, between pairs of electrodes, at a distance L, at the surface ($\mathbf{E} = \Delta V/L$).

It can be shown that for any ω:

$$\mathbf{E}(\omega) = \mathbf{Z}(\omega) \cdot \mathbf{B}(\omega) \tag{6.2}$$

where **Z** is a complex tensor which depends on the resistivity structure in the earth and ω is the angular velocity [s^{-1}]. In the general case for a plane wave falling on a nonhomogeneous earth, this tensor equation can be written as:

$$\begin{bmatrix} E_x \\ E_y \end{bmatrix} = \begin{bmatrix} Z_{xx} & Z_{xy} \\ Z_{yx} & Z_{yy} \end{bmatrix} \cdot \begin{bmatrix} B_x \\ B_y \end{bmatrix} \tag{6.3}$$

In the one-dimensional case, i.e. if the earth is homogeneous or horizontally stratified, then the resistivity is the same in all directions. In that case, we have $Z_{xx} = Z_{yy} = 0$ and $Z_{xy} = -Z_{yx}$.

If the resistivity structure is two-dimensional, that is, the resistivity is different depending on the direction, then Z_{xy} is not equal to Z_{yx}. Furthermore, the analysis gives two apparent resistivities, one in the direction of the geological strike and another one perpendicular to the two-dimensional structure. The depth of penetration, d, into the earth for an electromagnetic wave, is a function of resistivity, ρ, and the period $T = 2\pi/\omega$ of the incident magnetic field, and is given as:

$$d = 500\sqrt{T\rho}, \tag{6.4}$$

where d is given in m, T in seconds and ρ in Ωm (see Figure 6.4).

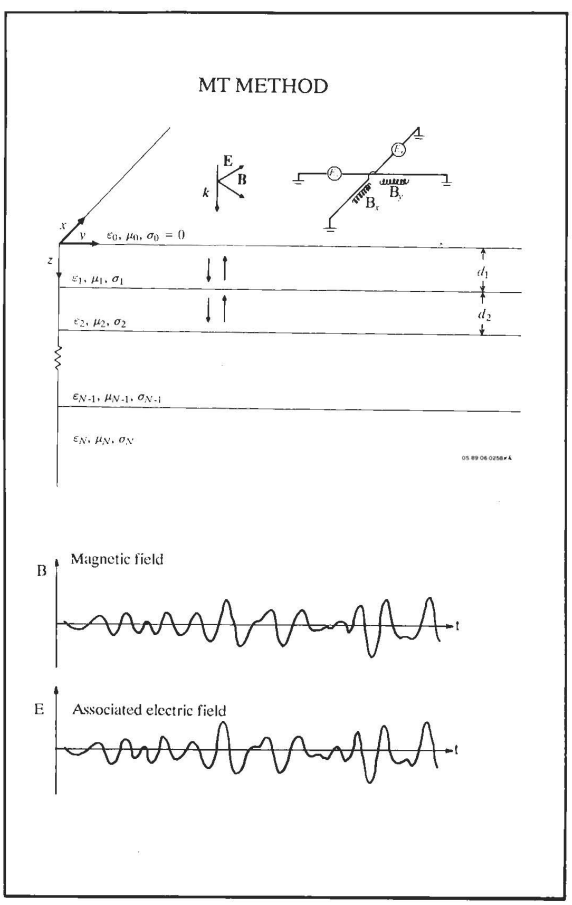

FIGURE 6.3: *Arrangement of magnetometers and potential electrodes in MT measurements*

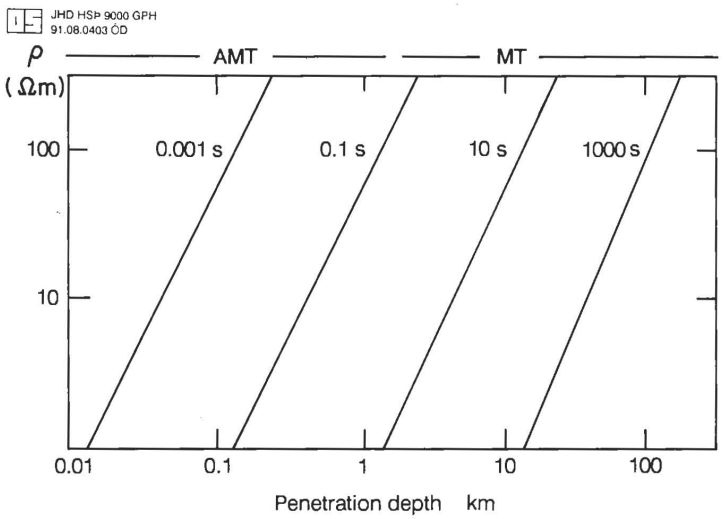

FIGURE 6.4: *The skin depth depends on the period and on resistivity*

For a homogeneous earth, it is easy to calculate the resistivity from the elements of the impedance tensor Z_{xy} and Z_{yx}. If the earth is not homogeneous, we define (similar to the DC-method) an apparent resistivity as the calculated resistivity as if the earth was homogeneous. The formula for the apparent resistivity is:

$$\rho_{a_{xy}} = \frac{1}{\omega}\frac{|E_x|^2}{|B_y|^2} = 0.2T|Z|^2 \quad [\Omega m] \tag{6.5}$$

and is analogous for $\rho_{a_{yx}}$. In the one-dimensional case, these resistivities are the same.

The procedure for MT and AMT soundings can be summarized as follows:

- Measurement of the horizontal components of the magnetic field, B_x and B_y and the induced electric field, E_y and E_x, both as a function of time for several hours (an hour for AMT, a day for MT)
- Fourier transforming the time series and calculating two apparent resistivities, $\rho_{a_{xy}}$ and $\rho_{a_{yx}}$ as a function of the frequency (period T)
- One-dimensional interpretation. Calculating a one-dimensional model which fits the measured data. Comparison with other results
- Two-dimensional interpretation
- Geological interpretation, geothermal model of the area

The MT method has mainly been used to investigate the deeper structures of the crust and upper mantle. In Iceland, it has been used to map bodies with anomalous low resistivities (see Figure 6.5) which are interpreted to be magma chambers or semi-fluid magma layers (Beblo et al., 1983; Hersir et al., 1984; Eysteinsson and Hermance, 1985). A good correlation has been found in many areas between anomalously high heat flow and the depth to a low resistive body measured with MT (see Figure 6.6) (Kaufman and Keller, 1981).

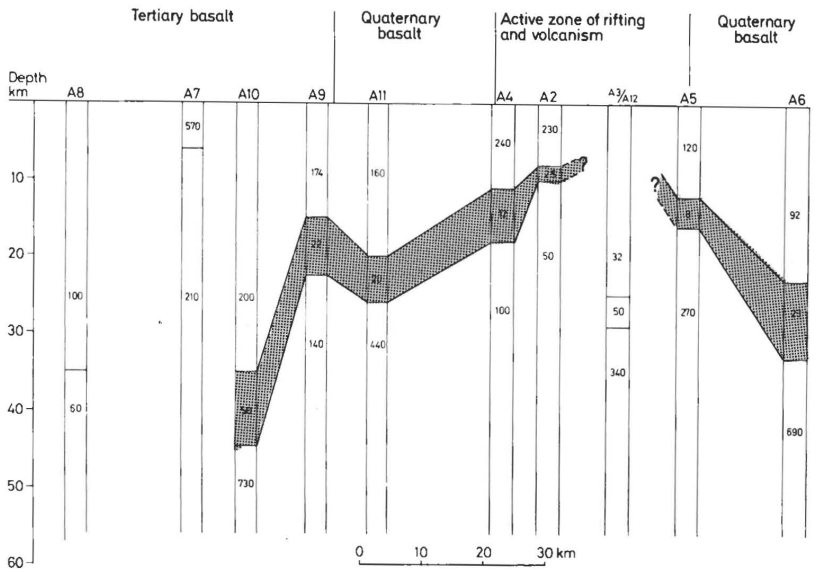

FIGURE 6.5: *Magnetotelluric pseudo-resistivity cross-section, crossing the constructive plate boundary in SW-Iceland. The depth to the good conductor (10-20 km) and its resistivity increase with age of the crust and the distance from the axial zone. The layer is interpreted as partially molten basalt, at a temperature of about 1100°C and a volume fraction of the melt phase in the range 10-20% (taken from Hersir et al., 1984)*

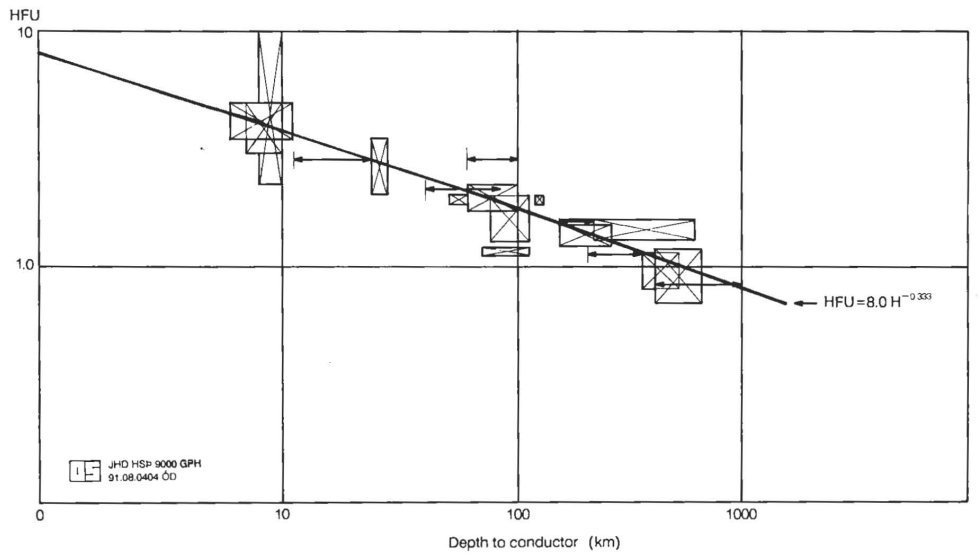

FIGURE 6.6: *Correlation between anomalous heat flow and the depth to a magma layer (modified from Kaufman and Keller, 1981)*

6.2 TEM (central-loop, grounded dipole)

The EM methods can be divided into two different categories depending on the measuring technique used:

- **Frequency domain methods:** Measurements made at several different discrete frequencies. The lower frequencies penetrate deeper into the earth than the higher frequencies
- **Time domain methods:** A current pulse is transmitted and the decay of the induced magnetic field is measured as a function of time. This gives information for a broad frequency range and, hence, broad depth range

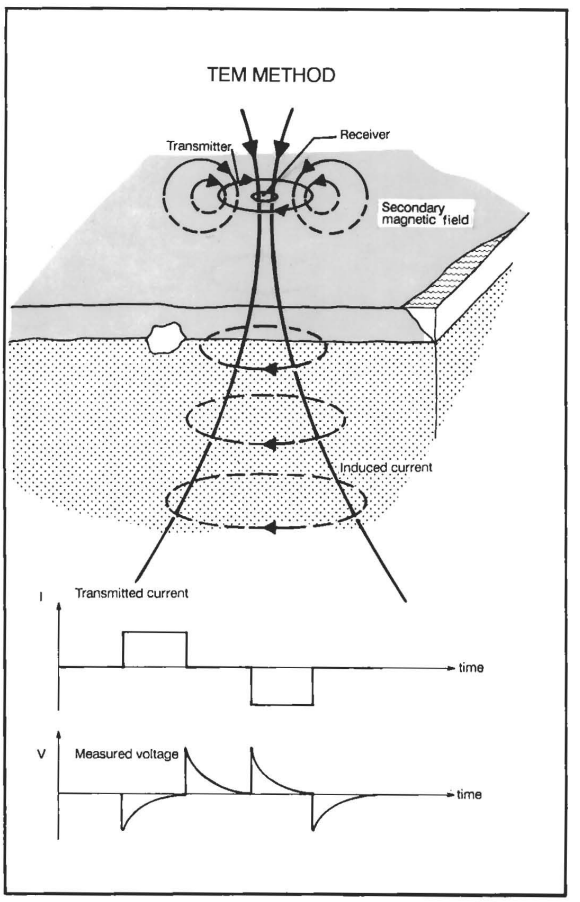

In the central-loop TEM sounding method, the current in the ground is generated by a time-varying field of a controlled magnitude generated by a source loop. A loop of wire is placed on the ground (about 300 m x 300 m) and a constant magnetic field of known strength is built up by transmitting a constant current into the loop. The current is then abruptly turned off. The decaying magnetic field induces electrical currents in the ground (see Figure 6.7). The current distribution in the ground induces a secondary magnetic field decaying with time. The decay rate of the secondary magnetic field is monitored by measuring the voltage induced in a receiver coil (or a small loop, some 10 m x 10 m) at the center of the transmitting loop. The current distribution and the decay rate of the secondary magnetic field depends on the resistivity structure of the earth. The decay rate, recorded as a function of time after the current in the transmitter loop is turned off, can therefore be interpreted in terms of the subsurface resistivity structure.

FIGURE 6.7: *The central-loop TEM sounding configuration*

The TEM signal is usually presented as an apparent resistivity (see Figure 6.8) given by the formula:

$$\rho_a\ (r,t) = \frac{\mu_0}{4\pi}\left[\frac{2\mu_0 A_r n_r A_s n_s}{5t^{5/2}V(r,t)}\right]^{2/3} \qquad (6.6)$$

where:

- t - time elapsed, after the current in the transmitter loop is turned off
- A_r - cross-sectional area of the receiver coil [m^2]
- n_r - number of windings
- μ_0 - magnetic permeability in vacuum [henry/m]
- A_s - cross-sectional area of the loop [m^2]
- n_s - number of windings in the loop

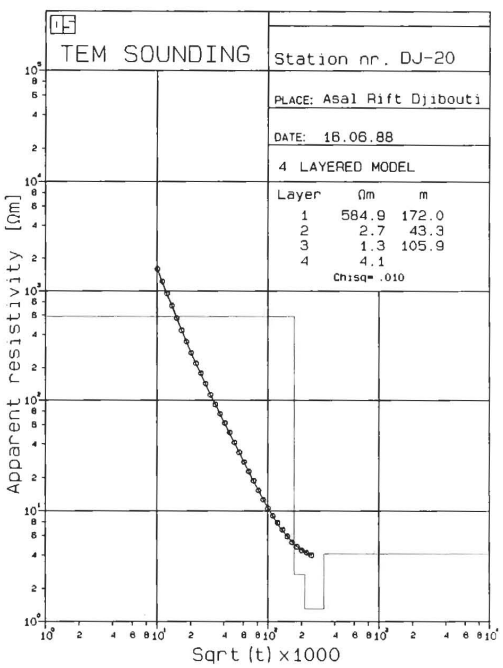

FIGURE 6.8: *One-dimensional interpretation of the apparent resistivity in a central-loop TEM sounding from the Asal Rift in Djibouti, Africa (Árnason et al., 1988)*

The apparent resistivity curve can be interpreted one-dimensionally in a PC-computer (Árnason, 1989) as shown in Figure 6.8. An example of the application of the central-loop TEM method is given in Figure 6.9. In the grounded dipole TEM sounding, the current source is a grounded dipole instead of a loop. The grounded dipole TEM sounding has a greater depth of penetration than the central-loop TEM sounding (see Keller et al., 1984).

The central-loop TEM sounding method has several advantages over the conventional Schlumberger DC-sounding method:

- The transmitter couples inductively to the earth and no current has to be injected into the

ground. This is most important where the surface is dry and resistive like dry fresh lava-fields or a desert

- The monitored signal is a decaying magnetic field, not an electric field at the surface. This makes the results much less dependent on local conditions at the receiver site. Distortions due to local resistivity inhomogeneities at the receiver site can be a severe problem in DC-soundings (remember Figure 5.6) as well as in MT soundings
- This method is much less sensitive to lateral resistivity variations than the DC-methods. Therefore, one-dimensional inversion is better justified in the interpretation of central-loop TEM soundings than in DC-soundings. Results from the Nesjavellir high-temperature geothermal field in Iceland show that one-dimensional interpretation of central-loop TEM soundings can basically give the same resolution as a much more time consuming and expensive two-dimensional modeling of DC-data (Árnason et al., 1987; Árnason, 1990)
- In DC-soundings the monitored signal is low when the subsurface resistivity is low, like in geothermal areas, whereas in TEM soundings the situation is the reverse, the lower the resistivity the stronger the signal

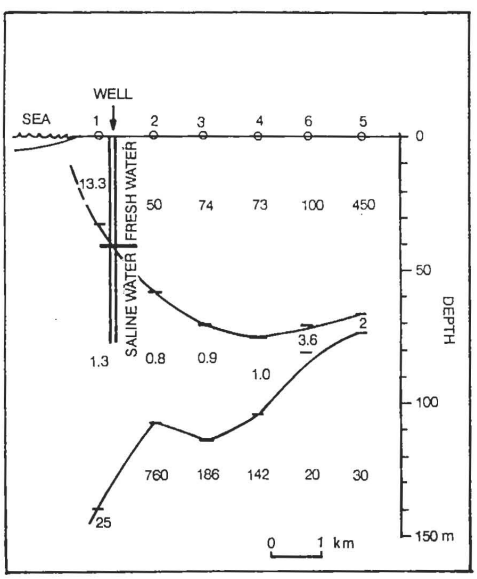

FIGURE 6.9: *Interpretation of central-loop TEM soundings from the south coast of Iceland. Drilling indicates that the low resistivity coincides with saline water (Björnsson and Eysteinsson, 1988)*

7. SELF POTENTIAL (SP), NATURAL ELECTRICAL POTENTIALS

If two electrodes are put into the ground and connected with an electrical wire to a millivoltmeter, an electrical potential will be observed between the electrodes. This potential is composed of an AC-component containing amplitudes in a broad frequency range caused by the magnetic micropulsations, and a DC-component. The DC-component is called the SP potential (spontaneous or self potential). Its causes can be fluid flow in the subsurface rocks, electrochemical reactions, temperature differences, mechanical activity and stress differences. The SP potential varies from place to place and its value is often in the range of a few tens of mV up to 1-2 V/km.

Interpretation: Significant and reproduceable SP-anomalies are related to many geothermal areas. They may have different causes and may or may not be related directly to the geothermal activity. The mechanism which generates these anomalies is not very well understood. Possible causes are:

- Temperature difference creating thermoelectrical potential
- Fluid flow of hot or cold water
- Conductive mineral deposits like graphite, pyrite or sulphide
- Chemistry variations in rock composition and pore fluid

As many different effects can cause an SP anomaly, it is difficult to make a significant quantitative interpretation of the measured data. Nevertheless, the SP method has been used extensively in geothermal exploration and has often provided valuable information along with results of other methods (see Figure 7.1). The most important applications have been in:

- Reconnaissance study
- Mapping the boundaries of high-temperature geothermal fields
- Tracing faults and fissures

In the last few years considerable effort has been put into quantitative modelling but much more work needs to be done in order to get a firm understanding of the SP phenomenon.

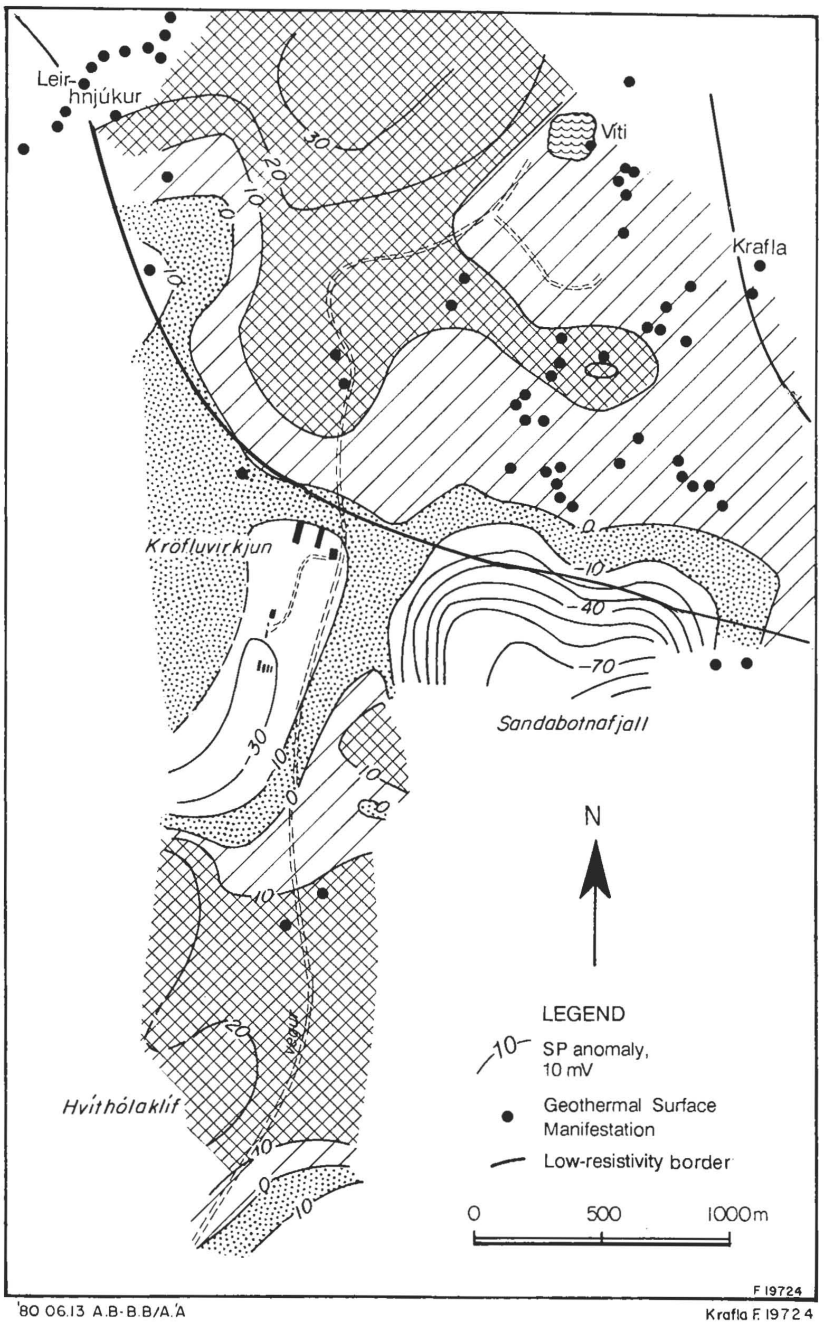

FIGURE 7.1: *SP survey of the Krafla high-temperature area in northern Iceland. Positive anomalies are correlated to surface geothermal activity and resistivity lows. The zero line is most likely running along a fault with a NW-SE trend (redrawn from Karlsdóttir et al., 1978; Björnsson, 1980; Árnason et al., 1984)*

8. MAGNETIC SURVEYS

8.1 Introduction

Magnetic methods are widely used in geothermal exploration and are often applied together with regional gravity and refraction measurements in mapping geological structures (structural method). The most important applications are in the following:

- Location and depth of concealed intrusives, tracing dykes and faults
- Locating buried lava, depth to basement
- Locating hydrothermally-altered areas and Curie point depth analysis
- Paleomagnetism

The magnetic field of the earth resembles the field of a large bar magnet located near the center of the earth, a dipole field (see Figure 8.1). Its origins are currents in a fluid conductive core. According to the definition of magnetic poles, the north-seeking end of a compass needle is a north pole. Hence, the magnetic south pole is near the geographic north pole of the earth.

The earth's magnetic field is not a pure dipole field but contains higher order pole components (80% dipole, 20% higher order poles). The lines are near-vertical close to the poles, and horizontal near the equator (see Figure 8.1). The total field strength is about 60,000 γ near the poles and 30,000 γ near the equator (γ = nT = 10^{-9} T [Tesla = Weber/m^2]).

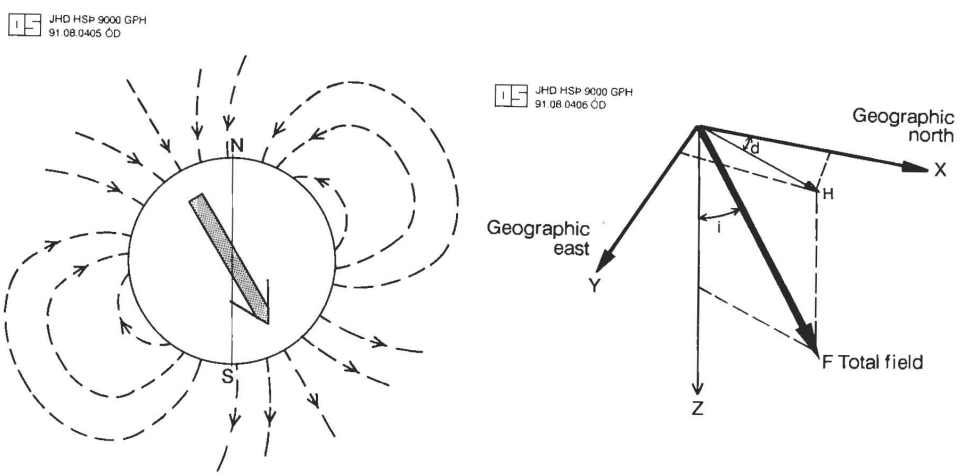

FIGURE 8.1: *To the left: The dipole field of the earth, the magnetic south pole is near the geographic north pole. To the right: Components of the magnetic field.* **F** = *total field vector,* **H** = *horizontal field vector, d = declination, i = inclination.* **F** = (F_x, F_y, F_z)

Large scale anomalies are, in many areas of the world, created by irregularities of the generation mechanism. The field also changes slowly with time, both in intensity and in location of poles. These changes are called secular variations. Reversals of the magnetic poles occur

irregularly about every 1 m.y. Major time periods with the same direction of the magnetic field are called magnetic epoches (Brunhes, 0-0.7 m.y. ago, Normal; Matuyama, 0.7-2.5 m.y. ago, Reversed; Gauss, 2.5-3.3 m.y. ago, Normal; Gilbert, 2.5-4.5 m.y. ago, Reversed). Shorter periods are called magnetic events.

There are also large distortions from outer space caused by the solar wind. Time variations with periods of seconds, minutes, hours and days are caused by the impact of the solar wind on the magnetosphere and ionosphere. Micropulsations are in the frequency range of 0.001 - 1,000 Hz, daily variations are of some 100 γ and during magnetic storms amplitudes above 500 γ are observed. These variations, which are utilized in MT and AMT surveys, must be considered when measuring minor spatial variations, and also in DC and EM electrical measurements (telluric noise).

8.2 Various types of magnetometers

Portable, for surveying:

Field balance needle	Mechanical instruments; for measuring vertical or horizontal
and dip needle:	components, intensity or direction
Fluxgate:	One component. Ground survey of ΔZ and for rock magnetism
Proton-precession:	Total field intensity. Ground survey of ΔF and for aeromagnetism

Less portable, for stationary work:

Fluxgate:	3-components
Coils:	1-3 components, also used in MT and AMT
SQUID:	1-3 components, also used in MT and AMT
Optically pumped:	(rubidium, cesium)
Variometers:	Moving magnets. For observatory use

The total magnetic field is a vector quantity having both direction and intensity (see Figure 8.1). With proton-precession magnetometers, only the intensity is measured. If the anomaly, ΔF, which is measured, is small compared to **F**, then the change of **F** in the direction of the total field (**F**) is actually measured. In high latitudes it is approximately equal to F_Z, but in low latitudes it is approximately equal to F_H.

8.3 The magnetic field - Quantities and units

The magnetic field or magnetic flux density is denoted with **B** and measured in the unit Tesla [T] or γ, where, γ = nT = 10^{-9} T [Tesla = Weber/m^2]. The earth's total magnetic field is 25,000-60,000 γ [25-60 kγ].

A magnetic field, B_0 can induce a magnetic field, B_M (magnetization field) in materials, which is proportional to the undisturbed external field B_0:

$$\mathbf{B}_M = k \cdot \mathbf{B}_0, \tag{8.1}$$

where k is the magnetic susceptibility [dimensionless].

The total magnetic field **B** is the sum of $\mathbf{B}_0$ and $\mathbf{B}_M$:

$$\mathbf{B} = \mathbf{B}_0 + \mathbf{B}_M = (1+k)\mathbf{B}_0 = \mu \mathbf{B}_0 \tag{8.2}$$

$\mu = 1+k$ is called the magnetic permeability [dimensionless].

The magnetic susceptibility, k, is a property of the material, describing its ability to enhance the local field. The magnetic permeability, μ, is the relative ability of the material to create local magnetic fields. Most materials have $0<k<10^{-5}$ and are paramagnetic. If k is small and negative, then it is diamagnetic. Materials, with $k \approx$ 1-4, are ferrimagnetic. Iron alloys may have $k \approx 10^1 - 10^6$, and are ferromagnetic.

Ferri- and ferromagnetism decreases with temperature and disappears entirely at a critical temperature called the Curie Point (see Figure 8.2). For the most common ferrimagnetic mineral in rocks, magnetite, the Curie Point is 580°C (Grant and West, 1965). Practically all magnetic minerals in the earth's crust are ferrimagnetic.

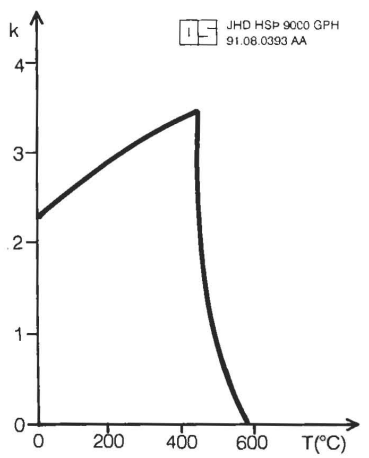

FIGURE 8.2. *A change in magnetic susceptibility of a sample of ferrimagnetic mineral (simplified from Nagata, 1961)*

[Sometimes the magnetic field is defined in a different way and denoted with **H** and measured in [A/m], i.e. $\mathbf{H} = \mathbf{B}_0/\mu_0$, where μ_0 is the magnetic permeability of free space and is a universal constant, equal to $4\pi \cdot 10^{-7}$ Weber/Am [Henries/m].]

Older cgs units are still frequently used in geomagnetics, instead of the more common SI-units. We have:

- $\mu_{SI} = \mu_{cgs}$
- $k_{SI} = 4\pi \cdot k_{cgs}$
- $\mathbf{B}_{SI}$ [Tesla] = $10^4 \mathbf{B}_{cgs}$ [Gauss]
- $\mathbf{H}_{SI}$ [A/m] = $4\pi \cdot 10^{-3} \mathbf{H}_{cgs}$ [Oersted]
- $\mathbf{B}_{M_{SI}}$ [Tesla] = $\mu_0 \mathbf{H}_M = \mu_0 \mathbf{M} = 4\pi \cdot 10^2 \mathbf{M}$ [A/m]

8.4 Magnetization of crustal rocks

In crustal material, two kinds of magnetization must be considered, i.e.:

- Induced magnetization, $\mathbf{M}_i$
- Permanent magnetization, $\mathbf{M}_p$

$\mathbf{M}_i$ has always the same direction as the ambient earth's field and the time constant is zero, i.e. it changes immediately by rotation of $\mathbf{B}_0$. For it, we have $\mathbf{M}_i = k \cdot \mathbf{B}_0 / \mu_0$.

$\mathbf{M}_p$ often predominates in igneous rocks. It depends upon the metallurgic properties and the thermal, mechanical and magnetic history of the specimen. $\mathbf{M}_p$ is sometimes divided into viscous magnetization, $\mathbf{M}_v$ with a time constant of $1\text{-}10^5$ years and remanent magnetization, $\mathbf{M}_R$ created by cooling below the Curie-point ($\approx$ 500-600°C) with a very long time constant around some 10^7 years (thermoremanent magnetization). In Tertiary and lower Quaternary basaltic lavas in Iceland, the magnetization is on the order of, $\mathbf{M}_i \approx 1$ A/m, $\mathbf{M}_v \approx 0.3$ A/m and $\mathbf{M}_R \approx$ 3-4 A/m (Kristjánsson, 1984). Hence, the thermoremanent magnetization is dominating.

8.5 Local magnetic anomalies

An anomaly is a local disturbance in the earth's magnetic field. It is caused by local changes in magnetization (magnetization contrast), i.e. changes in k ($\mathbf{M}_i$) and/or changes in $\mathbf{M}_p$. The total or effective magnetization is the net effect of $\mathbf{M}_i$ and $\mathbf{M}_p$, both of which may have different intensities and directions (see Figure 8.3). Changes in both magnetic susceptibility k and $\mathbf{M}_p$ create anomalies.

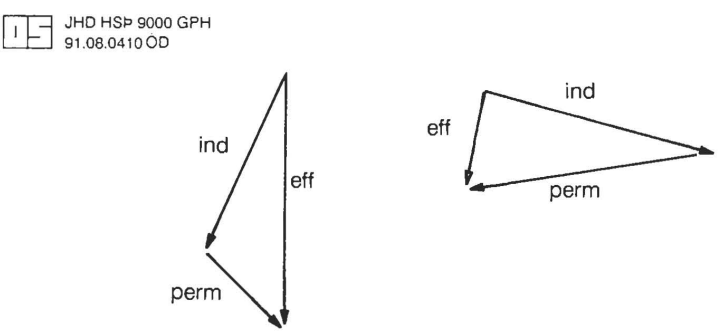

FIGURE 8.3: *Effective magnetization is composed of induced and permanent magnetization. The effective magnetization characterizes the magnetic anomaly*

A magnetic anomaly is characterized by the **direction** and **magnitude** of the effective magnetization, the **shape** of the anomalous body and its **position**. The most simple anomalies can be represented by monopoles (very long dipoles) and dipoles (see Figure 8.4). The dipole field varies as $1/r^3$, and the monopole field varies as $1/r^2$. (Actually no magnetic monopoles exist but the distribution of the magnetic field close to the one end of a very long bar magnet resembles a monopole field, and it is very convenient to use monopoles in calculations of model anomalies).

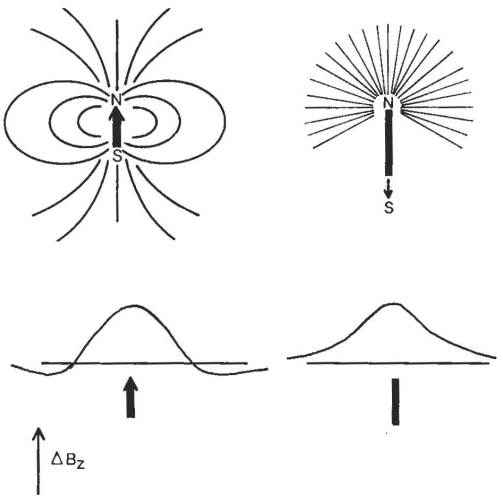

FIGURE 8.4: *Uppermost part: Magnetic field around a dipole and a monopole. Lowermost part: Magnetic anomalies over a dipole and a monopole*

It is possible to explain complicated anomalies as arrangements of dipoles and monopoles either in a line or sheet-like distribution of such poles. The same anomalous body shows different magnetic anomalies at different latitudes of the earth.

If the induced magnetization dominates or is the only reason for an anomaly, then an anomaly measured by a proton-precession magnetometer depends strongly on the direction of the total field **F**. In Iceland, for example, the inclination of **F** is close to 76°. Hence, the total field anomalies are approximately ΔZ anomalies.

In Icelandic low-temperature geothermal areas, ground magnetic measurements are often used to trace dykes which feed hot water to the surface (see Figure 8.5).

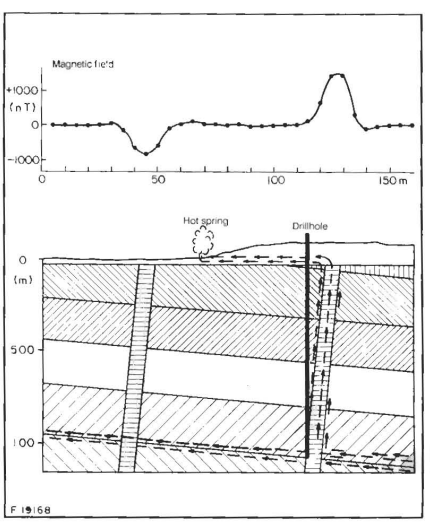

FIGURE 8.5: *Principle of ground-magnetic measurements across a basaltic dyke which feeds hot water to the surface (taken from Björnsson, 1980)*

8.6 Field procedure - Magnetics using a proton-precession magnetometer

Magnetic measurements are made at regular intervals along profiles or in a grid (see Figure 8.9). Spacing depends on the spatial wavelength of the expected anomaly. If Δx is the distance between measuring points and d the depth to the anomalous body, then $\Delta x/d$ should be less than 2 in order to be able to draw contour lines. $\Delta x/d$ should be less than 1 if boundaries of a buried body are to be traced or a vertical gradient to be calculated.

In low-temperature areas in Iceland, where dykes and faults are often traced, it is common to have 20 m between profile lines and 5 m between measuring points on each line. The magnetic sensor is on a staff 2-4 m above the surface or in a backpack (if some 5-10 γ accuracy is required). In aeromagnetic surveys of high-temperature geothermal areas, the flight height above ground is some 100 m and there are about 100 m between lines (see Figure 8.12). Readings are noted in a field notebook, on a dictaphone or digitally on a tape or into the memory of a computer.

Some precautions: Check the magnetic activity and avoid magnetic storms. Orient the sensor perpendicularly to the main field in order to get as strong a signal as possible. Keep away from AC-powerlines (50-100 m). Avoid magnetic material on the operator.

8.7 Data reduction and presentation

Profiles: Plotted profiles should be smooth and express the anomalies of interest. If noise is present (wavelength shorter than the anomaly) smoothing is done by tracing through the noise, calculating running averages, doing band-pass filtering or polynomial curve fitting (see Figure 8.6). If the anomalies of interest are superimposed on much broader anomalies or regional trend, this can be removed and the residual field presented (see Figure 8.6).

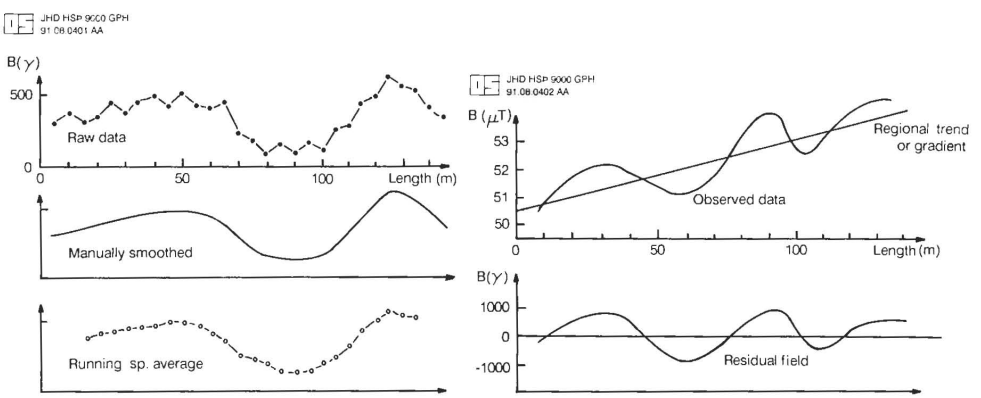

FIGURE 8.6: *Profile smoothing (to the left) and removal of trends (to the right) in magnetic measurements along a profile*

Contour maps: If data points are dense enough, contour lines showing constant field strength (iso-lines) can be drawn (see Figures 8.7, 8.10 and 8.12). Contour lines give good overview and general behavior of the anomalies. Profile maps often show many more details than contour maps (see Figure 8.9).

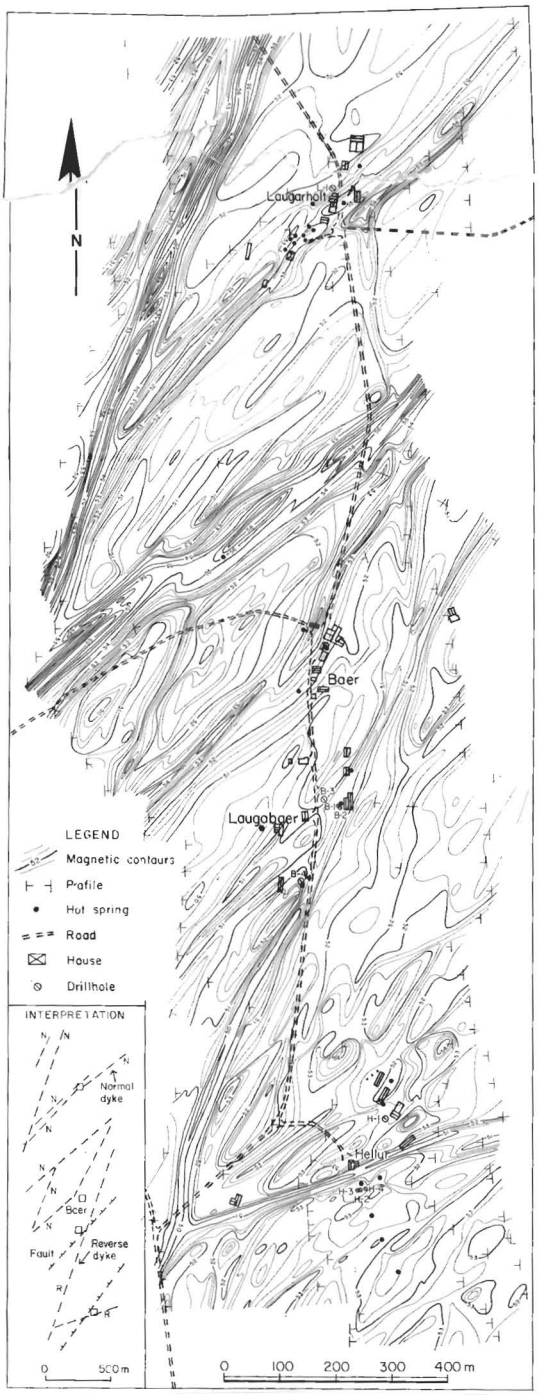

FIGURE 8.7: *Magnetic contour map of the Baer thermal field, W-Iceland. The clusters of hot springs are located where an active northerly trending fracture (not seen in the magnetic data) intersects northeasterly trending water bearing structures, dykes or faults (Georgsson et al., 1981)*

Figure 8.8 shows the structure of the Baer thermal field, W-Iceland. It illustrates how magnetic and geothermal mapping (Figure 8.7) can be the basis of simple geothermal models with the help of chemical data. Figure 8.11 shows the geological interpretation of the magnetic maps in Figures 8.9 and 8.10.

Advanced data reduction: A number of advanced techniques for data enhancement are available by using computer programs. The data points have to be dense.

- Vertical derivatives (gradients) often help in locating anomalies
- Upward and downward continuation of the measured field can be calculated in order to enhance high frequency or long wavelength spatial variations
- Filtering in one- or two-dimensions; band-pass, high-pass, low-pass
- Spectral analysis in one- or two-dimensions

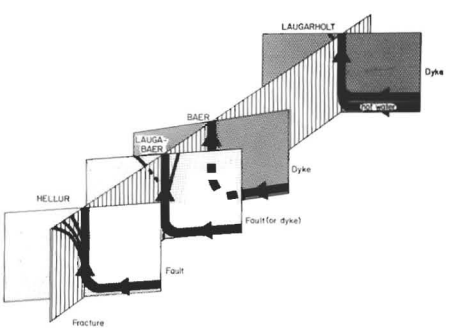

FIGURE 8.8: *A schematic illustration of the structure of the Baer thermal area, W-Iceland, mainly based on magnetic and geothermal mapping (Figure 8.7). Chemical data and drilling confirm that different clusters of hot springs are fed by separate aquifers (Georgsson et al., 1981)*

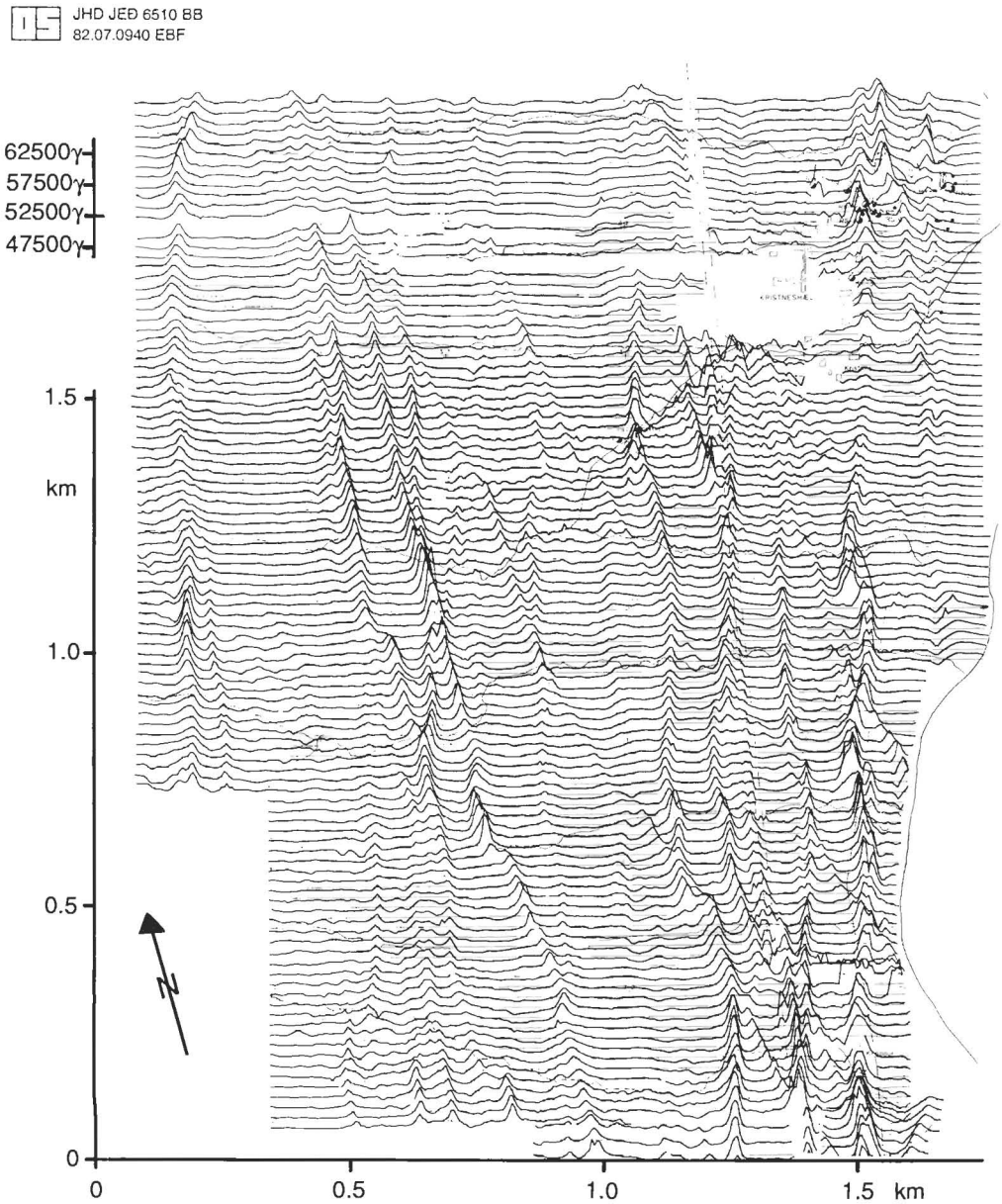

FIGURE 8.9: *Ground-magnetic survey from a low-temperature geothermal area at Hrafnagilshreppur in northern Iceland. Measured with a proton-precession magnetometer. Individual profiles are shown; 20 m are between profiles and 5 m between measuring points. Both faults and dykes can be seen as peaks (anomalies) forming lineations across the profiles (Björgvinsdóttir, 1982)*

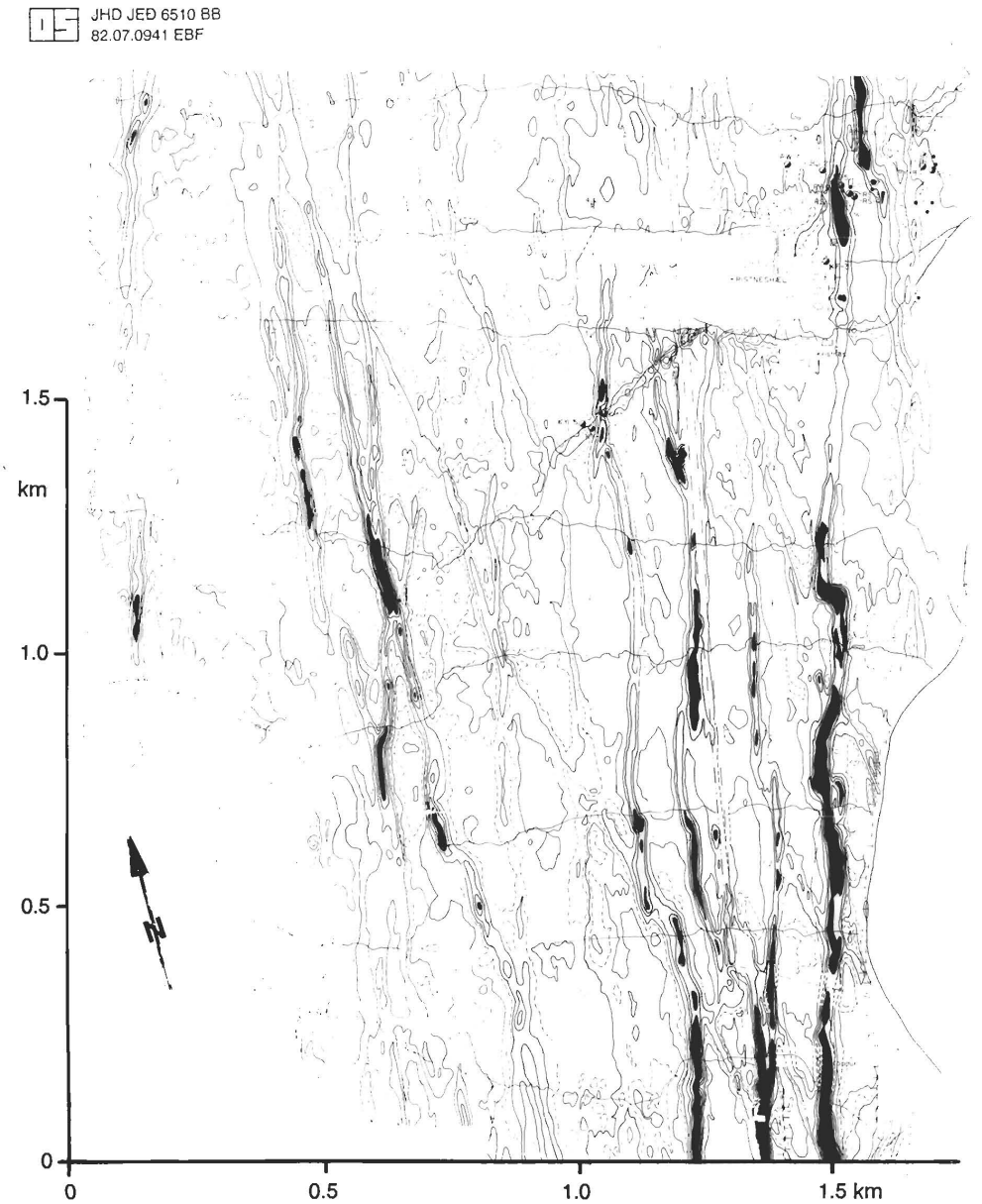

FIGURE 8.10: *Contour map from Hrafnagilshreppur based on the same data as in Figure 8.9. The profile map in Figure 8.9 and this contour map are different presentations of the same data set. It depends on the data density as to which presentation gives more information about the geological structures (Björgvinsdóttir, 1982)*

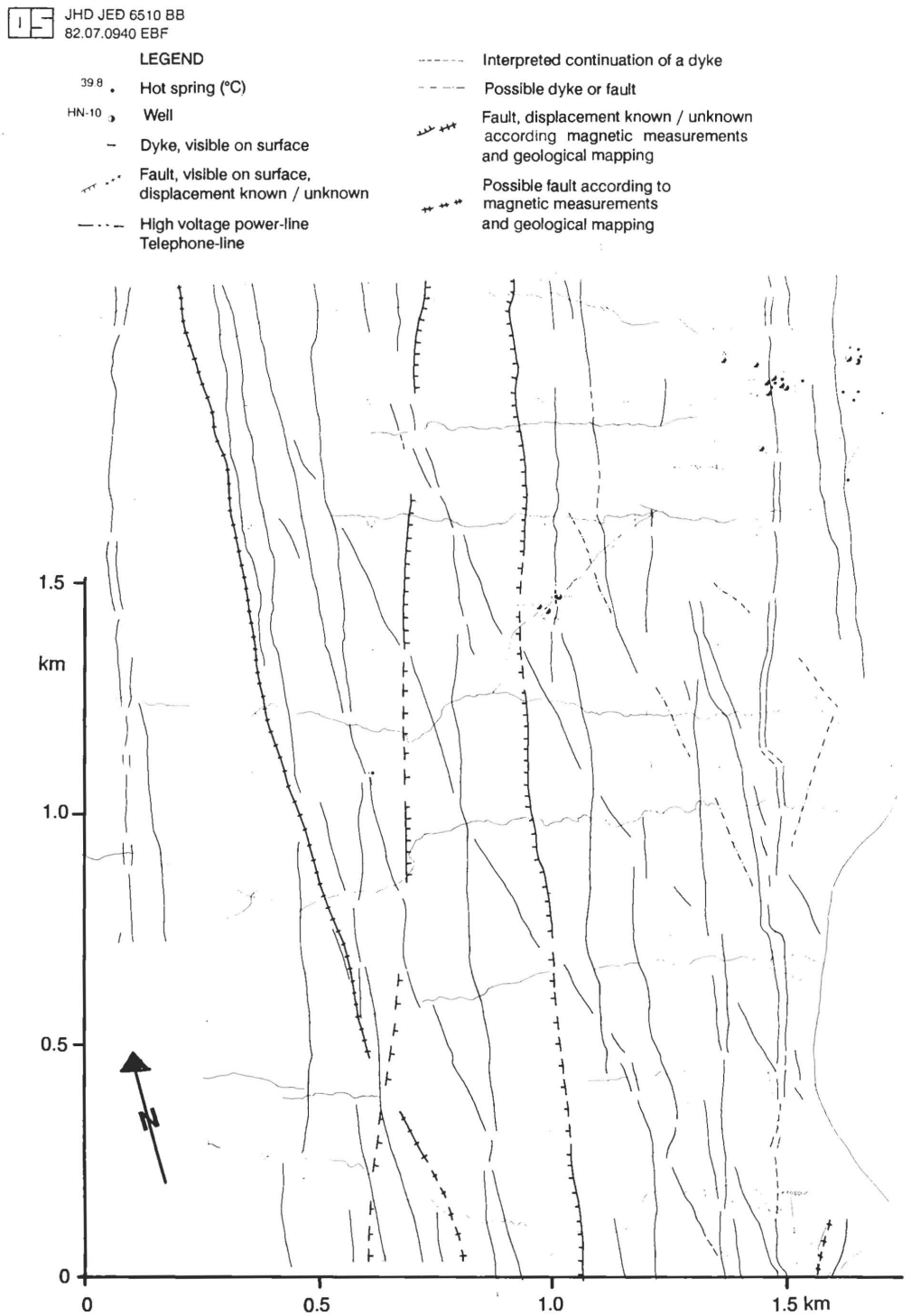

FIGURE 8.11: *Geological interpretation of the magnetic map from Hrafnagilshreppur based on the profile map in Figure 8.9 and the contour map in Figure 8.10 (Björgvinsdóttir, 1982)*

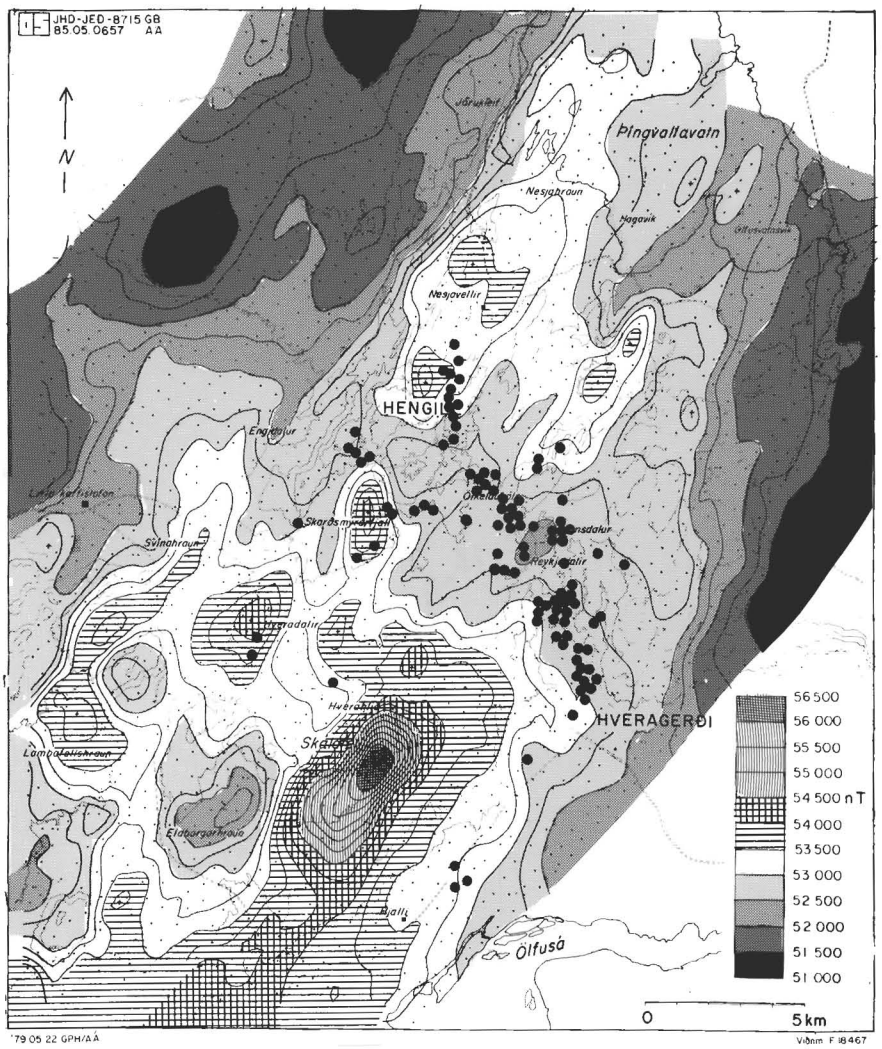

FIGURE 8.12: *Aeromagnetic map of the Hengill high-temperature geothermal area flown at 800 m a.s.l. Geothermal surface manifestation is shown as well (black dots). Contour-lines are drawn at 250 nT intervals. A positive anomaly trending NE-SW along the axis of the neo-volcanic zone is caused by normal magnetization of lavas from the Brunhes geomagnetic epoch. To the northwest and southeast, the magnetic field is lower because of reversed magnetized lavas from the Matuyama epoch. Within the central positive anomaly, there is a distinct negative linear anomaly (dotted) extending NW-SE, dissecting Hengill near its center. This anomaly coincides with the tectonic features with this orientation and nearly all fumaroles and hot springs are within this anomaly. The anomaly is most likely caused by hydrothermal alteration by geothermal fluids (taken from Hersir et al., 1990; Björnsson et al., 1986)*

9. GRAVITY SURVEYS

The gravity force between two masses, m_1 and m_2, at a distance r apart, is given by Newton's law of gravitation (m_1 is the apple and m_2 is the earth):

$$\mathbf{F} = G\frac{m_1 m_2}{r^2} \quad [N], \tag{9.1}$$

where G is the universal gravitation constant, $G = 6.670 \cdot 10^{-11}$ [$N\,m^2/kg^2$]. Galileo demonstrated that the gravitational acceleration of the earth, g, (or simply gravity) is the same for all bodies at a given place on the earth. This can be expressed as:

$$\mathbf{g} = \mathbf{F}/m = G \cdot M_{earth}/r^2 \tag{9.2}$$

The average gravity at the surface of the earth is $g \approx 9.81\ m/s^2$. But it is not a constant, i.e. it varies from place to place. One reason is that the earth is not an ideal sphere and it is rotating. Furthermore, different types of rocks in the crust and mantle have different densities and hence, different gravitational force.

In geothermal exploration, the gravity method is used to detect geological formations with different densities. Therefore, it is a typical structural method.

Gravity variations are measured with a gravimeter. These are very sensitive mechanical instruments which measure the change in acceleration (**g**) at one place relative to another reference place (relative measurements). The unit for acceleration is m/s^2. A gravity unit (g.u.) is equal to $10^{-6}\ m/s^2$. On the other hand, geophysicists usually use the unit, Gal (Galileo), which is equal to $1\ cm/s^2$ and the subunit milligal, or mgal [$0.001\ cm/s^2$]. A g.u. is equal to 0.1 mgal. The sensitivity of gravimeters is about 0.005 mgal.

In recent years, absolute gravimeters have been developed. They are already used in the field to measure gravity at selected base stations. Their accuracy is similar to the accuracy of conventional gravimeters.

In order to obtain information about the subsurface density from gravity measurements, it is necessary to make several corrections to the measured gravity values before they can be represented on a map and interpreted in terms of geological structures. The final corrected value for the gravity anomaly is called the Bouguer anomaly, Δg_B. The Bouguer anomaly is mainly used in exploration work. It can be expressed as:

$$\Delta g_B = g_M + C_{FA} - C_B + C_T - g_N, \tag{9.3}$$

where:

- g_M, measured gravity corrected for tidal effects (attraction of moon and sun) and drift in the gravimeter
- C_{FA}, elevation correction or free-air correction. It can be written as: $C_{FA} = 0.3086 \cdot H$, where H is the height of the station in m above sea-level
- C_B, correction for the excess mass material between the station and sea-level, Bouguer correction. It can be written as: $C_B = 0.04191 \cdot \rho \cdot H$, where ρ is the density [g/cm^3]. The density must be well known in order to be able to calculate the Bouguer correction

- C_T, topographical correction, correction for local terrain variations near the station. It is caused by distortion by hills and valleys. It can be written as: $C_T = \rho \cdot GL$, where GL is a parameter characterized by the topography around each station. The topographic correction (due to both hills and valleys) always decreases measured gravity
- g_N, normal reference gravity, according to an international formula. It takes into account the latitude of the station, i.e. the earth's shape (ellipsoid) and centrifugal acceleration

TABLE 9.1: *Bulk density for different rocks*

Rock type	ρ [g/cm^3]
Shale	2.00-2.65
Hyaloclastite	2.00-2.60
Limestone	2.25-2.80
Sandstone	2.20-2.70
Granite	2.65-2.75
Basalt	2.50-2.90
Diorite	2.70-2.95
Gabbro	2.85-3.10
Dunite	3.20-3.20

Density depends largely on rock composition and porosity. For fluid saturated rocks, we have:

$$\rho_b = \Phi \cdot \rho_F + (1-\Phi) \cdot \rho_M \qquad (9.4)$$

Where:

ρ_b - bulk density (see Table 9.1)
Φ - porosity
ρ_F - fluid density
ρ_M - matrix density, solid rock density, for basalts: $\rho_M \approx 2.9$ g/cm^3

Residual anomaly: To separate effects of shallow structures from deeper ones, a regional trend is subtracted (see Figure 9.1).

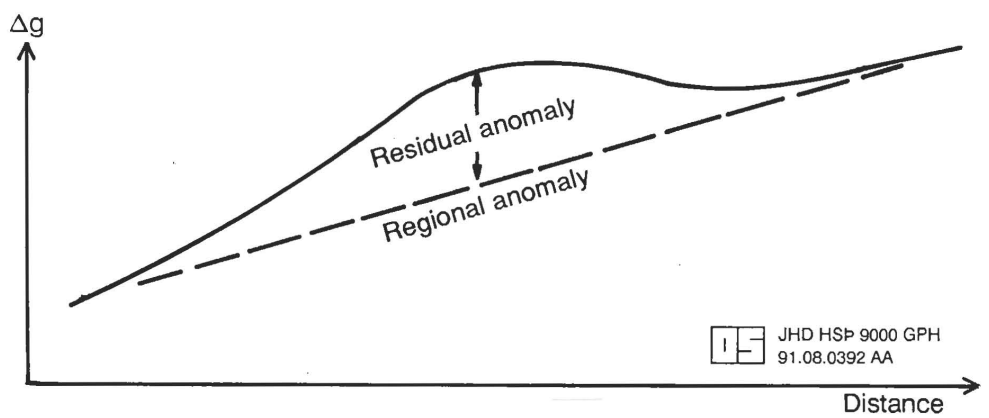

FIGURE 9.1: *Regional and residual anomaly*

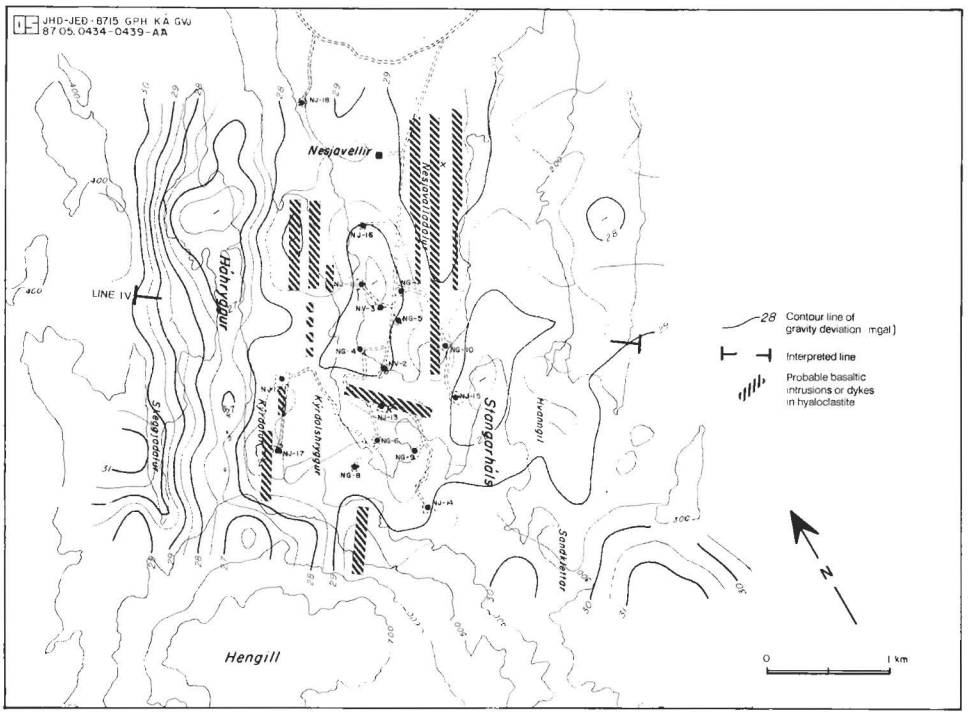

FIGURE 9.2: *Bouguer map of the Nesjavellir field based on density* 2.45 g/cm^3. *A gravity low is found in the low-density hyaloclastite filled graben in the volcanic zone. The measurements indicate intrusions in the youngest volcanic zones on both sides of the valley and at its southern rim. These intrusions seem to control the flow through the geothermal field (taken from Árnason et al., 1987; Árnason and Hersir, 1991)*

The value of the gravity method is greatly limited by the inherent ambiguity in the interpretation. Theoretically, an infinite number of density distributions fits a given gravity field. Additional information is needed for interpretation. The main value of the gravity method is, in conjunction with other information in structural investigations, to find massive intrusions and high porosity zones. It is an aid to geological mapping. Gravity maps and their application, and two-dimensional modelling of a gravity profile are shown in Figures 9.2-9.5.

Some possible causes of density contrasts and gravity anomalies in geothermal fields are as follows:

- Basement depth variation (sedimentary area)
- Intrusive rocks (possible heat sources)
- Alteration, cementation, due to thermal effect (sediments, volcanics)
- Porosity variations, pore fluid (water, steam)
- Faults, dykes

Mass extraction from a geothermal field under exploitation can be monitored by gravity and ground elevation measurements. This has been done in the Wairakei geothermal field in New-Zealand (Allis, 1982). Subsurface magma movement can also be monitored in this way, e.g. Krafla caldera, NE-Iceland (Johnsen et al., 1980).

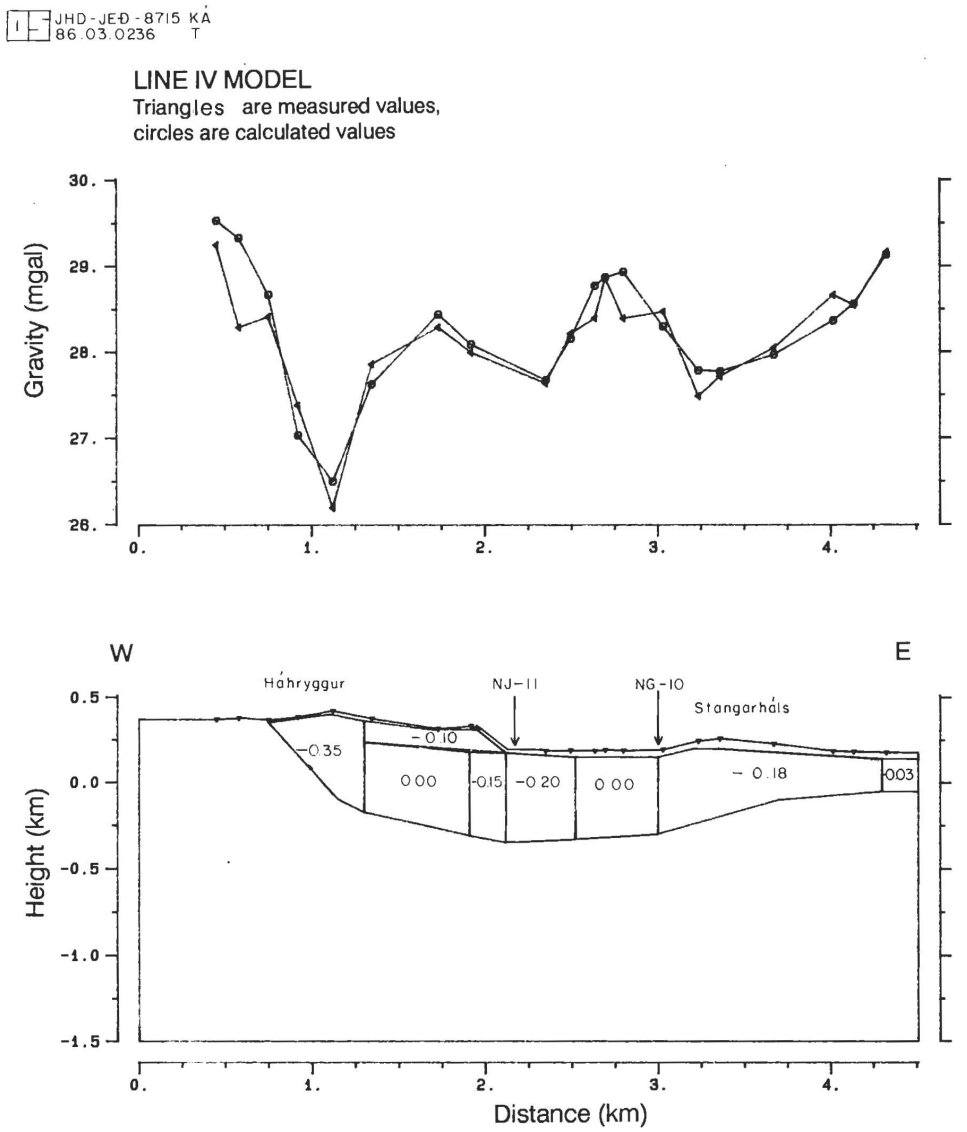

FIGURE 9.3: *Two-dimensional modelling of a gravity profile from the Nesjavellir high-temperature geothermal field based on density* 2.45 g/cm^3. *NJ-11 and NG-10 are drillholes number 11 and 10, respectively. (Figures 5.11 and 5.12 show two-dimensional interpretation of resistivity data along the same profile.) For location of the profile, see Figures 9.2 and 5.9. Figures denote deviation from the average density* 2.45 g/cm^3. *Two intrusions in the low-density hyaloclastite filled graben are detected (taken from Árnason et al., 1986; Árnason and Hersir, 1991)*

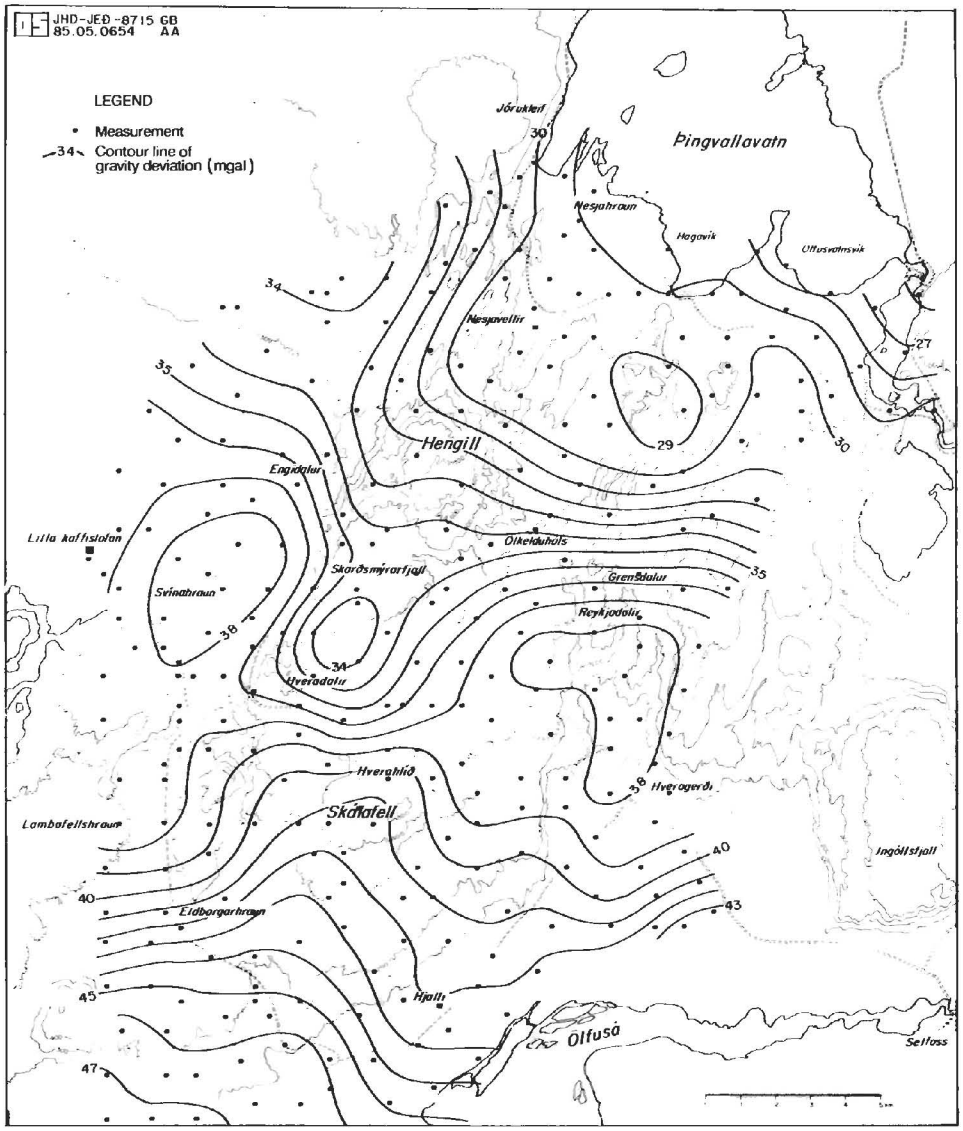

FIGURE 9.4: *Bouguer map of the Hengill high-temperature geothermal area based on density* 2.3 g/cm^3. *Contour-lines are drawn at 1 mgal intervals. The map shows a regional trend, higher values closer to the coast. This is in agreement with the Bouguer anomaly of Iceland, which has the shape of a bowl with a minimum of -40 mgal in the central part and increasing to 40-50 mgal in the coastal areas (Þorbergsson et al., 1990). A gravity low can be traced along the axis of the volcanic zone, in particular southwest of mountain Hengill (taken from Hersir et al., 1990; Björnsson et al., 1986)*

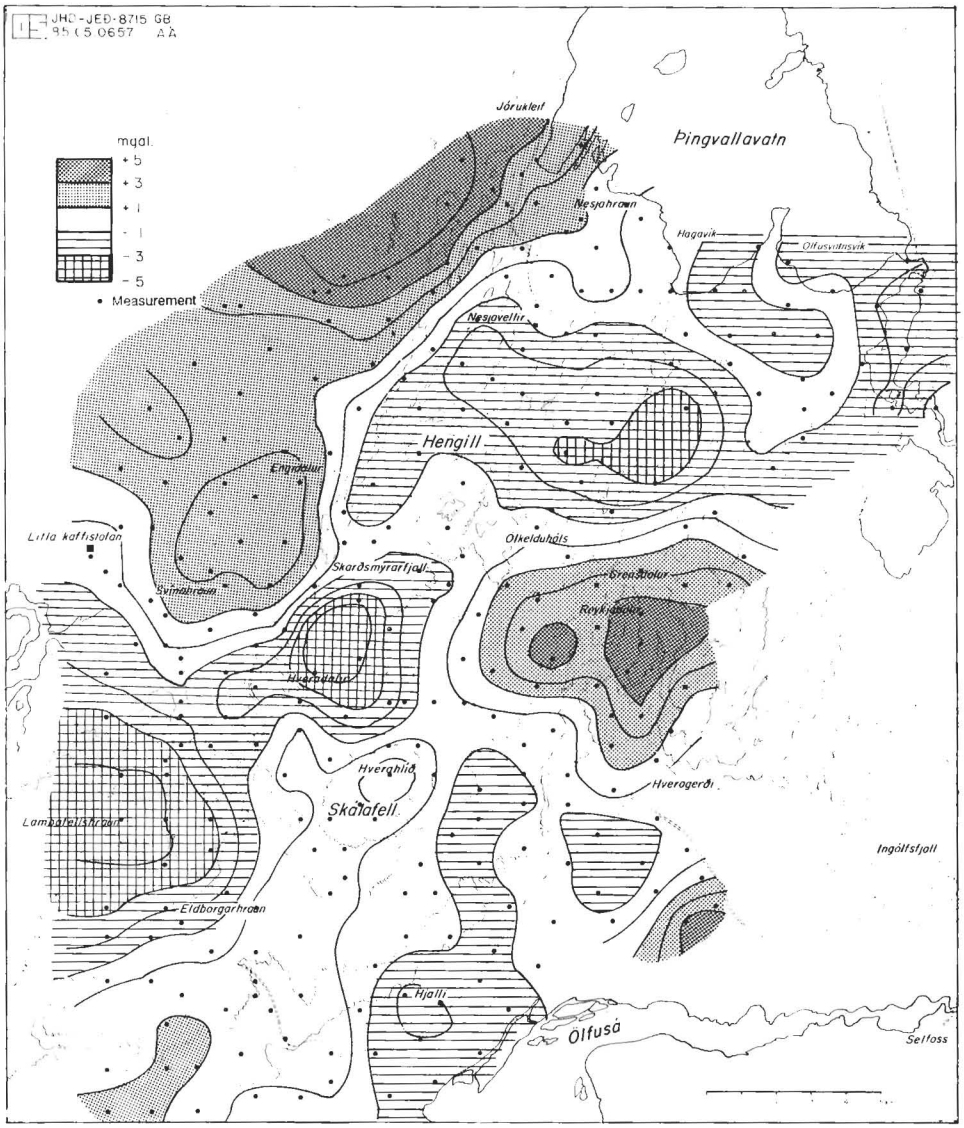

FIGURE 9.5: *Residual Bouguer map of the Hengill high-temperature geothermal area based on density 2.3 g/cm^3. Contour-lines are drawn at 1 mgal intervals. The regional trend in the Bouguer map (Figure 9.4) has been removed to produce the residual Bouguer map. There is an elongated NNE trending gravity low along the axis of the volcanic zone. It is presumably caused by the low density hyaloclastites with high porosity. Furthermore, less mineral deposits, thinner crust and low groundwater level in the highlands within the highly fractured rock of the Hengill fissure swarm close to the rift axis compared to the area outside the rift axis, could also contribute to lower gravity values. A distinct gravity high is located above the extinct Hveragerði central volcano caused by dense cool intrusions and high degree of alteration. Another gravity high is west of Hengill above the extended lava shield Húsmúli (taken from Hersir et al., 1990; Björnsson et al., 1986)*

10. SEISMIC SURVEYS

10.1 Seismic waves

Elastic waves travel with different velocities in different rock types. They are initiated at a point by explosion, vibrators or by sudden tectonic movements, like earthquakes. At a number of other points, the arrival times and the nature of the waves can be recorded. The waves are refracted and reflected by discontinuities in the rock formations.

The properties of elastic material are described by constants, or modulus, which specify the relationship between different types of stresses, s, and strain, l. Within the limits of elasticity, s [N/m^2] is proportional to l [m/m] (Hooke's law). In the case of a simple linear tension or compression we have:

$$s = E \cdot l \quad ; \quad E = \text{Young's modulus} \quad [N/m^2] \tag{10.1}$$

The bulk modulus, k, is the ratio of pressure change to relative volume change. The shear modulus, μ, or rigidity is the s/l ratio by simple tangential stress or shear. The Poisson's ratio, σ, is a measure of change in shape of an elastic body, i.e. relative change in diameter divided by relative change in length. Only two of these four constants (E, k, μ and σ) are independent.

There are two types of elastic body waves. In compressional waves (longitudinal, primary or P-waves) the material movements are along the travel direction of the wave path. In shear waves (transverse, secondary or S-waves) the material movements are perpendicular to the direction of the wave path. These waves are shown in Figure 10.1.

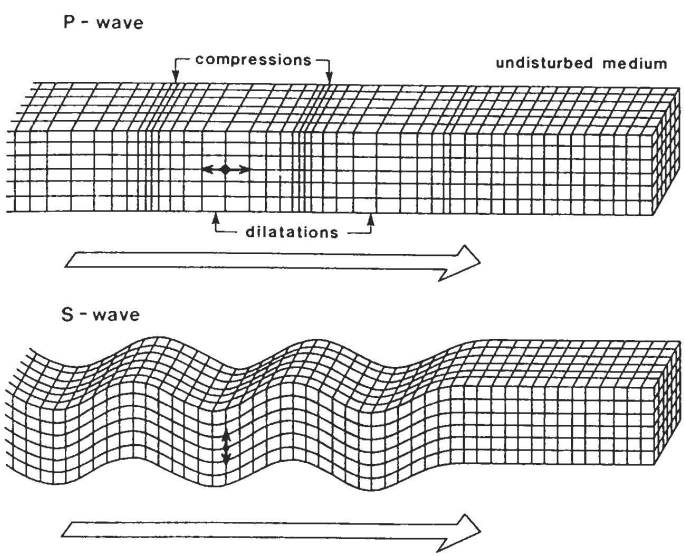

FIGURE 10.1: *Particle motions in P- and S-waves (taken from Kearey and Brooks, 1984)*

The velocities of the P-and S-waves, respectively, are given by:

$$V_P = \sqrt{\frac{k+4/3\cdot\mu}{\rho}} \quad \text{and} \quad V_S = \sqrt{\frac{\mu}{\rho}}, \tag{10.2}$$

where:

k - bulk modulus
μ - shear modulus, equal to 0 in molten rocks
ρ - density

V_S is equal to 0 in fluids. Therefore, S-waves are strongly attenuated or disappear completely when seismic waves travel through partially molten rocks or magma chambers.

In addition to the body waves (P and S), which travel across an elastic medium, there are other types of waves which travel along the surface of a body or along interfaces of different layers. Their velocities are lower than V_S.

In any material the ratio V_P/V_S can be expressed in terms of Poisson's ratio (σ). Poisson's ratio is the ratio of the transverse contraction to the longitudinal extension when a rod is stretched.

$$\frac{V_P}{V_S} = \sqrt{\frac{2(1-\sigma)}{(1-2\cdot\sigma)}} \tag{10.3}$$

Poisson's ratio can be measured from seismic wave arrivals. Values for σ from 0.0 (no lateral change in size) to 0.5 (a complete volumetric compensation) can be expected. For rubber and water we have σ equal to 0.5, but for cork σ is equal to 0. A body having σ equal to 0.25 is called Poisson's or an ideal elastic body. If V_S is low, the ratio V_P/V_S becomes high and σ approaches 0.5 (see Figure 10.2). For σ equal to 0.25, the V_P/V_S ratio becomes $\sqrt{3}$. These values are valid for the average crustal and upper mantle rocks. Significant deviations are observed in nature.

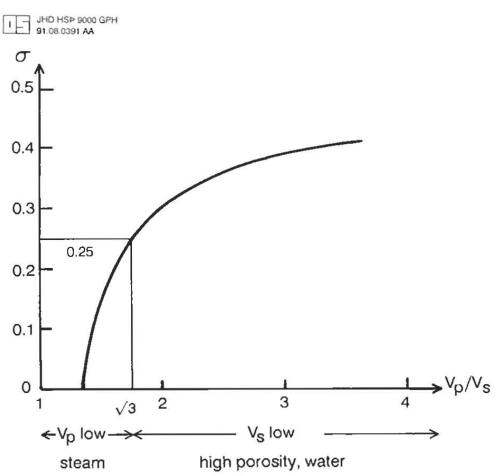

FIGURE 10.2: V_P/V_S *as a function of Poisson's ratio (σ) and conditions in a geothermal system*

σ is an indicator of fracturing. Increased fracturing of fluid-filled rock will lead to an increase in σ. This is due to a slight decrease in V_P and a significant decrease in V_S. On the other

hand, if the fractures are filled with air or steam, the opposite effect on σ occurs because of a large decrease in V_P.

In a geothermal environment, Poisson's ratio is typically in the range of 0.25 to 0.30 for normally saturated rocks. Poisson's ratios of 0.13 to 0.16 have been noted over the production zone at The Geysers in California, USA, and values of 0.25 and higher outside of it (Majer and McEvilly, 1979; Gupta et al., 1982). The low Poisson's ratio, in part, corresponds to a decrease in P-wave velocity.

An empirical relationship exists between P-wave velocity and porosity (Φ), given by (see e.g. Flóvenz et al., 1985):

$$\Phi_t = 1.97 \cdot V_P^{-1} - 0.32 \qquad (10.4)$$

There exists, as well, an empirical relationship between resistivity and porosity (Archie's law, see Equation 4.6 and Figure 4.3). Therefore, P-wave velocity and resistivity are empirically related (see Figure 10.3).

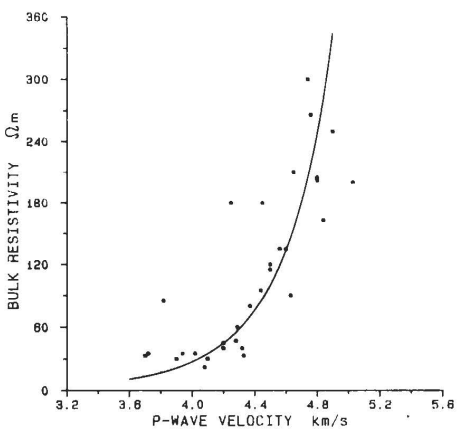

FIGURE 10.3: *Bulk resistivity at 500 m depth versus P-wave velocity at 500 m depth (taken from Flóvenz et al., 1985)*

Seismic methods can be divided into passive and active seismic methods, depending on whether the source of seismic energy is natural or man-made.

- **Passive seismic methods** detect seismic activity in the earth and can give information about sound velocity, attenuation and S-wave shadows. Seismic activity gives information about active faults and permeable zones. S-wave shadows can indicate partial melt and magma chambers. The seismic activity that is studied in geothermal exploration is:
  - **Ground noise (micro-seismicity)** generated by the geothermal system (from boiling and/or convective flow)
  - **Micro-earthquakes and earthquakes** on active fault planes, hydraulic fracturing and tensile cracking of cooling intrusions

- **Active seismic methods** detect sound velocity distribution and anomalies in the earth and attenuation. Sound velocity distribution gives structural information, information about density, texture and porosity. Attenuation can give information about temperature and

fluid-filled fracture zones. The active seismic methods are:

- **Seismic refraction** which gives good information about stratigraphy, faults, intrusions and geological structure
- **Seismic reflection** which gives more or less the same information as refraction but with better resolution
- **Teleseismic method** gives information about velocity anomalies, attenuation and S-wave shadows
- **VSP (Vertical Seismic Profiling).** Measurements are made with a geophone at various depths in a borehole and shots on the surface. Sometimes the location of the surface shots is varied. VSP has been useful for obtaining the acoustic properties of individual lithologic units and detecting reflections from near-vertical discontinuities

The active seismic methods are expensive and, therefore, not used routinely in geothermal exploration.

10.2 The passive seismic method - Earthquake studies

An earthquake is a movement of the earth along a new or pre-existing fault or fissure caused by a regional stress field. The nonelastic rupture is usually some tens or hundreds of meters for a small earthquake and can be regarded as a point source at some distance. The source place is called hypocenter and its projection up to the surface of the earth is called epicenter.

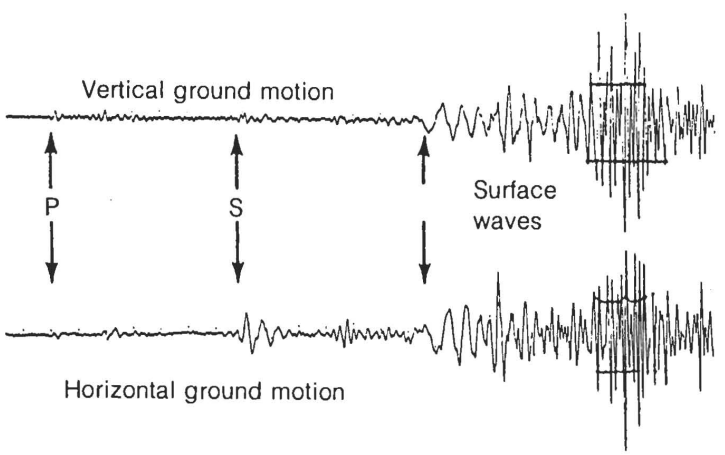

FIGURE 10.4: *A seismogram showing P-waves, S-waves and surface waves (taken from Press and Siever, 1974)*

A measure of the energy release (E) is the Richter M factor or **magnitude** which is a logarithmic scale.

$$\log E = A + B \cdot M; \quad B \approx 1.4 \tag{10.5}$$

An earthquake of magnitude 5 is about 10 times stronger (ten times more energy release) than an earthquake of magnitude 4. Earthquakes and micro-earthquakes give information on

the stress field and the tectonic nature of the area where they occur. Observation of seismic waves gives information on the properties of the transmission path from source to receiver (seismometer) (see Figure 10.4).

Earthquakes occurring within a specific area, i.e. those which are generically related, follow an inverse linear relationship between log (number of earthquakes, N) and magnitude, M (see Figure 10.5). The slope of the line log N = f(M) is called b-slope and is often about -1. This means that, for a given time interval, earthquakes with magnitude equal to M-1 are 10 times more frequent than greater earthquakes with magnitude equal to M. This can be expressed as:

$$\log N = a - b \cdot M \qquad (10.6)$$

The b-slope is less than 1 for strong rocks, and around 2-3 in inhomogeneous stressed volcanic rocks. When $b \leq 1.4$, small earthquakes cannot release all the stress; large earthquakes inevitably occur. When $b \geq 1.4$, all occurring earthquakes have $M_{max} \leq 5$.

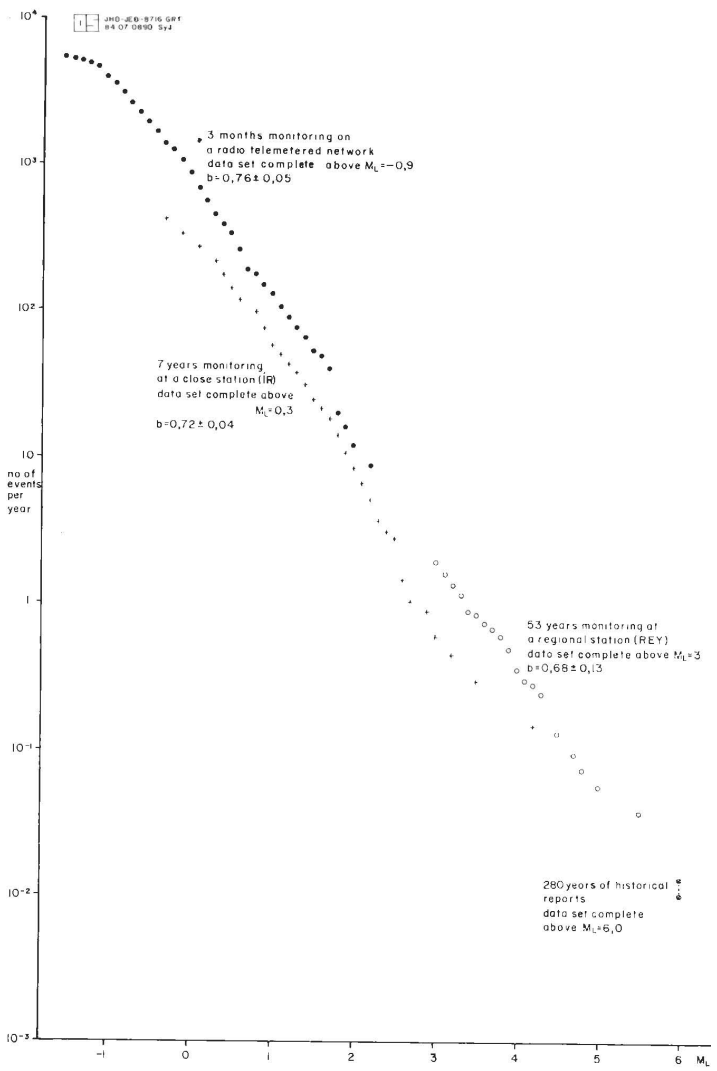

FIGURE 10.5: *A composite number-magnitude plot from the Hengill area in SW Iceland. The plot is based on three sets of data: 3 years monitoring of micro-earthquakes, 30 years monitoring at regional stations, and historic records. The b-slope is about 0.7-0.8 (taken from Foulger, 1984)*

The location of a hypocenter is estimated from the arrival times of P- and S-waves at several stations. Thereby, it is assumed that the source is a point and that the seismic waves travel through a transversely uniform earth (horizontal layers).

In principle an epicenter can be found from four P-arrival times. A better method is to use both S- and P-arrival times at three or more stations. The arrival times are read from the seismograms. If the distance travelled is denoted with r, the arrival times with t_S and t_P, the velocities with V_P and V_S and the origin time of the event with t_0, then

$$\frac{r}{V_S} - \frac{r}{V_P} = (t_S - t_0) - (t_P - t_0) = t_S - t_P \qquad (10.7)$$

or:

$$r = \frac{(t_S - t_P) \cdot V_S \cdot V_P}{V_P - V_S} \qquad (10.8)$$

This means that if the velocities, V_P and V_S, are known, then the distance to the earthquake can be found from the difference in the arrival times of the waves.

Some geothermal areas are characterized by an increased number of earthquakes, other show similar seismic activity as the region around and some geothermal areas even define a seismic gap (no seismic activity). Seismic studies have been used to investigate the regional tectonics where a geothermal area is located. As the tectonics and geological settings control the nature of most geothermal areas, the passive seismic method can deliver valuable information about the nature of geothermal systems.

In order to create and maintain a geothermal system, it is necessary to have high permeability, a heat source and water.

- **High permeability** is, in most geothermal systems, due to seismically active fractures. Continuing fracturing is necessary if chemical precipitation tends to fill pore spaces. This is most likely true both for high- and low-temperature geothermal systems. On the Reykjanes peninsula in SW-Iceland, several high-temperature geothermal systems are located where a seismically active zone intersects tectonically active fissure swarms (see Figure 10.6)
- **Heat source.** This can be a magma chamber or cooling intrusion or just a high geothermal gradient
- **Micro-earthquakes and earthquakes** have been observed to be created by hydraulic fracturing and tensile cracking of cooling intrusions in the roots of the Hengill high-temperature area in SW-Iceland (Foulger, 1984)
- **S-waves** are heavily attenuated when they pass through a partially molten or liquid rock (magma chamber) or may disappear completely from the records. This phenomenon has been used to localize and map the extent of a magma chamber beneath the high-temperature area in the Krafla caldera, NE-Iceland (Einarsson, 1978) (see Figure 10.7)
- **P-waves** are attenuated in hot intrusions (see Figure 10.8)
- **P-waves** from distant big earthquakes are delayed in hot intrusions below geothermal fields (see Figure 10.9)

In addition to earthquakes, a continuous seismic noise has been observed in some geothermal fields. This ground noise (micro-seismicity) is generated by the boiling or rapid flow of water at depth within the system.

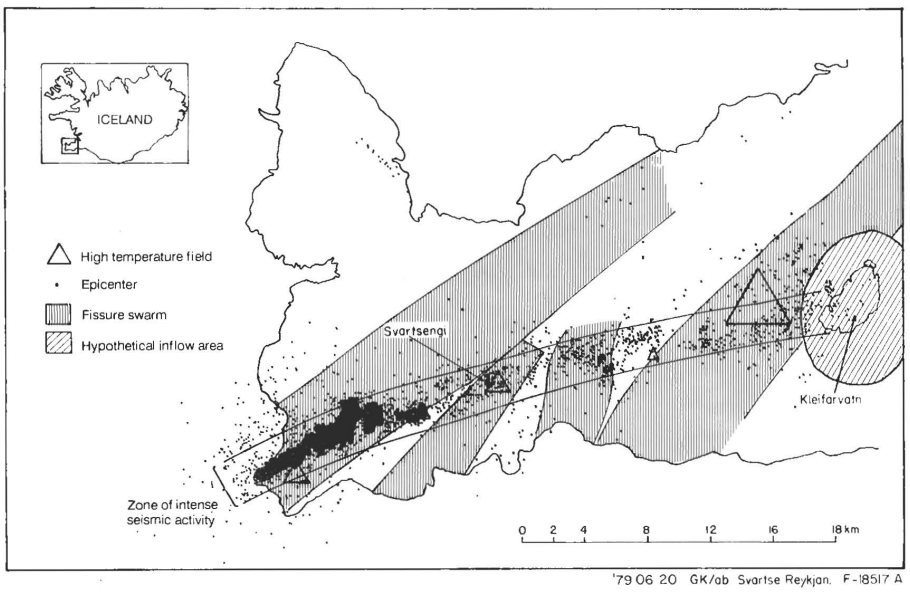

FIGURE 10.6: *Earthquakes on the Reykjanes peninsula in SW-Iceland. The high-temperature fields are located at the intersection of tectonically active fissure swarms and the seismically active zone (data from Sveinbjörn Björnsson, in: Kjaran et al., 1980)*

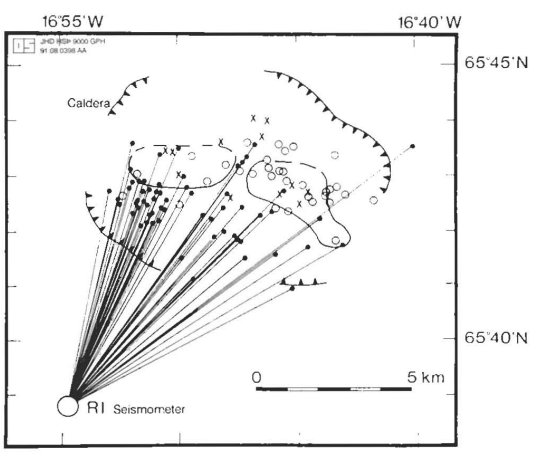

FIGURE 10.7: *S-wave paths to the seismometer, RI in the Krafla caldera, NE-Iceland. Epicenters of earthquakes that are recorded with a clear S-wave are marked with a black dot, open circles denote earthquakes with no recorded S-wave at RI. Earthquakes of intermediate character are marked with X. Two separate areas of maximum attenuation of S-waves are delineated. The attenuation is interpreted as being caused by magma in some kind of a magma chamber (taken from Einarsson, 1978)*

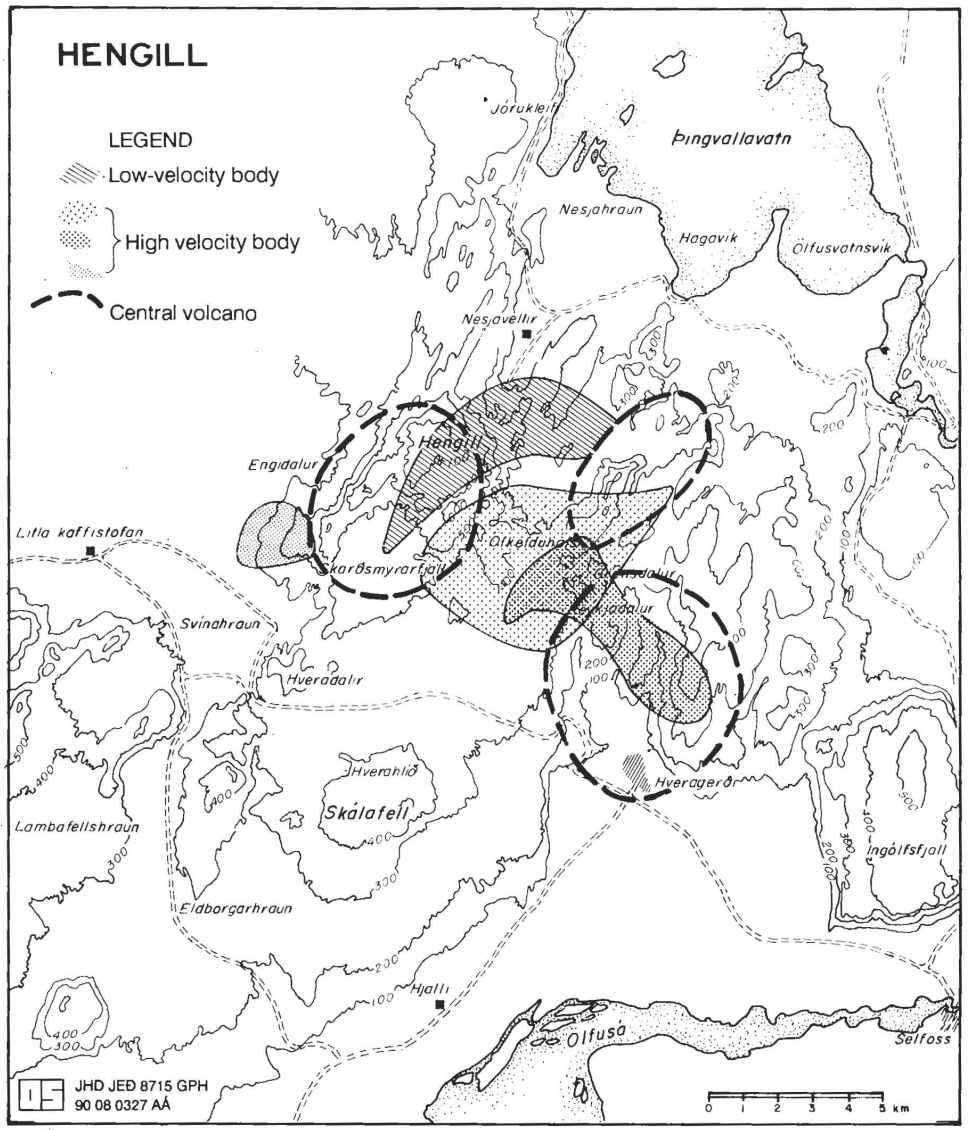

FIGURE 10.8: *Tomographic inversion of the Hengill area, based on 2,409 P-wave arrival times from 158 earthquakes. Three high-velocity bodies (dense rock types) and one low-velocity body (hot and light rock types) were found. Two of the high-velocity bodies coincide with extinct central volcanoes, underlain by solidifying magma chambers. (Compare this figure with the gravity map, shown in Figure 9.5) The low-velocity body coincides with the Hengill system which probably contains magma in disconnected pockets (modified from Foulger and Toomey, 1989)*

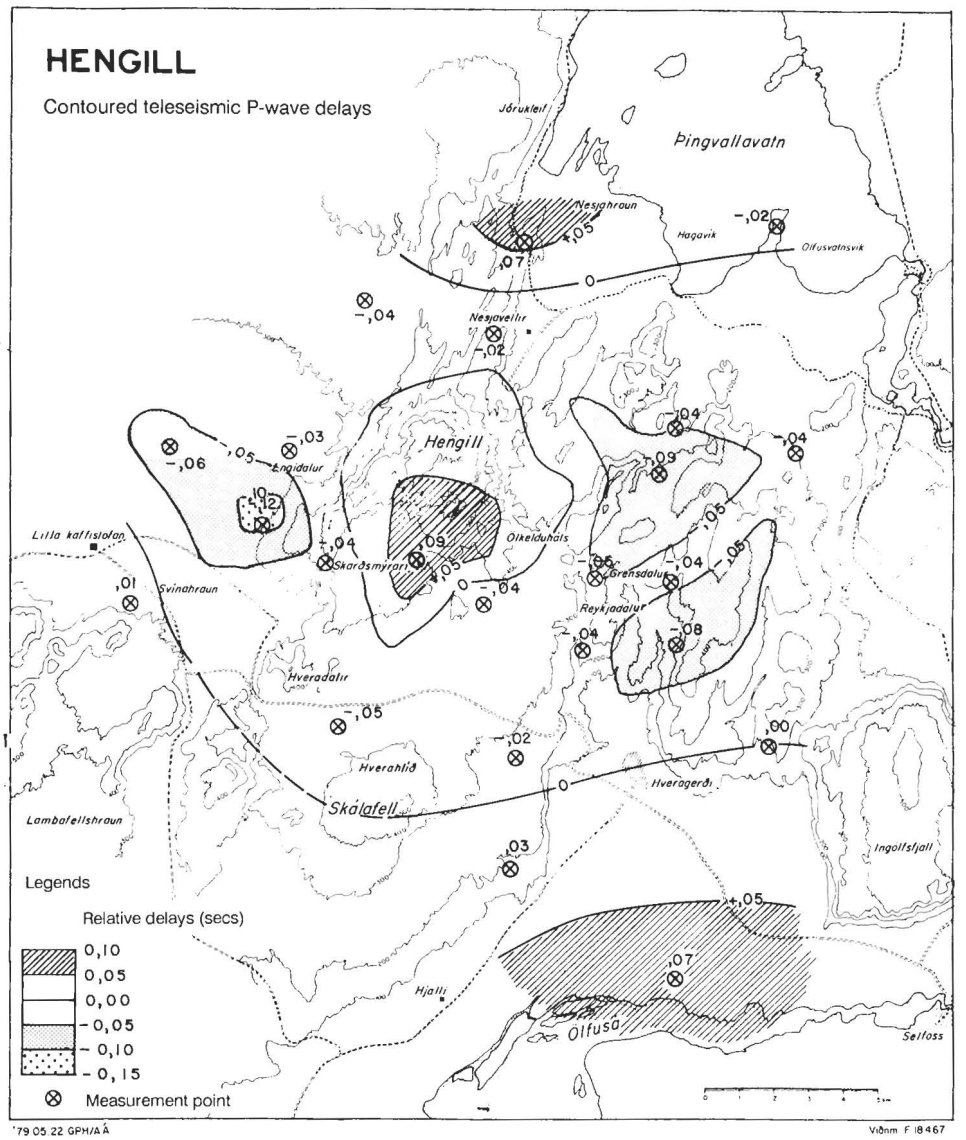

FIGURE 10.9: *Teleseismic data of the Hengill area based on 328 arrival times of 21 teleseismic event. Three high-velocity bodies and one low-velocity body were found (modified from Foulger, 1984)*

10.3 The active seismic method - Refraction and reflection

Active seismic methods have been highly developed and utilized in oil exploration, but have, until recently, not been widely used in geothermal exploration.

One of the reasons is the high cost. A seismic survey costs much more than any other exploration method. The cost for a reflection survey is about 5,000 US dollars per line km compared to a 2,000 m deep production well which costs about 1,000,000 US dollars. This does not seem to be very high. But we have to consider that oil is, in most places, of much higher economic importance than hot water and steam.

Another reason is the uncertainty in interpretation of reflection data from volcanic areas. Many geothermal fields are located in geologically complex areas, whereas the oil fields are in horizontal sedimentary layers.

The most important seismic methods are the seismic reflection method and the seismic refraction method. In both cases, a seismic wave is generated by an explosion or by vibration. The seismic signal is observed in a systematic way with many geophones (seismometers) and analyzed digitally with sophisticated computer programs.

The seismic methods, especially the reflection method, have much higher resolving power than most other exploratory techniques. It delivers a detailed picture of the crustal layers, depth and slope and location of faults and displacements as well as folding structures in sediments.

Seismic refraction has been used to a limited extend in geothermics. The resolving power is too limited to give detailed information about the structure of individual geothermal fields. It is used in shallow engineering work and in investigating the deep crustal structure.

Seismic reflection has given poor results in some geothermal areas but has also shown very useful results in other geothermal fields. Figure 10.10 shows a good quality seismic section from a volcanic terrain near Mineral Hot Springs in USA. Basalt flows are shown interbedded with gravel and alluvium and can easily be traced. Faulting is apparent as well as thinning out of the basalt layers. A geothermal area with a low electrical resistivity is associated with a down-drop fault block in the center of the section (see Figures 10.10 and 10.11) (Keller, 1981).

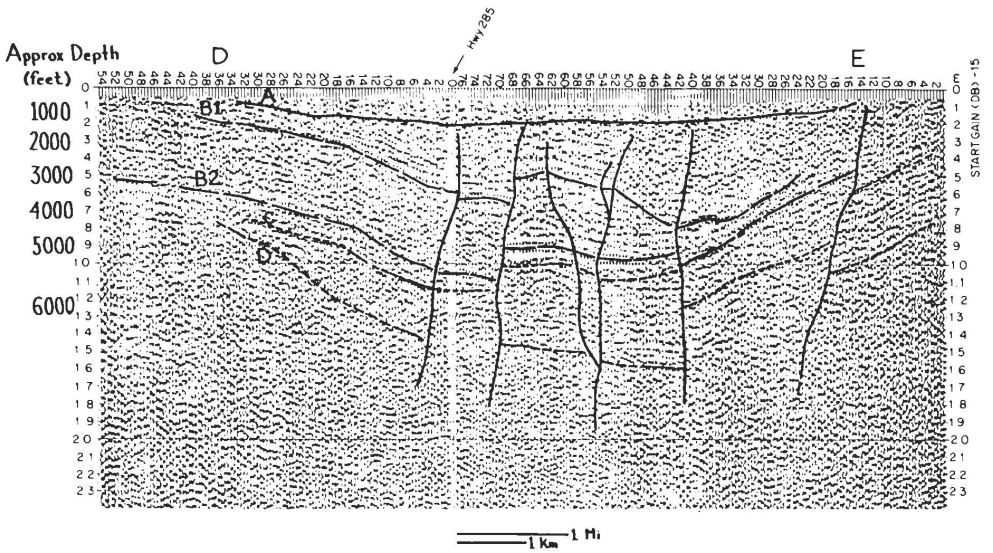

FIGURE 10.10: *Seismic reflection profile in the vicinity of Mineral Hot Springs (Central Colorado, USA). Events B1 and B2 are volcanic flows, C is flow bottom, D is probably Palaeozoic carbonate sequence. Near-vertical lines are faults (taken from Keller, 1981)*

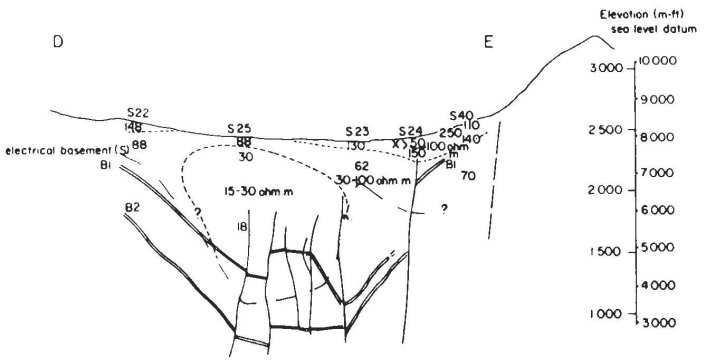

FIGURE 10.11: *Resistivity cross-section interpreted from Schlumberger soundings along the same profile as the seismic section shown in Figure 10.10. Reflective horizons from Figure 10.10 are shown. An area of relatively low resistivity, which is believed to represent the reservoir feeding the mineral hot springs, is seen to be associated with a down-drop fault block which is traced by the surface of the basalt flows (taken from Keller, 1981)*

11. PLANNING OF GEOTHERMAL PROJECTS - THE ROLE OF GEOPHYSICS

It is of utmost importance to plan, in detail, every geothermal exploration and exploitation before a power plant or direct-use installation is designed. Good planning minimizes risks and saves money. The role of geophysical exploration is important in this procedure. In this chapter, we will discuss the major steps in initiating a geothermal project and investigate what role geophysics plays in the different parts of the exploration and exploitation phases.

The major steps in planning geothermal projects are the following:

- Reconnaissance (regional) survey
- Detailed survey (prospect exploration)
- Exploratory drilling
- Appraisal study - Test drilling
- Project design
- Construction
- Production

There is one major difference between exploration and utilization of geothermal energy, on the one hand, and most other kinds of energy (like hydropower, nuclear energy and fossil fuel) on the other hand. The nature of a geothermal reservoir, and the amount of available energy, is usually not known in the beginning. Hence, an extensive surface exploration, exploratory drilling and reservoir testing must be done before the project can be designed and built without taking too much risk. Surface exploration (geology, geophysics etc.) costs only a small fraction of what the drillholes cost, and the drillholes are usually only a minor part of the total cost of the power plant. Therefore, it is important to take the above listed steps in proper succession, i.e. start with the exploration in order to site the wells, then drill wells and test the reservoir before the power plant is designed and built. It is important to realize that the first low-cost pre-drilling steps usually take just as long, or even longer time, than the drilling and reservoir evaluation steps. In order to save time, some investors have started drilling and building geothermal power plants without performing sufficient exploration, often with fatal results.

Reconnaissance (regional) survey: The purpose is to delineate geothermal areas, identify possible drilling fields and assign them priorities for further exploration. This phase may take some 2-3 years. The investigated area is relatively big, or some 10 x 10 km, mapped in scale e.g. 1:50,000. The most important geophysical methods are:

Airborne methods (magnetics, infra-red)
Gravity survey
Resistivity soundings (Schlumberger)
Dipole profiling
AC-methods, TEM, MT, AMT
Micro-earthquake studies
Seismics

A geological map is made of the area, which shows all major tectonic features, distribution of surface geothermal manifestations, etc., and the chemistry of hot springs and fumaroles is investigated.

The results of a reconnaissance survey is a first geological model of the geothermal system and identification of the best targets for further exploration.

Detailed survey (prospect exploration): The purpose is to delineate the selected prospect field, locate faults and fissures (aquifers) and site exploratory wells. This phase may take 1-3 years for each prospect field within a major geothermal area. The detailed survey is confined to a confined area, some 2 x 2 km and the mapping scale is usually around 1:10,000. The most important geophysical methods are:

DC-resistivity profiling
TEM soundings, and various EM methods (VLF, AMT)
Ground magnetics
Gravity survey
SP
Seismics
Temperature gradient in 1-100 m holes

A detailed geological map is made and the chemistry of thermal water and gas is studied in more detail.

The result is an improved model of the geothermal system, location of possible aquifers and upflow zones. The results are used to site the first exploratory wells.

Exploratory drilling: The purpose is to discover a geothermal reservoir, find the base temperature and investigate the chemical composition of the fluid. Further, the first estimate of the reservoir parameters is found. During this phase, often 1-3 wells are drilled some 1-2 km deep. The same geophysical methods are applied as in step 2. The result is an improved model of the geothermal reservoir and siting of appraisal wells. A prefeasibility report is made.

Appraisal study - Test drilling: The purpose is to prove sufficient production for an initial generation plant and obtain data for the design of a geothermal plant. Several more wells are drilled and the same geophysical methods applied as in steps 3 and 4 to site the wells. Further tasks are reservoir evaluation, resource assessment, preliminary design of the plant and feasibility studies. The result is a feasibility report and possibly the decision to build a plant.

Project design: This phase consists of production drilling, production testing, reservoir simulation, project planning, design of the plant, preparation of tender documents and reservoir tests.

Construction

Production

Along with the production of power, it is necessary to monitor and evaluate the response of the reservoir continuously.

REFERENCES

Abouriche, M., 1989: *Temperature measurements at the surface and in shallow drillholes.* UNU G.T.P., Iceland, Report 8, 46 pp.

Allis, R.G., 1982: *Geologic controls on shallow hydrologic chances at Wairakei field.* 4th New Zealand Geothermal Workshop, Proceedings. Part 1, 139-144.

Archie, G.E., 1942: *The Electrical Resistivity Log as an Aid in Determining some Reservoir Characteristics.* Tran. AIME, 146, 54-67.

Árnason, Knútur, 1984: *The effect of finite potential electrode separation of Schlumberger soundings.* 54th Annual International SEG meeting, Atlanta, Extended abstracts, 129-132.

Árnason, Knútur, 1989: *Central Loop Transient Electromagnetic Soundings Over a Horizontally Layered Earth.* National Energy Authority of Iceland report, OS-89032/JHD-06, 129 pp.

Árnason, Knútur, 1990: *Central-loop transient electromagnetic soundings in geothermal and ground water exploration, a step forward.* Geothermal Resources Council, Transactions, vol. 14, part II, 845-850.

Árnason, Knútur: *Inductive Electromagnetic coupling in Schlumberger soundings.* Unpublished manuscript.

Árnason, Knútur, Eyjólfsson, Brynjólfur, Gunnarsson, Karl, Sæmundsson, Kristján, and Björnsson, Axel, 1984: *Krafla-Hvíthólar, jarðfræði- og jarðeðlisfræðikönnun (Krafla-Hvíthólar, geological and geophysical exploration).* National Energy Authority of Iceland report (in Icelandic), OS-84033/JHD-04, 61 pp.

Árnason, Knútur, Haraldsson, Guðmundur Ingi, Johnsen, Gunnar V., Þorbergsson, Gunnar, Hersir, Gylfi Páll, Sæmundsson, Kristján, and Snorrason, Snorri Páll, 1985: *Nesjavellir. Jarðfræði- og jarðeðlisfræðileg könnun 1985. Áfangaskýrsla (Nesjavellir. Geological and geophysical exploration 1985. Preliminary report).* National Energy Authority of Iceland report (in Icelandic), OS-85088/JHD-47 B, 52 pp.

Árnason, Knútur, Haraldsson, Guðmundur Ingi, Johnsen, Gunnar V., Þorbergsson, Gunnar, Hersir, Gylfi Páll, Sæmundsson, Kristján, Georgsson, Lúðvík S., and Snorrason, Snorri Páll, 1986: *Nesjavellir. Jarðfræði- og jarðeðlisfræðileg könnun 1985 (Nesjavellir. Geological and geophysical exploration 1985).* National Energy Authority of Iceland report (in Icelandic), OS-86014/JHD-02, 125 pp.

Árnason, Knútur, Haraldsson, Guðmundur Ingi, Johnsen, Gunnar V., Þorbergsson, Gunnar, Hersir, Gylfi Páll, Sæmundsson, Kristján, Georgsson, Lúðvík S., Rögnvaldsson, Sigurður Th., and Snorrason, Snorri Páll, 1987: *Nesjavellir-Ölkelduháls - Yfirborðsrannsóknir 1986 (Nesjavellir-Ölkelduháls - Surface exploration 1986).* National Energy Authority of Iceland report (in Icelandic), OS-87018/JHD-02, 112 pp.

Árnason, Knútur, Björnsson, Grímur, Flóvenz, Ólafur G., and Haraldsson, Einar H., 1988: *Geothermal resistivity survey in the Asal Rift in Djibouti. Volume II: Survey data.* National Energy Authority of Iceland report, OS-88031/JHD-05, 57 pp.

Árnason, Knútur, and Hersir, Gylfi Páll, 1988a: *One dimensional inversion of Schlumberger resistivity soundings. Computer program, description and user's guide.* UNU G.T.P., Iceland, Report 8, 59 pp.

Árnason, Knútur, and Hersir, Gylfi Páll, 1991: *Surface geophysical exploration of the Nesjavellir geothermal field, SW-Iceland.* Unpublished manuscript, 23 pp.

Beblo, M., Björnsson, Axel, Árnason, Kolbeinn, Stein, B., and Wolfgram, P., 1983: *Electrical conductivity beneath Iceland - constraints imposed by magnetotelluric results on temperature, partial melt, crust- and mantle structure.* J. Geophys., vol. 53, 16-23.

Björgvinsdóttir, Bára, 1982: *Segulmælingar í Hrafnagilshreppi í Eyjafirði (Magnetic ground survey at Hrafnagilshreppur in Eyjafjörður).* National Energy Authority of Iceland report (in Icelandic), OS-82100/JHD-15, 23 pp.

Björnsson, Axel, 1980: *Jarðhitaleit og rannsókn jarðhitasvæða með jarðeðlisfræðilegri könnun (Geophysical methods used in geothermal exploration).* Náttúrufræðingurinn (in Icelandic), vol. 50, no. 3-4, 227-249.

Björnsson, Axel, 1990: *Jarðhitarannsóknir. Yfirlit um eðli jarðhitasvæða, jarðhitaleit og vinnslu jarðvarma (Geothermal exploration).* National Energy Authority of Iceland report (in Icelandic), OS-90020/JHD-04, 49 pp.

Björnsson, Axel, Hersir, Gylfi Páll, and Björnsson, Grímur, 1986: *The Hengill high-temperature area SW-Iceland: Regional geophysical survey.* Geothermal Resources Council, Transactions, vol. 10, 205-210.

Björnsson, Axel, Axelsson, Guðni, and Flóvenz, Ólafur G., 1990: *Uppruni hvera og lauga á Íslandi (The Nature of Hot Spring Systems in Iceland).* Náttúrufræðingurinn (in Icelandic), vol. 60, no. 1, 15-38.

Björnsson, Grímur, and Eysteinsson, Hjálmar, 1988: *Viðnámsmælingar á Meðalfellssandi í júlí 1988 (Resistivity soundings at Meðalfellssandur in July, 1988).* National Energy Authority of Iceland report (in Icelandic), OS-88061/JHD-31 B, 7 pp.

Coudert, J.M., Lejeune, J.M., Rojas J. and Varet, J., 1985: *Normal-gradient geothermal energy: Technical and economic characteristics.* In: 1985 International Symposium on Geothermal Energy, edited by Claudia Stone. International volume. Geothermal Resources Council, 77-84.

Dakhnov, V.N., 1962: *Geophysical Well Logging.* Q. Colo. Sch. Mines, vol. 57, no. 2, 445 pp.

Einarsson, Páll, 1978: *S-wave shadows in the Krafla caldera in NE Iceland, evidence for a magma chamber in the crust.* Bull. Volcanol., vol. 41, 187-195.

Eysteinsson, Hjálmar, and Hermance, J.F., 1985: *Magnetotelluric measurements across the eastern neovolcanic zone in south Iceland.* J. Geophys. Res., vol. 90, no. B12, 10,093-10,103.

Flóvenz, Ólafur G., 1984: *Jarðhitinn á Reykjum í Fnjóskadal (The geothermal area at Reykir in Fnjóskadalur, northern Iceland).* Náttúrufræðingurinn (in Icelandic), vol. 53, 165-175.

Flóvenz, Ólafur G., 1984a: *Application of the head-on resistivity profiling method in geothermal exploration.* Geothermal Resources Council, Transaction, vol. 8, 493-498.

Flóvenz, Ólafur G., Georgsson, Lúðvík S., and Árnason, Knútur, 1985: *Resistivity Structure of the Upper Crust in Iceland.* J. Geophys. Res., vol. 90, no. B12, 10,136-10,150.

Flóvenz, Ólafur G. and Sæmundsson, Kristján, 1991: *Geothermal Atlas of Europe. Explanatory text for Iceland.*

Foulger, G. R., 1984: *The Hengill Geothermal Area: Seismological Studies 1978-1984.* Raunvísindastofnun Háskólans, Hitaveita Reykjavíkur, Orkustofnun. OS-84073/JHD-12, 196 pp.

Foulger, G. R., and Toomey D. R., 1989: *Structure and Evolution of the Hengill-Grensdalur Volcanic Complex, Iceland: Geology, Geophysics, and Seismic Tomography.* J. Geophys. Res., vol. 94, no. B12, 17,511-17,523.

Garland, G. D., 1979: *Introduction to geophysics (mantle, core and crust).* Saunders, 494 pp.

Georgsson, Lúðvík S., Jóhannesson, Haukur, and Gunnlaugsson, Einar, 1981: *The Baer thermal area in western Iceland: Exploration and exploitation.* Geothermal Resources Council, Transaction, vol. 5, 511-514.

Goldstein, N.E., 1988: *Subregional and detailed exploration for geothermal-hydrothermal resources.* Geothermal science and technology, vol. 1, no. 4, 303-432.

Grant, F.S., and West, G.F., 1965: *Interpretation theory in applied geophysics.* McGraw-Hill, 585 pp.

Gupta, H.K., Ward, R.W., and Lin, T.L., 1982: *Seismic wave velocity investigation at The Geysers-Clear Lake geothermal field, California.* Geophysics, vol. 47, 819-824.

Haenel, R., Rybach, L., and Stegena, L. (editors), 1988: *Handbook of terrestrial heat-flow density determination with guidelines and recommendations of the international heat flow commission.* Kluwer academic publishers, 486 pp.

Hersir, Gylfi Páll, 1988: *Correcting for the Coastal Effect on the Apparent Resistivity of Schlumberger Soundings.* National Energy Authority of Iceland report, OS-88019/JHD-10 B, 13 pp.

Hersir, Gylfi Páll, Björnsson, Axel, and Pedersen L.B., 1984: *Magnetotelluric survey across the active spreading zone in southwest Iceland.* J. Volcanol. Geotherm. Res., vol. 20, 253-265.

Hersir, Gylfi Páll, Björnsson, Grímur, and Björnsson, Axel, 1990: *Eldstöðvar og jarðhiti á Hengilssvæði. Jarðeðlisfræðileg könnun (Volcanos and geothermal fields in the Hengill area. Geophysical exploration).* National Energy Authority of Iceland report (in Icelandic), OS-90031/JHD-06, 93 pp.

Hersir, Gylfi Páll, Björnsson, Grímur, Björnsson, Axel, and Eysteinsson, Hjálmar, 1990a: *Eldstöðvar og jarðhiti á Hengilssvæði. Jarðeðlisfræðileg könnun - Viðnámsmæligögn (Volcanos and geothermal fields in the Hengill area. Geophysical exploration - Resistivity data).* National Energy Authority of Iceland report (in Icelandic), OS-90032/JHD-16 B, 89 pp.

Hjartarson, Árni, Hersir, Gylfi Páll, and Smárason, Ómar Bjarki, 1988: *Ísafjarðardjúp. Náttúrulegar aðstæður til fiskeldis (Ísafjarðardjúp. Natural conditions for fish farming).* National Energy Authority of Iceland report (in Icelandic), OS-88012/VOD-05 B, 58 pp.

Hochstein, M.P. (editor), 1982: *Introduction to geothermal prospecting.* Geothermal Institute, University of Auckland, 155 pp.

Jessop, A.M., and Lewis, T., 1978: *Heat flow and heat generation in the Superior Province of the Canadian Shield.* Tectonophys., vol. 50, 55-77.

Johnsen, Gunnar, V., Björnsson, Axel, and Sigurðsson, Sven, 1980: *Gravity and elevation changes caused by magma movement beneath the Krafla caldera, northeast Iceland.* J. Geophys., vol. 47, 132-140.

Karlsdóttir, Ragna, Johnsen, Gunnar, Björnsson, Axel, Sigurðsson, Ómar, and Hauksson, Egill, 1978: *Jarðhitasvæðið við Kröflu. Áfangaskýrsla um jarðeðlisfræðilegar rannsóknir 1976-1978 (Krafla geothermal area. Preliminary report on geophysical exploration 1976-1978).* National Energy Authority of Iceland report (in Icelandic), OS JHD 7847, 40 pp.

Kaufman, A.A., and Keller G.V., 1981: *The magnetotelluric sounding method.* Elsevier Scientific Publishing Company, 595 pp.

Kaufman A.A., and Keller G.V., 1983: *Frequency and transient soundings.* Elsevier Scientific Publishing Company, 685 pp.

Kearey, P., and Brooks, M., 1984: *An introduction to geophysical exploration.* Blackwell scientific publications, 296 pp.

Keller, G.V., 1980: *Geophysical methods in prospecting for geothermal resources.* In: Geophysical aspects of the energy problem, edited by Rapolla, A., Keller, G.V., and Moore, D.J., Elsevier Scientific Publishing Company, 51-82.

Keller, G.V., 1981: *Exploration for geothermal Energy.* In: Developments in Geophysical Exploration Methods-2, edited by Fitch, A.A., Applied Science Publisher Ltd, London, 107-149.

Keller, G.V., and Frischknecht, F.C., 1966: *Electrical methods in geophysical prospecting.* Pergamon Press, 527 pp.

Keller, G.V., Pritchard, J.I., Jacobson, J.J., and Harthill, N, 1984: *Megasource time-domain electromagnetic sounding methods.* Geophysics, 993-1,009.

Kjaran, Snorri Páll, 1977: *Theoretical and Numerical Models of Groundwater Reservoir Mechanism.* National Energy Authority Hydraulic Laboratory, 196 pp.

Kjaran, Snorri Páll, Elíasson, Jónas, and Halldórsson Gísli Karel, 1980: *Svartsengi. Athugun á vinnslu jarðhita (Svartsengi. Exploration of geothermal utilization).* National Energy Authority of Iceland report (in Icelandic), OS80021/ROD10-JHD17, 98 pp.

Koefoed, O., 1979: *Geosounding Principles 1, Resistivity sounding measurements.* Elsevier Scientific Publishing Company, 270 pp.

Kristjánsson, Leó, 1984: *Notes on paleomagnetic sampling in Iceland.* Jökull, vol. 34, 67-76.

Lamb, H., 1932: *Hydrodynamics.* Dover Publications, New York, 738 pp.

Lumb, J.T., 1981: *Prospecting for geothermal resources.* In: Geothermal systems: Principles and case histories, edited by Rybach, L., and Muffler, L.J.P., John Wiley & Sons Ltd, 77-108.

Majer, E.L., and McEvilly, T.V., 1979: *Seismological investigations at The Geysers geothermal field.* Geophysics, vol. 44, 246-249.

Nagata, Takesi, 1961: *Rock magnetism.* Maruzen Co., Tokyo, 350 pp.

Noble, J.W., and Ojambo, S.B., 1976: *Geothermal exploration in Kenya.* Proc. 2nd UN Sympos. on the Development and Use of Geothermal Resources, vol. 1, 189-204.

Orellana, E., and Mooney, H.M., 1966: *Master tables and curves for vertical electrical sounding over layered structures.* Interscienia, Madrid, 123 pp.

Pálmason, Guðmundur, 1975: *Geophysical Methods in Geothermal Exploration.* Proceedings 2nd UN Symposium on the Development and Use of Geothermal Resources, 1,175-1,184.

Pálmason, Guðmundur, Arnórsson, Stefán, Friðleifsson, Ingvar Birgir, Kristmannsdóttir, Hrefna, Sæmundsson, Kristján, Stefánsson, Valgarður, Steingrímsson, Benedikt, Tómasson, Jens, and Kristjánsson, Leó, 1979: *The Icelandic Crust: Evidence from Drillhole Data on Structure and Processes.* In: Deep Drilling Results in the Atlantic Ocean: Continental Margins and Paleoenvironment. AGU, Maurice Ewing Ser., vol. 3, 43-65.

Parasnis, D.S., 1973: *Mining geophysics.* Elsevier Scientific Publishing Company, 395 pp.

Parasnis, D.S., 1979: *Principle of applied geophysics.* Chapman and Hall, 275 pp.

Press, F., and Siever, R., 1974: *Earth.* Freeman and Company, 945 pp.

Quist, A.S., and Marshall, W.L., 1968: *Electrical conductances of aqueous sodium chloride solutions from 0 to 800 °C and at pressures to 4000 bars.* Journ. Phys. Chem., vol. 72, 684-703.

Rink, M., and Schopper, J.R., 1976: *Pore structure and physical properties of porous sedimentary rocks.* Pure Appl. Geophys., 114, 273-284.

Rybach, L., 1976: *Radioactive heat production: A physical property determination by the chemistry of rocks.* In: The physics and chemistry of minerals and rocks, edited by Strens, R.G.J., John Wiley & Sons Ltd, 309-318.

Rybach, L., 1981: *Geothermal systems, conductive heat flow, geothermal anomalies.* In: Geothermal systems: Principles and case histories, edited by Rybach, L., and Muffler, L.J.P., John Wiley & Sons Ltd, 3-36.

Rybach, L., 1986: *Amount and significance of radioactive heat sources in sediments.* In: Thermal modeling in sedimentary basins, edited by Burrus, J., Editions Technip, 311-322.

Sass, J.H., Lachenbruch, A.H., and Munroe, R.J., 1971: *Thermal conductivity of rocks from measurements on fragments and its application to heat flow determinations.* J. Geophys. Res., vol. 76, 3,391-3,401.

Sharma, P.V., 1976: *Geophysical methods in geology.* Elsevier Scientific Publishing Company, 428 pp.

Stefánsson, Valgarður, Axelsson, Guðni, and Sigurðsson, Ómar, 1982: *Resistivity Logging of Fractured Basalts.* In: Proceedings of Eight Workshop Geothermal Reservoir Engineering, Stanford University, Stanford Calif., 189-195.

Telford, W.M., Geldart, L.P., Sheriff, R.E., and Keys, D.A., 1976: *Applied geophysics.* Cambridge University Press, 860 pp.

Tulinius, Helga, Smárason, Ómar Bjarki, Tómasson, Jens, Friðleifsson, Ingvar Birgir, and Hermannsson, Guðlaugur, 1986: *Hitastigulsboranir árið 1984 á höfuðborgarsvæði. Holur NS-14 til HS-22 (Thermal gradient wells in 1984 in the neighborhood of the capital. Wells NS-14 to HS-22).* National Energy Authority of Iceland report (in Icelandic), OS-86060/JHD-22 B, 38 pp.

Uyeda, S., 1988: *Implications.* In: Handbook of terrestrial heat-flow density determination with guidelines and recommendations of the international heat flow commission, edited by Haenel, R., Rybach, L., and Stegena, L., Kluwer academic publishers, 317-351.

Vozoff, K., 1972: *The magnetotelluric method in the exploration of sedimentary basins.* Geophysics, vol. 37, 98-141.

Ward, S.H., 1983: *Controlled source electromagnetic methods in geothermal exploration.* UNU G.T.P., Iceland, Report 4, 46 pp.

Ward, S.H., Ross H.P., and Nielson D.C., 1981: *Exploration Strategy for High-Temperature Hydrothermal System in Basin and Range Province.* Am. Ass. Petr. Geological Bull., vol. 65, 88-102.

Ward, S.H., and Sill, W.R., 1983: *Resistivity, induced polarization, and self potential methods in geothermal exploration.* UNU G.T.P., Iceland, Report 3, 94 pp.

Ward, S.H., and Wannamaker, P.E., 1983: *The MT/AMT electromagnetic method in geothermal exploration.* UNU G.T.P., Iceland, Report 5, 107 pp.

Wright, P.M., Ward, S.H., Ross, H.P., and West R.C., 1985: *State-of-the-art geophysical exploration for geothermal resources.* Geophysics, vol. 50, 2,666-2,699.

Þorbergsson, Gunnar, Magnússon, Ingvar Þór, and Pálmason, Guðmundur, 1990: *Þyngdarmæligögn og þyngdarkort af Íslandi (Gravity data and gravity map of Iceland).* National Energy Authority of Iceland report (in Icelandic), OS-90001/JHD-01, 50 pp.